National Technical University of Athens
Scholl of Civil Engineering
Laboratory of Soil Mechanics

1-dof system lying on square foundation : Monotonic and cyclic loading

P2011SQF2

Edition 1.0

Authors :

I. Anastasopoulos
Dr. Civil Engineer

P. Kokkali
Civil Engineer

A. Tsatsis
Civil Engineer

Approved by :

G. Gazetas
Professor, NTUA
Director of LSM

/03/2011

Phone: +30 210 772 3383, Fax: +30 210 772 2405
E-mail : soildyn@civil.ntua.gr
http: www.civil.ntua.gr/labs/geotech/gr/soildyn

1 INTRODUCTION

Over the last decades the earthquake engineering community has realized that non-linear response is unavoidable in the case of strong seismic incidents, exceeding the design limits. To this end, current seismic codes ensure that structural members can sustain dynamic loads exceeding their capacity without collapsing (ductility design), that failure is guided to less important members of the structure, and that failure is in the form of non-brittle mechanisms (capacity design). This capacity design concept, however, is exclusively addressed to the superstructural elements, while a contrasting restriction for elastic foundation response is posed, implemented through the adoption of overstrength design factors and the demand for increased Factors of Safety (FS).

Recent research, though, indicates that allowing non-linear response to take place at foundation level may reduce the ductility demands and limit the inertia transmitted to the superstructural elements by dissipating earthquake energy [Paolucci, 1997; Pecker, 1998, 2003; FEMA 356, 2000; Martin & Lam, 2000; Faccioli et al., 2001; Gazetas et al, 2003; Kutter et al., 2003; Gajan et al, 2005; Paolucci et al., 2008; Kawashima et al., 2007; Gajan & Kutter, 2008; Anastasopoulos et al. 2010a; Raychowdhury & Hutchinson, 2010]. Non linear response manifests by means of geometrical nonlinearity (i.e. uplifting from the supporting soil), interface nonlinearity (sliding at soil-foundation level) and mobilization of bearing capacity failure mechanisms. Thus, the incorporation of the non-linear soil –foundation interaction in the design of new buildings and retrofit of existing buildings is of paramount importance. However, lack of confidence in the ability to accurately design foundations with the desired capacity and energy dissipation characteristics, as well as concerns about permanent deformations beneath the footing and perceived lack of certainty in material properties (especially soil properties), have hindered the use of non-linear soil-foundation-structure interaction in the design.

Motivated by this lack of confidence, an experimental study has been conducted at the Laboratory of Soil Mechanics of NTUA in order to investigate the metaplastic response of 1-dof systems on surface square foundations, subjected to displacement control lateral pushover loading. The objective of this series of experiments was to shed light on some of the most important factors that affect the non-linear response of shallow foundation-structure systems when loaded well into their non-linear range. Primarily, this parametric investigation was conducted with respect to the design FS_v values, accomplished both by altering the superstructure mass and by utilizing different soil profiles. Secondly, the role of the sand relative density was examined by utilizing three cohesionless soil deposits. Moreover, the effect of the load history was investigated in terms of horizontal displacement amplitude and number of cycles. Finally, the potential effectiveness of shallow soil improvement was explored in an attempt to limit the uncertainties relating to the nonlinear soil response.

The experiments were conducted in the framework of the Research Project “DARE” (“Soil - Foundation - Structure Systems Beyond Conventional Seismic Failure Thresholds : Application to New or Existing Structures and Monuments”) and were carried out by Dr. I. Anastasopoulos, P. Kokkali, A. Tsatsis and E. Papadopoulos. The complete series of experiments consists of 34 experiments conducted between 07/04/2011 and 30/05/2011 (**Table 1**).

2 EXPERIMENTAL SETUP

2.1 SANDBOX

The sandbox where the experiments were performed is illustrated in **Figure 1**. Its internal dimensions, length - width - height are *1.48 m x 0.78 m x 0.645 m*, respectively. Transparent barriers have been placed at the two opposite larger sides of the box, in order to better observe the experimental procedure. These barriers are a combination of Plexiglas and glass. Plexiglas has been placed at the external side so that rigidity and durability are achieved, whereas glass has been put at the internal side, in order to minimize friction and simultaneously avoid scratching the Plexiglas.

2.2 PUSHOVER APPARATUS

The horizontal displacement is applied through a pushover apparatus, which consists of a servomotor joined to a screw-jack actuator (**Figure 2**). The servomotor is controlled by computer where the desired diplacement, acceleration and velocity can be selected. A device capable of measuring the applied load (load cell) is connected at the edge of the actuator. In this case, the load cell has a loading capacity of *200 kg*. The actuator is fixed at the model at the height of the center of mass through a pin and clevis attachment. A linear guideway intercepts between the actuator and the connection device. This system enables the structure to freely settle, slide and rotate, while the loading point remains at the level of the center of mass without producing parasitic inclined loading in the vertical direction.

2.3 FOUNDATION–SUPERSTRUCTURE MODEL

Figure 3 displays the model used in the experiments (in 3D, elevation and plan view). This particular concept of foundation-superstructure model was adopted due to its versatility. Its design gives the opportunity of altering the slenderness ratio (*h/B*), by adjusting the height of the slab supporting the superstucture mass. In addition, the desired Factor of Safety against vertical loads (FSv) can be acquired by placing the appropriate mass on the slab (*Figure 4*). In this series the model weights *35, 70* and *100 kg*. The mass-supporting slab placed at height equal to three times the foundation width B achieving a theoretical slenderness ratio *h/B = 3*. However, since the dead weight of the model is *30 kg*, the actual center is slightly lower than estimated resulting in aspect ratios *h/B = 2.3*, *2.6* and *2.8* in the three cases, respectively. The mass-supporting slab is supported through two columns, instead of a central one, for stability in the out-of-plane direction. Every component of the superstrusture is made of steel.

The foundation of the model is a square footing of dimensions *15 x 15 x 2 cm*. The ultimate capacity against vertical loads of this particular foundation was measured in the framework of a previous series of experiments conducted at NTUA (P2011SQF1) where the vertical load capacity of square foundations on homogeneous and two-layered soil profiles was investigated (LSM, March 2011). The footing is made of alluminium of density $2.7\ g/cm^3$ weighting only *1.22 kg*, avoiding this way significant deviation of the center of mass from the desired point. Finally, sandpaper has been placed under the foundation to achieve the desired friction angle of the foundation-sand interface.
No attempt was made to simulate the flexiibility and strength of the columns, so that the response be governed by the soil-foundation behavior.

2.4 INSTRUMENTATION

The model was instrumented to allow direct recording of both load and displacements. **Figure 5** shows the instrumentation adopted throughout the whole series. Load was measured by a load cell connected at the edge of the actuator as already mentioned. For the measurement of horizontal and vertical dislacements of the model, wired and laser displacement transducers were utilized. Two laser displacement transducers were used to measure the horizontal displacement of the footing, acquiring this way measurements for both sliding of the model and potential out-of-plane rotation. An extra wired displacement transducer was connected to the mass-supporting slab for a direct measurement of the horizontal displacement imposed. In the same manner, four wired displacement transducers were used to measure the vertical displacement of each corner of the slab, obtaining thus, the rotation of the model in both directions and the settlement of the system. The data from all the instruments were gathered through proper cables and saved in the record system of the Laboratory. In addition, visual data were obtained using high definition cameras, when necessary.

2.5 MODEL PREPARATION

Model preparation begins with sand layering within the sandbox. Dry Longstone sand, an industrially produced fine and uniform quartz sand, was used in the experiments. The respective gradation curve is shown in **Figure 6a**. In order to evaluate the characteristic parameters of the soil material, several tests have been conducted at the Laboratory of Soil Mechanics. The friction angle of the sand at the critical state has been found to be $\varphi_{cs} = 29.5^o$.

Sand layering is succeeded through an appropriate electronically controlled device of the Laboratory, shown in **Figure 6b** and **6c**. Through this sand raining system, it is possible to choose and audit the mechanical characteristics of the soil. This procedure is called sand pluviation. In order to achieve the desired density, the height measured from the bottom of the sandbox, the aperture of the device and the velocity of the soil hopper are defined. The selection of the suitable values of these three parameters is made according to **Figure 6d**, which summarizes the results of an experimental series performed to calibrate this particular device.

Three types of sand samples with relative density **D_r = 93 %, D_r = 65 %** and **D_r = 45 %** were used in this experimental series. The parameters regarding sand pluviation are shown in the following table. In each experiment the soil deposit in model scale was about 50 cm depth.

Soil	*Density D_r*	*Raining Parameters*		
		Aperture	*Pluviation Height*	*Velocity*
Dense Sand	93%	2 mm	0.9 m	12.3 cm/s
Sand of Medium Density	65%	4 mm	0.9 m	12.3 cm/s
Loose Sand	45%	10 mm	0.9 m	12.3 cm/s

Table 2. Raining parameters of soil samples used in the experimental series.

After sand layering is completed, the model is placed on four jacks attached to the sandbox which enable us to place the model on the desired position both horizontally and vertically. Due to the heavy weight of the system, this is achieved using a crane bridge, . Once the model has been placed on the jacks, the sandbox is moved to the prescribed location for the test. The whole system is aligned to the loading plane, as defined by the pushover apparatus. Then the model is carefully lowered to touch the soil. To monitor this procedure, electronic spirit levels are placed on the superstructure to certify that the foundation is placed parallel to the soil surface, with no inclination in both directions. The above procedure is adopted in order to assure that horizontal loading is central, preventing any out of plane movement. Once this routine is completed, the instruments mentioned above are installed and connected to the recording system. Initial and final measurements are taken before and after each load pack, respectively, regarding the force displayed on the load cell and the foundation inclination, for verification purposes.

3 EXPERIMENTAL RESULTS

The following section provides the results of the experiments, sorted primarily according to the mass of the superstructure and secondarily according to the type of the soil profile. In each experiment, information regarding the structural system, the soil properties and the load type are provided. The experimental results are presented in terms of moment–rotation and settlement–rotation curves and they all refer to model scale.

As already mentioned the systems were subjected to monotonic and slow cyclic horizontal loading. Since the displacement amplitude and the sequence of horizontal loading plays a vital role in the behavior of the foundation, three different types of cyclic load protocols were adopted in the series of experiments. **Type I**, the primary load protocol, consists of *14* cycles of increasing displacement, ranging from *2 mm* to *40 mm*. **Type II** consists of *7* cycles of increasing amplitude ranging from *4 mm* to *40 mm*. **Type III** consists of *31* cycles, divided into *10* cycles of *4 mm*, *10* cycles of *8 mm*, *5* cycles of *16 mm*, *3* cycles of *24 mm* and *3* cycles of *40 mm*, in increasing order. For all load types, the displacement was imposed in load packs in order to achieve the desired speed and avoid any dynamic effects.

4 DISCUSSION

4.1 INVESTIGATION ON HOMOGENEOUS SOIL PROFILES

In a first attempt to investigate the key response parameters of the problem, three systems with the same foundation but different superstructure mass were tested, lying on sand of varying density. The selection of the parameters was deliberately made so that the examined systems demonstrate distinctly different behavior, from strictly uplift–dominated to strictly sinking response.

First, the effect of the vertical load of the structure (**FS_V**) is discussed. Secondly, the density of the soil profile is examined. Finally, the effect of the load protocol for cyclic loading is studied.

Some of the results extracted are compared to Large Shaking Table experiments that took place at Public Works Research Institute (PWRI) Tsukuba, Japan, in order to validate the experimental findings of the current project.

4.1.1 *The Effect of FS_v*

The factor of safety against vertical loads is an indicative parameter of the overall response of a foundation–superstructure system and determines the interplay between uplifting and soil yielding. While 1-dof systems with small FS_V tend to accumulate settlement and soil yielding prevails at large rotation amplitudes, lightly loaded ones tend to uplift from the supporting soil even for small angles of rotation and soil plastification is concentrated on foundation edges.

Experiments P2011SQF2-001, 006, 007, 008, 009, 030 demonstrate the qualitatively different response of systems with different FS_v during horizontal monotonic and cyclic loading (TYPE I). The different values of FS_V are achieved by modifying the superstructure mass while all the systems lie on the same homogeneous soil deposit (Dense Sand).

Monotonic loading

The comparison in terms of moment–rotation and settlement–rotation is shown in **Figure 4.1**. With respect to moment–rotation curves the heavier the foundation, the larger bearing capacity M_u is displayed, with the relatively heavily loaded system ($FS_V = 5$) exhibiting ultimate moment $M_u = 0.042\ kNm$, the moderately loaded one $M_u = 0.036\ kNm$ and the lightly loaded one $M_u = 0.025\ kNm$. In terms of ultimate rotation ϑ_u, it can be evidently observed that the larger the safety factor, the ϑ_u of the system approaches that of the corresponding rigid block on rigid base ($\vartheta_c = arctan(b/2h) = 0.165\ rad$). This is expected considering the low ground compliance due to the reduced load of the foundation.

As depicted in **Figure 4.1b**, the factor of safety also determines the response in terms of settlement–rotation. Three distinct types of response can be observed : The lightly loaded system ($FS_V = 14$) displays a dominantly uplifting response. In contrast, the relatively heavily loaded system ($FS_V = 5$) settles for a wide range of rotation, while it uplifts only for great rotation amplitudes. Regarding the moderately loaded model ($FS_V = 7$), the response lies somewhere between the two, but still closer to that of the light one.

Though rotational stiffness is not expected to depend on the structural vertical load, **Figure 4.1c** reveals a dependency on the FS_V. Indeed, K_ϑ increases as the FS_V becomes greater. However, rotational stiffness is tied to the shear modulus G, which for sands is an increasing function of the confinement stresses. For reduced scale experiments, confinement stresses are mostly attributed to the surcharge imposed by the superstructure. Thus, the heavily loaded systems demonstrate greater rotational stiffness than the lighter ones.

Figure 4.2 plots the comparison of the critical load combinations as derived from the aforementioned experiments with the failure envelopes proposed by Butterfield and Gottardi (1994) for shallow footings on sand, for FS_V values *5*, *7* and *14.* Some slight differences can be noticed. Although for the relatively heavy system the measured and the calculated values of maximum horizontal load and maximum moment compare really well, that's not the case for the less heavily loaded systems. The measured load in the two remaining cases proves to be larger than the estimated values. Due to low stress field that unavoidably exists in *1g* reduced scale experiments, the calculated FS_V value diverges from the actual one, as the friction angle is greater than estimated. This is more noticeable when the model is not loaded significantly,. Hence, the comparison is less satisfactory for the cases of $FS_V = 7$ and *14.*

Cyclic loading

The correlation of FS_V with the moment developed and the evolution of settlement with respect to rotation is observed during cyclic loading for the aforementioned systems (experiments P2011SQF2-006, 008, 030), as well. In addition, there are some additional features, representative of the type of the response for each of the three differently loaded systems.

Figure 4.3 shows the moment–rotation curves derived for cyclic loading of TYPE I. Regarding the shape of the cyclic loops, qualitative differences are observed as the FS_V increases. The loops demonstrate an oval shape for the case of $FS_V = 5$, whereas for the large safety factor ($FS_V = 14$) the loops are clearly S–shaped. Compared to the monotonic backbone curves, the relatively heavily loaded system displays overstrength in moment, whereas the loops of the lightly loaded system are enveloped by the respective monotonic curves.

At this point, it should be mentioned that asymmetries observed at the curves derived from the cyclic pushover tests are attributed to deviations from the idealized conditions that unavoidably exist in an experimental procedure.

As inferred from the monotonic tests, the heavier the structure, the more the response is governed by sinking rather than uplifting and vice versa. During cyclic loading the response of the systems is similar (**Figure 4.4**). In particular, the relatively heavy system ($FS_V = 5$) settles throughout the whole load pack and only limited uplifting can be observed. On the other hand, for the case of the light one ($FS_V = 14$) uplifting is noteworthy and the accumulated settlement per cycle is significantly lower. At the end of the test the settlement of the relatively heavy system reaches *1.9 cm*, whereas that of the light one reaches *75 %* less than that of the heavy one. As for the case of $FS_V = 7$ the response is dominated by both uplifting and accumulation of settlement..

These differences can be explained as follows : When the heavy system reaches the maximum rotation at each cycle, soil yielding occurs and becomes more extensive as the rotational amplitude increases. As the system returns to its initial position permanent deformation of the soil results in substantial settlement of the system, even though the system might have instantly lost contact with the supporting soil during loading. On the other hand, the light system looses contact from the supporting soil even for small angles of rotation and soil yielding is limited near the edges of the foundation. Uplifting becomes even more intense for large values of rotation. Hence, when returning to the initial position settlement is significantly lower than for the heavily loaded system.

The qualitative different response can also be observed in **Figure 4.5** that shows the evolution of settlement with respect to horizontal displacement amplitude. It is evident that for the larger displacement amplitudes, the difference in settlement between the three different systems increases. This happens because systems with high FS_v demonstrate clearly uplifting response in large displacement amplitudes, whereas in small amplitudes all systems demonstrate sinking response differing only in absolute values.

Summarizing the above, as the systems get heavier the response is dominated by sinking rather than uplifting. However, it should be noticed that in the cases studied sinking response was observed for a moderate FS_V value ($FS_V = 5$). For a system lying on clay with the same FS_V value, the response would be identified with uplifting rather than sinking, since the settlement or uplifting response is coupled with the nature of the supporting soil.

Hence, for a system even heavier than those studied, the response would be governed by sinking exclusively. Indeed, this is demonstrated in **Figure 4.6**, where the cyclic response of a system with $FS_V = 2.6$ (system with $m_{str} = 100kg$ lying on sand of medium density $D_r = 65$ %) is shown. In this case, not only overstrength of the order of *100 %* is displayed, but also the system clearly settles during the whole load pack.

4.1.2 *The Effect of Soil Density D_r*

As demonstrated above, FS_V proves to be a crucial factor regarding the response of shallow foundations subjected to horizontal loading and consequently subjected to earthquake loading. However, the FS_V value cannot unambiguously define the system's capacity or performance. In experiments P2011SQF2-001, 015, 025, 030 two similar structures that have the same theoretical slenderness ratio ($h/B = 3$) and the same $FS_V = 5$ are subjected to monotonic and cyclic loading (TYPE I) and their performance is compared. The difference between these two structures lies in the fact that the soil deposit is different in each case, being a very dense sand of relative density $D_r = 93\%$ in the first case and a loose sand of relative density $D_r = 45\%$ in the second one. Of course, this means that in order to achieve the same FS_V, the superstructure mass is different.

Figure 4.7 reveals a satisfactory qualitative comparison between the examined systems. In terms of moment developed during cyclic loading, both systems exhibit overstrength compared to the respective static backbone curves, whereas the shape of the hysteretic loops imply that uplifting is limited (oval shaped loops). This kind of response is characteristic of their relatively small FS_V value. With respect to settlement–rotation curves, both systems respond to the imposed loading mainly through sinking rather than uplifting. The accumulation of settlement with the cycles is dominant, limited uplifting is noticed and particularly at large displacement amplitudes. The final settlement is of the same order for both systems (*1.9 cm* and *2.1 cm*, respectively).

The performance of these two systems, though, is far from identical, despite the fact that the factor of safety is the same in both cases. A big difference is observed in the moment capacity as derived from the monotonic tests. The system lying on dense sand has ultimate moment capacity around four times that of the system lying on loose sand ($M_u = 0.042\ kNm$ and $M_u = 0.011\ kNm$, respectively). Moreover, in the first case the overstrength developed during cyclic loading is less than in the second case.

Regarding ultimate rotation, the systems lying on dense sand clearly exhibits smaller ultimate rotation. In addition, as depicted at the settlement–rotation curves, there is a small, though significant, difference in the response of these systems. The monotonic curves reveal that the system founded on dense sand uplifts for a greater range of rotation whereas the system lying on loose sand settles for a notably larger range of rotation amplitudes.

Figure 4.8 depicts the dimensionless monotonic moment–rotation curves for the compared systems. The respective curves of the corresponding rigid blocks on rigid base are also shown. Moment is normalized with the ultimate moment sustained by the corresponding rigid block on rigid base and rotation is normalized with the critical angle of overturning of the corresponding rigid block ($B = 0.15$ m $2h = 0.9$ m). Taking into account that the systems have the same FS_V, the same dimensionless response would be expected. However, significant discrepancies are noticed.

In order to explain the differences observed we should consider the following : The aspect ratio slightly differs in the two cases, as already mentioned, due to the difference in the mass distribution. Hence, in the first case (system on dense sand) the center of mass is located higher than in the second case (system on loose sand). As a result the more slender system overturns at a smaller angle. Indeed, the ϑ_{ult} is closer to that of the corresponding theoretical rigid block ($h/B = 3$) for the lighter system.

Moreover, the difference between the dimensionless moment is also remarkable. The nature of the two soil deposits differs substantially and the inherent tendency to the development of overstrength due to dilatancy for the dense sand partially explains this difference. However, the discrepancies might be attributed to the different slenderness of the systems and the failure mechanisms developed. As the aspect ratio increases, ultimate moment is achieved for greater rotation amplitudes. As a result, second order effects have already become important, reducing the ultimate moment that can be sustained. This is the case of the system lying on loose sand, which due to its smaller aspect ratio and stiffness of the soil–foundation system results in significantly lower moment capacity.

4.1.3 *The Effect of the Change in Load Protocol*

Real earthquake records exhibit a wide range of horizontal displacement amplitudes and a varying number of loading cycles. Hence, in order to evaluate the performance of 1-dof systems on surface foundations during cyclic loading the effect of the load protocol with respect to the number of cycles and the displacement amplitude has been investigated and is presented herein.

Figure 4.9 depicts the moment–rotation and settlement–rotation curves derived from the cyclic pushover tests P2011SQF2-010, 011, 030. In these experiments, the system that carries a structural mass $m_{str} = 100\ kg$ and lies on dense sand is subjected to Type I, Type II and Type III cyclic lateral loading. These different load protocols reach the same displacement amplitude but with different ways. Type I consists of *14* cycles of increasing displacement, ranging from *2 mm* to *40 mm*. Type II consists of *7* cycles of increasing displacement ranging from *4 mm* to *40 mm*. Type III consists of *31* cycles, divided into *10* cycles of *4 mm*, *10* cycles of *8 mm*, *5* cycles of *16 mm*, *3* cycles of *24 mm* and *3* cycles of *40 mm*, in increasing order.

The performance of the system with respect to moment–rotation curves (**Figure 4.9a**) is analogous in the examined load protocols. The shape of the loops is similar and the overstrength developed compared to the static backbone curves is of the same order. Moreover, rotational stiffness does not seem to be affected by the number of cycles or by previous loading steps.

On the other hand, the response in terms of settlement differs substantially. While the total settlement accumulated in Type I is *1.9 cm*, it is only *1.1 cm* in Type II. As for Type III, it reaches *2.1 cm*. In brief, the settlement–rotation curves highlight that the accumulated settlement is an increasing function of the displacement amplitude and the number of cycles.

Nevertheless, the increase of settlement with the number of cycles is not linear. In the framework of illuminating the role of the number of cycles the results of the experiment P2011SQF2-019 are presented and discussed herein. This particular test refers to a foundation–superstructure system with $m_{str} = 35\ kg$ on loose sand and is subjected to Type III cyclic test. As already mentioned, Type III cyclic test consists of *5* load packs. The first one consists of 10 cycles of 4 mm, the second one of 10 cycles of 8 mm, the third one of *5* cycles of *16 mm*, the fourth one of *3* cycles of *24 mm* and the last one of *3* cycles of *40 mm*. **Figures 4.10** and **4.11** show the accumulated settlement in each load pack (*δw*) with respect to rotation and the additional settlement per cycle (*δw_i*, where *i* refers to each cycle) as a percentage of the total settlement of the load pack (*$\Sigma\delta w$*).

The following can be inferred : In the first three loading packs ($\delta = 4$, *8* and *16 mm*, respectively) the rate that the system accumulates settlement reduces with the increase of the number of cycles. This is especially evident in the first two loading packs that consist of a great number of cycles. In these cases, the major percentage of settlement occurs during the first cycles and the additional settlement gradually reduces as densification of the supporting soil takes place. However, this behavior is not apparent in the two remaining cases ($\delta = 24$ and *40 mm*), where there is no specific trend noticed, probably because of the small number of cycles.

The effect of the load protocol is shown in **Figure 4.12** through a different perspective. The additional settlement with respect to rotation is plotted for the systems mentioned in the previous section with $FS_V = 5$ (system with $m_{str} = 100\ kg$ on dense sand and system with $m_{str} = 35\ kg$ on loose sand), when subjected to load Types I and III. For the case of cyclic test Type III the additional settlement δw at each rotation ϑ is the average settlement for the number of cycles that took place at this specific amplitude. The selection of this variable was deliberately made in order to directly compare the response in terms of additional settlement for the two loading types. In both cases, the dotted line that represents Type III is below the solid line (Type I) signing that the major percentage of settlement takes place during the first cycle of loading. The difference between the two curves is more distinct for the system lying on loose sand. This means that the foundation on loose soil deposit is more sensitive to the load protocol as densification can take place in a greater extent.

4.1.4 *Comparison to Large Scale 1g Experiments*

In order to validate the findings of the current experimental project, a qualitative comparison is made between a specific case studied and results derived from large scale 1g experiments realized at the Public Works Research Institute, Tsukuba, Japan (2005).

In order to compare similar cases the systems shown in **Figure 4.13** were chosen. The foundation–superstructure system studied at PWRI consists of a square footing lying on dense sand ($D_r = 85\ \%$) with a slenderness ratio $h/B = 1.8$ and a safety factor against vertical loads $FS_V = 16$. This system was subjected to two different loading protocols similar to Type I and Type III as shown in detail in **Figure 4.14**. The compared system studied in the framework of the current project lies on dense sand (D_r = 93 %), has slenderness ratio $h/B = 3$ and $FS_V = 14$. Since the systems exhibit some differences the comparison cannot be direct and only a qualitative evaluation of their performance during cyclic loading can be made.

Figure 4.14 displays the comparison in terms of moment–rotation and settlement–rotation (or horizontal displacement) for the load protocol of the increasing displacement amplitude (**Figure 4.14a**) and the load protocol with numerous cycles at each displacement amplitude (**Figure 4.14b**). In both load protocols, the compared systems demonstrate qualitative similar response both in terms of moment and settlement. Regarding the loading protocol with the numerous cycles, no degradation in the moment developed is noticed due to the previous cycles. However, since the static backbone curve for the system studied at PWRI is not provided we cannot make a comparison between the static and the cyclic response.

As far as settlement evolution is concerned, even though the systems have different slenderness ratio and the system studied at PWRI might be more vulnerable to sliding and less to rocking, their response is uplift dominated as indicated by the settlement–rotation (or horizontal displacement) plots. The evolution of settlement with respect to the loading cycles and displacement amplitudes is analogous in both cases.

Hence, this satisfactory qualitative comparison points out that the results derived from this reduced 1-scale experimental series can adequately capture the cyclic response of 1-dof systems on surface footings encouraging further investigation of their metaplastic response.

4.2 Shallow Soil Improvement

Civil engineering practice does not take complete advantage of non linear soil–foundation–structure interaction yet. Apart from the concern about permanent deformations beneath the footing, lack of confidence in accurately designing foundations with the desired capacity has hindered the adoption of foundation rocking or mobilization of bearing capacity as fuse mechanisms.

The foundation capacity and the overall response of the system strongly depend on soil properties that cannot be easily defined. Aiming to remedy this problem and at the same time to achieve the desired performance, the case of soil improvement at shallow depth is investigated. Since the rocking mechanism has a relatively shallow area of effect, it is reasonable to assume that an improvement of small depth would improve the performance of the system.

This assumption is put to the test herein, investigating two different scenarios. The first one represents the case where the inaccurate estimation of the soil properties leads to reduced FS_V value, thus deteriorating the performance of the system particularly in terms of settlement. In order to model this scenario, the estimated soil profile was selected to be very dense sand ($D_r = 93\ \%$), while the actual soil profile was sand of medium density ($D_r = 65\ \%$). The model was loaded with superstructure mass $m_{str} = 100\ kg$, resulting in the first case in $FS_V = 5$ and in the second case in $FS_V = 2.6$. Two cases of improvement were explored. First, the “poor” soil was improved at depth z

equal to the foundation width *B* (*z/B = 1*), and in the ensuing a smaller improvement depth was chosen (*z/B = 0.5*). Although, as previously discussed, the behavior between the two extreme cases is not qualitatively that different (both systems exhibit sinking response), this investigation primarily aimed at showing the effectiveness of shallow soil improvement as a measure of limiting the uncertainties that could lead to excessive settlement, beyond design, after strong earthquake shaking.

The second case of soil improvement was examined under a different perspective : In common practice, there are many times that a structure has to be founded on poor soil that does not provide the desired safety margins. In such case, a possible solution is the improvement of the upper soil layer so that a satisfactory performance can be achieved.

This is the concept of the second scenario of soil improvement examined, where its effectiveness as an a priori measure of performance enhancement, both in terms of augmenting the system's capacity and decreasing the cumulative settlement, is evaluated. The studied system carries a mass $m_{str} = 35\ kg$ and is founded on loose sand ($D_r = 45\ \%$) whereas the ideal case would be a dense soil deposit ($D_r = 93\ \%$). Hence, soil improvement of varying depths is examined. First, a relative shallow soil improvement is examined (*z/B = 0.25*) and the depth of the improvement gradually increases so that the desired performance is approached.

4.2.1 *Shallow Improvement on sand of Medium Density*

Consider the cases shown in **Figure 4.15** where the estimated soil profile consists of dense sand (D_r = 93 %), thus achieving a factor of safety FS_V = 5. However, the actual soil profile is poorer, consisting of sand of medium density (D_r = 65 %). In this case the factor of safety yields : FS_V = 2.6. As already discussed, these systems have similar behavior in qualitative terms. In brief, both of them develop overstrength in moment during cyclic loading (**Figure 4.15a**), while sinking prevails as demonstrated in settlement–rotation plots (**Figure 4.15b**). Of course, in absolute terms the differences are noteworthy, especially regarding the ultimate moment sustained during static pushover tests and the total settlement due to cyclic loading.

In order to eliminate the uncertainties regarding strength and settlement response, the poor soil deposit is improved at depths $z = 0.5B$ and $z = B$, where B is the foundation width (**Figure 4.16**), yielding factors of safety against vertical loads $FS_V = 3.1$ and 4.1, respectively. These soil–foundation–superstructure systems are subjected to monotonic and cyclic lateral loading and their effectiveness is discussed herein.

Figure 4.17 displays the results of monotonic tests in terms of moment–rotation, settlement–rotation and rotational stiffness for both the homogeneous and the two-layered soil profiles. The response of the systems in terms of moment capacity has been improved. In particular, for the case of $z/B = 0.5$ the system reaches *67%* of the moment capacity of the ideal system (on dense sand), while for $z/B = 1$ this percentage is even higher reaching *88%*. Slight differences are also noticed in the ultimate rotation angle, which decreases as the soil deposit gets poorer. Of course, this is in accordance with the correlation of the FS_V value with ϑ_{ult}, as previously noticed.

Regarding the settlement response during static lateral loading, the range of rotation amplitudes that the systems settle is different, with the case $z/B = 0.5$ being closer to the poor soil and the case $z/B = 1$ being closer to the dense profile, but still mostly exhibiting sinking response and uplifting only for great angles. Focusing on the dense soil profile and $z/B = 1$ it seems that the two curves are parallel from a rotational amplitude on, with their difference being the extra settlement the latter has accumulated at small rotation amplitudes. As the system rotates to a greater extent and contact with the supporting soil is reduced, the distribution of stresses is shallower, thus affecting more the upper layers. Consequently the role of the improved stratum becomes dominant.

Nevertheless, this cannot be observed for *z/B = 0.5*, where the depth of the soil improvement is not sufficient to "isolate" the high stress field at the upper layer.

Finally, rotational stiffness is enhanced due to the presence of the upper stiffer layer for the cases of soil improvement for every rotation angle. It is noteworthy that in terms of rotational stiffness the two crusts examined are very effective, increasing it up to the respective of the dense sand. In fact, for small ϑ values the two crusts appear to have larger rotation stiffness than the dense sand. This should be attributed to inaccuracies in the experimental measurements.

In the ensuing, the performance of the improved systems during cyclic loading is assessed for load protocols Type I and III. The moment–rotation and settlement–rotation curves derived from tests of Type I are shown in ***Figure 4.18***. As far as moment is concerned, all the systems have similar behavior exhibiting overstrength compared to the respective monotonic curves. The loop shapes display a lot of similarities, something to be expected considering the two homogeneous profiles do not demonstrate themselves sharp differences, due to the $FS_V s$ being close. The development of overstrength in moment for small and moderate safety factors has already been observed for homogeneous profiles and indeed the smaller the FS_V the greater the overstrength factor. This trend stands for two layered profiles, too. As a result, all four systems reach the same ultimate moment during cyclic loading, however, for the systems with the small FS_V values this happens after a certain number of cycles. Hence, the development of moment is not dictated by soil quality and foundation–superstructure properties seem to play more important role than the presence of the upper stiffer layer.

However, this is not the case for the evolution of settlement. As noted in the corresponding charts in **Figure 4.18b**, the system on loose sand settles about 3.5 cm while the one on dense sand settles approximately 1.9 cm. When the upper layer is improved for z = 0.5B there is 20 % reduction in settlement (2.8 cm), whereas when the improvement is deeper (z = B) the performance approaches the ideal dense profile, reaching the same final settlement.

In addition, **Figure 4.19** shows the secant rotational stiffness K_ϑ with respect to rotation as obtained at Type I cyclic pushover tests. In particular, **Figure 4.19a** gives a schematic illustration of the calculation of the rotational stiffness at each loading cycle. At every loop realized the maximum and minimum ϑ values and the corresponding moment values are obtained and used for the calculation of the secant rotational stiffness. As indicated by the respective diagram, the denser the soil–foundation system the greater the rotational stiffness. Some divergences are observed at the first amplitudes that are attributed to flaws of the experimental procedure and inaccurate measurements. However, the compared curves are very close for great rotational amplitudes when degradation has occurred and due to the limited contact with the supporting soil the upper soil layers mainly contribute to the stiffness of the system.

The same observations regarding moment and settlement can be made for cyclic loading Type III (**Figure 4.20**). The improvement is effective regardless the load protocol, as evidenced by the respective charts. All systems respond by developing overstrength and reaching the same moment in this case too, while the reduction in settlement is substantial, reaching *12%* for *z/B = 0.5* and *44%* for *z/B = 1*.

Hence, the performance in terms of settlement is very satisfactory, verifying the concept of shallow improvement for elimination of uncertainties and reduction of settlement. The only thing to be considered in such scenario is whether these values of settlement are within the acceptable limits, which of course depends on many factors and is beyond the context of this project.

4.2.2 *Shallow Improvement on Loose sand*

The second scenario investigated herein, refers to soil improvement as an a priori measure of performance enhancement. To model this case of particular interest, the lightly loaded foundation–superstructure system (*m = 35 kg*) is founded on a poor soil deposit ($D_r = 45\%$) resulting to $FS_v = 5$ (**Figure 4.21**). The system in this case has an ultimate moment capacity in monotonic loading that reaches a mere $M_{ult} = 0.011$ *kNm*, while when subjected to slow-cyclic loading, it exhibits a sinking response, as depicted in settlement–rotation plot. The performance of the system in this case is considered inadequate and an effort is made to enhance it using a shallow soil improvement of a stiffer soil stratum consisting of dense sand ($D_r = 93\%$). In order to evaluate the system's response with the soil improvement, the response of the system on dense sand is analyzed at first. In particular, assuming that the foundation soil consists exclusively of this stiffer soil, the factor of safety against vertical loads would reach $FS_v = 14$, resulting to a dominantly uplifting response, with an ultimate moment capacity in monotonic loading of $M_{ult} = 0.025$ *kNm*. Subsequently, three solutions of soil improvement are examined, $z/B = 1$, $z/B = 0.5$ and $z/B = 0.25$ as schematically illustrated in **Figure 4.22**, as an effort to optimize the enhancement in the system's response as opposed to the depth of the improvement. The first case refers to improving the soil at a layer of depth equal to the foundation width, yielding a $FSv = 9.8$. Then the depth is reduced to $z/B = 0.5$, resulting to a $FSv = 7.1$, and finally to $z/B = 0.25$ achieving a factor of safety FSv = 5.6.

Figure 4.23 displays the results of monotonic tests in terms of moment–rotation, settlement–rotation and rotational stiffness for the three cases of soil crusts used. The presence of the lines that refer to the homogeneous soil deposits serves the purpose of comparing and evaluating the enhanced performance. The response of the systems in terms of moment capacity has been improved. In particular, for the case of $z/B = 0.5$ the system reaches *72%* of the moment capacity of the ideal system (on dense sand), while for *z/B = 1* this percentage is even higher reaching 80%. In contrast, the shallower crust of depth *z/B = 0.25* does not increase considerably the moment capacity (a mere *9.1%* increase in ultimate moment capacity compared to loose sand). The same can also be noticed in settlement – rotation plots. The shallower crust does not alter the response of the system, which practically exhibits an exclusively sinking response. However, increasing the depth of the crust to *z/B = 0.5* the difference in the response is significant and the performance enhancement is satisfactory. The effect of the *z/B = 1* soil improvement is spectacular, leading to performance identical to that of homogeneous dense sand.

In the ensuing, the examined systems are subjected to cyclic loading. In terms of moment–rotation (**Figure 4.24**), the improved systems result in about the same ultimate moment M_{ult} = *0.020 kNm*. Nevertheless, this does not indicate the all three cases of soil improvement are equally effective. As depicted in settlement-rotation plots (**Figure 4.25**), in the case of *z/B = 1* the system displays practically the same response with the corresponding homogeneous dense profile. In qualitative terms, the system responds through uplifting and the final settlement is limited. Indeed, the accumulated settlement reaches *5.9 mm* while for the dense sand the accumulated settlement reaches *4.5 mm.*

The presence of shallower dense upper layer *z/B = 0.5* proves to be effective as well. In particular, the final settlement reaches *9.9 mm*, resulting in a *53%* reduction compared to the original poor soil. However, the effectiveness of the improvement is limited when the depth is further reduced to *z = 0.25B* where the accumulated settlement reaches *15.2 mm*, reduced only by *27%*.

Figure 4.26 shows the evolution of rotational stiffness with the rotation amplitude for both the homogeneous and the improved profiles. As already noticed in the previous chapter, the secant rotational stiffness increases as the depth of the soil improvement increases.

Similarly to the case of load protocol Type I, in the case of loading type III, the effectiveness of shallow soil improvement is proved as well, despite the increased number of cycles. The cases of crusts of depth $z/B = 1$ and $z/B = 0.5$ are remarkably efficient, leading to a decrease in the accumulated settlement of the order of *70%* and *62%* compared to the poor soil profile. In contrast, the crust of depth $z/B = 0.25$ does not adequately enhance the performance of the system since the respective decrease is only *18%*.

Nonetheless, whether the improvement in the response of the systems is judged adequate or not depends on the desired performance state and the design limitations.

4.2.3 *Effectiveness of crusts*

The previously presented study showed that shallow soil improvement of depth at least equal to half the foundation width is efficient in terms of settlement reduction. However, this deduction does not reveal the whole truth as the effectiveness of the crust depends on the rotation amplitude. In the present section, emphasis is given in this parameter.

Figure 4.30 presents the additional settlement δw depending on the rotation angle amplitude as derived from the Type I cyclic loading of the system with $m_{str} = 35\ kg$. Each rotation amplitude corresponds to a single loading cycle as defined by Load protocol Type I and δw refers to the additional settlement in each cycle (i.e., having subtracted the settlement accumulated in the previous cycles). Obviously, the curve that corresponds to the original poor soil profile is above the other ones, since in this case the settlement is excessive, and after all this is the unsatisfying scenario to be improved. The three curves corresponding to the two-layered profiles gradually diverge from the curve of the loose sand, with the curve referring to $z/B = 1$ almost coinciding with the dense sand. However, this chart reveals a detail of paramount importance. In small rotation amplitudes, both curves referring to $z/B = 1$ and 0.5 crusts are relatively further from the ideal dense sand profile and seem to be closer to the response of the poor unimproved profile. This is an indication that the crusts are not equally effective in every range of rotation angle amplitude.

In order to quantify the effectiveness of the crusts with respect to rotation angle, an effectiveness ratio is introduced. The ratio of the distance of each curve corresponding to the cases of soil improvement from the respective curve of the dense sand, to the distance between the original and the ideal soil deposit is considered (schematically illustrated in **Figure 4.29**). In particular this effectiveness ratio is given by the following formula :

$$\boldsymbol{a} = 1 - \frac{\delta w_i - \delta w_{dense}}{\delta w_{loose} - \delta w_{dense}}$$

Through this ratio, the contribution of the upper stiff layer to settlement reduction is evaluated. Consider the two extreme cases : when this ratio equals to 1 the settlement response is identical to the response of the system founded on the ideal dense soil, whereas when this ratio is equal to zero the settlement response of the system is identical to the that on the original poor soil. As a result, when this ratio tends to 1 the improvement is very effective whereas when it tends to zero the effect of the crust is negligible.

In **Figure 4.30** the effectiveness ratio ***a*** is plotted with respect to the rotation amplitude for every case of soil improvement examined for the system with $m_{str} = 35\ kg$ on loose sand $D_r = 45\%$. Apparently, there is a correlation between the performance enhancement and the rotation angle. All cases of soil improvement tend to reach a maximum level of effectiveness for large rotation angles. This figure also verifies that the effectiveness of the crust depends on its depth. The crust with depth equal to foundation width results an effectiveness ratio that tends to 1, implying thus response equivalent to that of the ideal dense profile. For the case of improvement at a depth equal to half the foundation width ($z/B = 0.5$) this ratio is satisfactorily high reaching *80%*. For the remaining case of $z/B = 0.25$, ***a*** tends to a mere *50%* demonstrating inadequate response compared to the previously two cases. It is worth mentioning that all three cases of soil improvement depicted in **Figure XX** reach their maximum level of effectiveness at approximately the same rotation angle ($\vartheta = 0.04\ rad$).

The major finding drawn from this specific figure is that, as opposed to large rotation amplitudes, the effectiveness of the crust is minimized at small rotation levels. The case of depth $z/B = 1$ is representative of this trend, since $\boldsymbol{a}$ decreases from 1 at rotation amplitudes greater than $\vartheta = 0.04\ rad$ down to 0.4 for $\vartheta = 0.0035$ rad. Likewise, in the two other cases z/B =0.5 and z/B = 0.25 for rotation amplitudes $\vartheta = 0.0035$ rad $\boldsymbol{a}$ yields 0.06 and 0.025, respectively.

This response indicates that during small amplitude cyclic loading a shallow soil improvement is not that effective in terms of settlement as in large amplitudes. The explanation is simple. At small rotation amplitudes the foundation maintains full contact with the supporting soil and stresses are distributed to greater extend, affecting thus the underlying deposit of poor soil. As a result, the role of the underlying soil in settlement accumulation is significant. On the other hand, as the system rotates at greater amplitudes, the effective width of the foundation is reduced, resulting to shallower stress bulb. Hence, the contribution of the upper stiffer layer is dominant.

The same trend can be noticed in case of load protocol Type III. In this case, however, the settlement depicted in **Figure XX** refers to the average additional settlement obtained in each rotation level δw_{aver}. The effectiveness ratio $\boldsymbol{a}$ is an increasing function of the rotation angle ϑ in this case as well. There are, however, some distinct differences with the previous case of load protocol Type I. Primarily, the three curves referring to the crusts do not begin from greater effectiveness levels than before. The curve corresponding to the deeper case of improvement $z/B = 1$ demonstrate a starting effectiveness ratio of $a = 0.9$ instead of $a = 0.4$, the respective curve referring to $z/B = 0.5$ begins at $a = 0.8$, while the shallower crust $z/B = 0.25$ begins at $a = 0.1$. This is of course attributed to the fact that this loading protocol begins from rotation amplitudes $\vartheta =$

0.0075 rad, i.e., twice the as much as that of Type I. Moreover, in contrast to Type I loading, in this case the crust of depth *z/B = 0.5* ultimately reaches an effectiveness ratio equal to *1* instead of *0.8*. In summary, it can be inferred that shallow soil improvement can be very effective at large rotation levels, but lacks sufficiency at small rotation angles where the contribution of the poorer underlying soil is significant.

5 CONCLUSIONS

In the framework of this series of experiments, the response of a rigid 1-dof oscillator was examined, when subjected to combined shear and moment loading both monotonically as well as cyclic, slowly induced. The scope of this series was to decode the effect of some of the most influential parameters governing the phenomenon, aiming at the increase of confidence in non linear response of the foundation as a fuse mechanism against strong shaking incident. Moreover, the effectiveness of using a layer of soil improvement was examined, in view of limiting the inaccuracies concerning the soil properties, as well as in view of using a healthier soil crust as a measure of performance enhancement. This investigation was conducted for various cases of crust depth, in order to explore the effect on the performance of the foundation–structure system. The main conclusions drawn from this study can be summarized as follows:

- The factor of safety against vertical loads is a crucial parameter regarding both the monotonic and the cyclic response. For the range of the FSv values examined, the increase in FSv results in a decrease of the ultimate moment capacity and in an increase in the ultimate overturning angle. During cyclic loading, systems with small FSv values exhibit sinking response and develop overstrength in moment capacity. On the other hand, as the FSv increases the response becomes uplift dominated.

- Even though the FSv value plays an important role in the response of the system, it cannot unambiguously define the performance of the system and soil stiffness should also been accounted for.
- As far as load protocol is concerned, it has been shown that it does not affect the ultimate moment developed nor the rotational stiffness, but in terms of settlement, the number of cycles and the displacement amplitude increase the accumulated settlement.
- Shallow soil improvement proved to be an effective way of eliminating uncertainties related to soil properties, as well as a measure of performance enhancement of systems lying on poor soil deposits. Though it was shown that cyclic response leads to approximately the same moment capacity for the systems under consideration with or without a crust, the contribution of the crusts in settlement reduction is significant.
- The effectiveness of the crust proved to be an increasing function of its depth. In both cases examined, the crusts of depth at least equal to half of the foundation width proved to be very effective. On the other hand, the case of the shallower crust examined did not considerably change the performance of the structure.
- It has also been shown that the soil improvement achieves great level of effectiveness as the rotation amplitude increases, whereas its effectiveness is minimized in small rotation amplitudes where the contribution of the poorer soil leads to increase in settlement.

6 REFERENCES

Anastasopoulos I., Gazetas G., Loli M., Apostolou M, N. Gerolymos, (2010a), "Soil Failure can be used for Seismic Protection of Structures", *Bulletin of Earthquake Engineering*, Vol. 8, pp. 309–326.

Faccioli E., Paolucci R., Vivero G., (2001), "Investigation of seismic soil– footing interaction by large scale cyclic tests and analytical models", *Proc. 4th International Conference on Recent Advances in Geotechnical Earthquake Engrng and Soil Dynamics*, Paper no. SPL-5, San Diego, California.

FEMA356 (2000), Prestandard and Commentary for the Seismic Rehabilitation of Buildings. Federal Emergency Management Agency, Washington DC, 2000.

Gazetas G., Apostolou M., Anastasopoulos I. (2003), "Seismic Uplifting of Foundations on Soft Soil, with examples from Adapazari (Izmit 1999, Earthquake)", *BGA Int. Conf. on Found. Innov., Observations, Design & Practice*, Univ. of Dundee, Scotland, September 25, pp.37-50.

Gajan S., Phalen JD., Kutter BL., Hutchinson TC., Martin G., [2005] "Centrifuge modeling of load deformation behavior of rocking shallow foundations." *Soil Dynamics and Earthquake Engineerin*g 25(7-10), 773-783.

Gajan S., Kutter BL. [2008] "Capacity, settlement and energy dissipation of shallow footings subjected to rocking" *Journal of Geotechnical and Geoenvironmetal Engineering*, ASCE 134(8), 1129-1141.

Kawashima K., Nagai T., Sakellaraki D., [2007] "Rocking seismic isolation of bridges supported by spread foundations" *Proc. 2nd Greece–Japan workshop : Seismic Design, Observation, and Retrofit of Foundations*, Tokyo, 3-4 April, pp 254-265.

Kutter BL., Martin G., Hutchinson TC., Harden C., Gajan S., Phalen JD., [2003] *" Status report on study of modeling of nonlinear cyclic load - deformation behavior of shallow foundations. "* In : PEER workshop, University of California, Davis, March 2003.

Martin G.R., and I. P. Lam, (2000), "Earthquake Resistant Design of Foundations : Retrofit of Existing Foundations", *Proc. GeoEng 2000 Conference*, Melbourne.

Paolucci R. [1997] "Simplified evaluation of earthquake induced permanent displacements of shallow foundations." *Journal of Earthquake Engineering* 1, 563-579.

Pecker A., (1998), "Capacity Design Principles for Shallow Foundations in Seismic Areas", *Proc. 11th European Conference on Earthquake Engineering*, A.A. Balkema Publishing.

Paolucci R. Shirato M., Yilmaz MT. [2008] "Seismic behavior of shallow foundations : shaking table experiments vs. numerical modeling." *Earthquake Eng. Struct. Dyn.* 37(4), 577-595.

Pecker A., (2003), "A seismic foundation design process, lessons learned from two major projects : the Vasco de Gama and the Rion Antirion bridges", *ACI International Conference on Seismic Bridge Design and Retrofit*, La Jolla.

Raychowdhury P., Hutchinson T.C. [2010] "Performance of seismically loaded shearwalls on nonlinear shallow foundations*" Int. J. Numer. Anal. Meth. Geomech.*, published online.

6. Figures

Experiment	Date	System properties		Description of Experiment	
		mass (kg)	FS_v	Soil Properties	Lateral Pushover Loading
P2011SQF2 - 001	7/4/2011	100	5	*Dense Sand*	*Monotonic*
P2011SQF2 - 002	11/4/2011	100	5	*Dense Sand*	*Cyclic* TYPE I
P2011SQF2 - 003	12/4/2011	100	5	*Dense Sand*	*Cyclic* TYPE I
P2011SQF2 - 004	13/4/2011	100	2.6	*Sand of Medium Density*	*Monotonic*
P2011SQF2 - 005	14/4/2011	100	5	*Dense Sand*	*Cyclic* TYPE I
P2011SQF2 - 006	15/4/2011	70	7	*Dense Sand*	*Cyclic* TYPE I
P2011SQF2 - 007	18/4/2011	70	7	*Dense Sand*	*Monotonic*
P2011SQF2 -008	19/4/2011	35	14	*Dense Sand*	*Cyclic* TYPE I
P2011SQF2 - 009	20/4/2011	35	14	*Dense Sand*	*Monotonic*
P2011SQF2 - 010	21/4/2011	100	5	*Dense Sand*	*Cyclic* TYPE II
P2011SQF2 - 011	26/4/2011	100	5	*Dense Sand*	*Cyclic* TYPE III
P2011SQF2 - 012	28/4/2011	100	2.6	*Sand of Medium Density*	*Cyclic* TYPE I
P2011SQF2 - 013	29/4/2011	100	3.1	*Improvement on Sand of Medium Density* z/B = 0.5	*Cyclic* TYPE I
P2011SQF2 - 014	2/5/2011	100	4.1	*Improvement on Sand of Medium Density* z/B = 1	*Cyclic* TYPE I
P2011SQF2 - 015	3/5/2011	35	5	*Loose Sand*	*Cyclic* TYPE I
P2011SQF2 - 016	4/5/2011	35	9.8	*Improvement on Loose Sand* z/B = 1	*Cyclic* TYPE I
P2011SQF2 - 017	4/5/2011	35	7.1	*Improvement on Loose Sand* z/B = 0.5	*Cyclic* TYPE I
P2011SQF2 - 018	5/5/2011	35	7.1	*Improvement on Loose Sand* z/B = 0.5	*Cyclic* TYPE III
P2011SQF2 - 019	5/5/2011	35	5	*Loose Sand*	*Cyclic* TYPE III
P2011SQF2 - 020	6/5/2011	35	5.6	*Improvement on Loose Sand* z/B = 0.25	*Cyclic* TYPE I
P2011SQF2 - 021	6/5/2011	35	5.6	*Improvement on Loose Sand* z/B = 0.25	*Cyclic* TYPE III
P2011SQF2 - 022	10/5/2011	35	14	*Dense Sand*	*Cyclic* TYPE III
P2011SQF2 - 023	11/5/2011	35	9.8	*Improvement on Loose Sand* z/B = 1	*Cyclic* TYPE III
P2011SQF2 - 024	12/5/2011	35	9.8	*Improvement on Loose Sand* z/B = 1	*Monotonic*
P2011SQF2 - 025	13/5/2011	35	5	*Loose Sand*	*Monotonic*
P2011SQF2 - 026	16/5/2011	35	7.1	*Improvement on Loose Sand* z/B = 0.5	*Monotonic*
P2011SQF2 - 027	17/5/2011	35	5.6	*Improvement on Loose Sand* z/B = 0.25	*Monotonic*
P2011SQF2 - 028	18/5/2011	100	3.1	*Improvement on Sand of Medium Density* z/B = 0.5	*Cyclic* TYPE III
P2011SQF2 - 029	19/5/2011	100	3.1	*Improvement on Sand of Medium Density* z/B = 0.5	*Monotonic*
P2011SQF2 - 030	20/5/2011	100	5	*Dense Sand*	*Cyclic* TYPE I
P2011SQF2 - 031	23/5/2011	100	2.6	*Sand of Medium Density*	*Cyclic* TYPE III
P2011SQF2 - 032	25/5/2011	100	4.1	*Improvement on Sand of Medium Density* z/B = 1	*Monotonic*
P2011SQF2 - 033	26/5/2011	100	4.1	*Improvement on Sand of Medium Density* z/B = 1	*Cyclic* TYPE III
P2011SQF2 - 034	30/5/2011	35	9.8	*Improvement on Loose Sand* z/B = 1	*Monotonic*

Table 1. Timetable of the full series of experiments conducted.

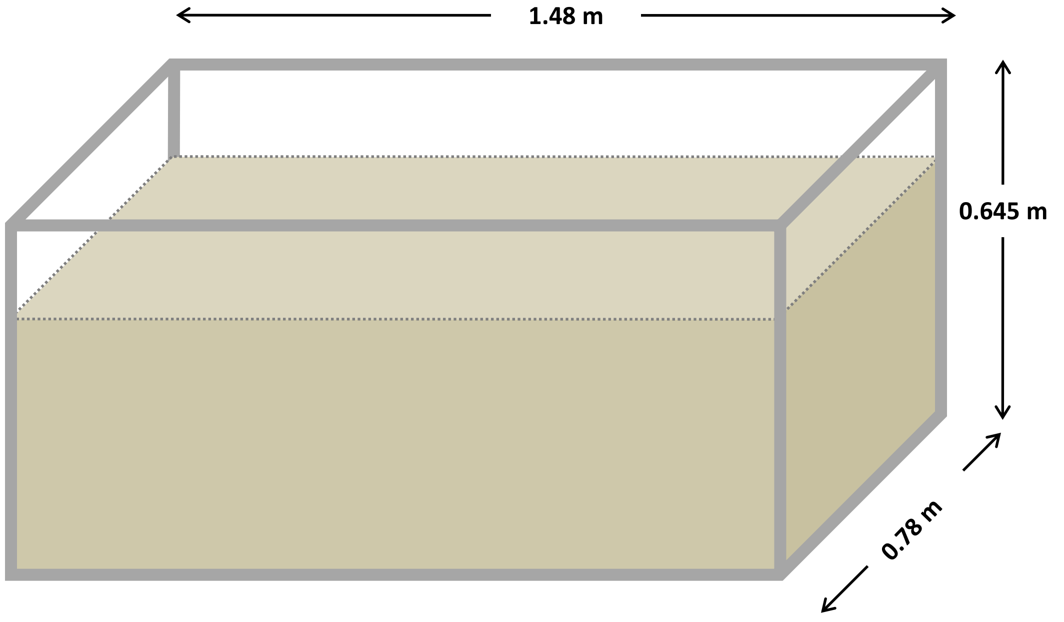

Figure 1. Schematic illustration of the sandbox used in the experimental series.

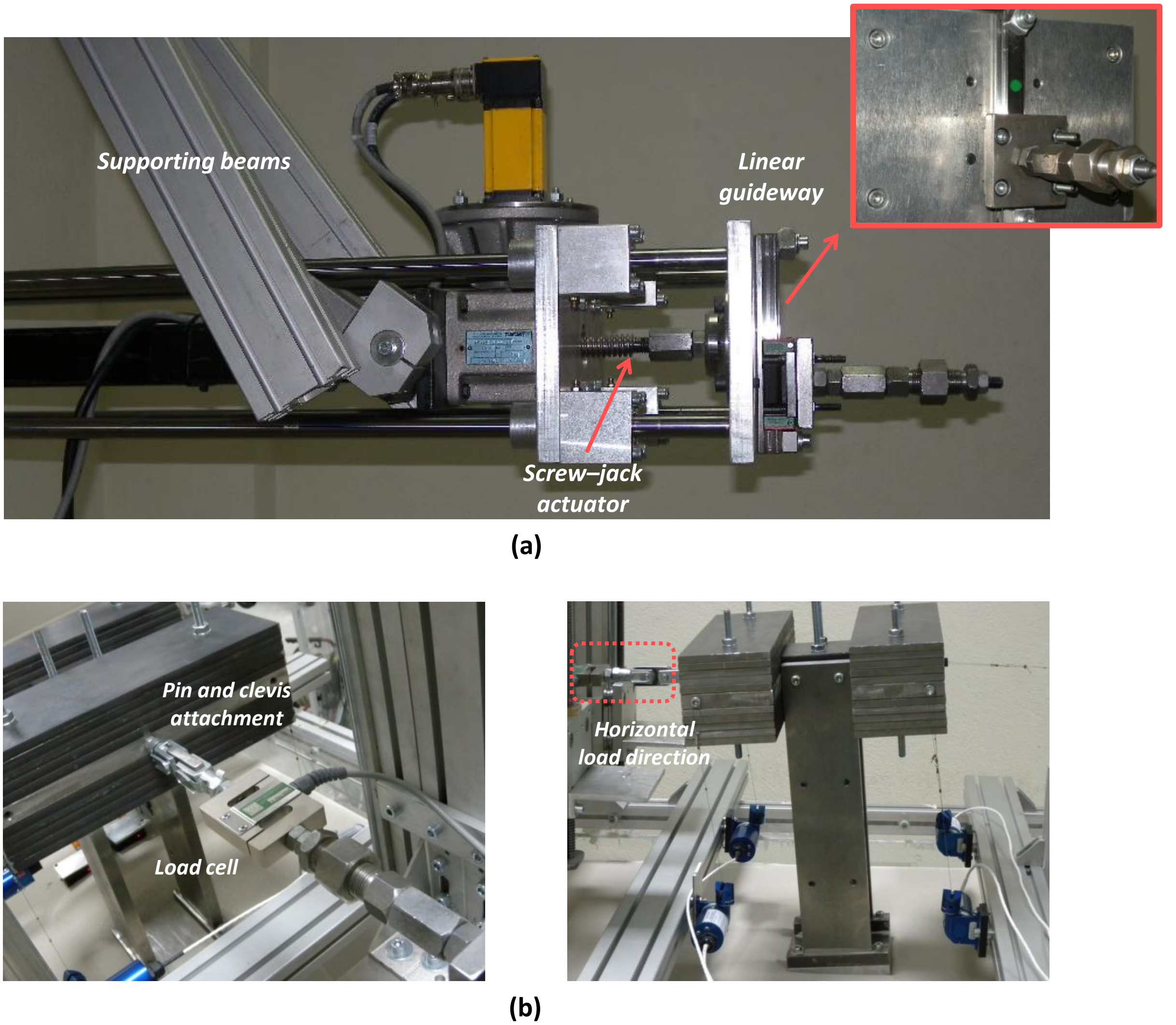

Figure 2. **(a)** Photograph of the pushover apparatus **(b)** device assembly (*linear guideway* & *pin and clevis attachment*) used to achieve horizontal load application at any rotation amplitude.

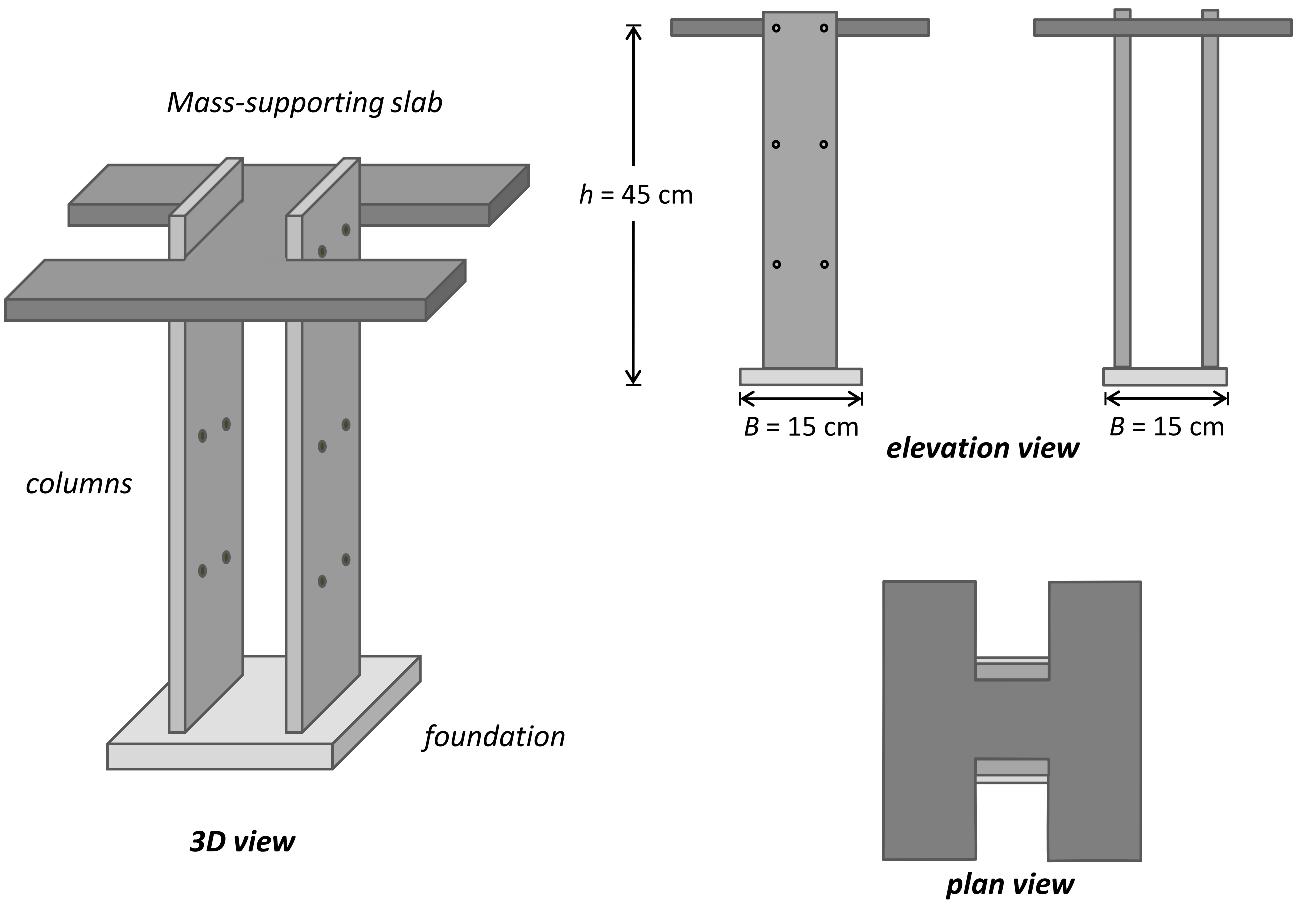

Figure 3. Schematic illustration of the foundation–superstructure model used in the experimental series.

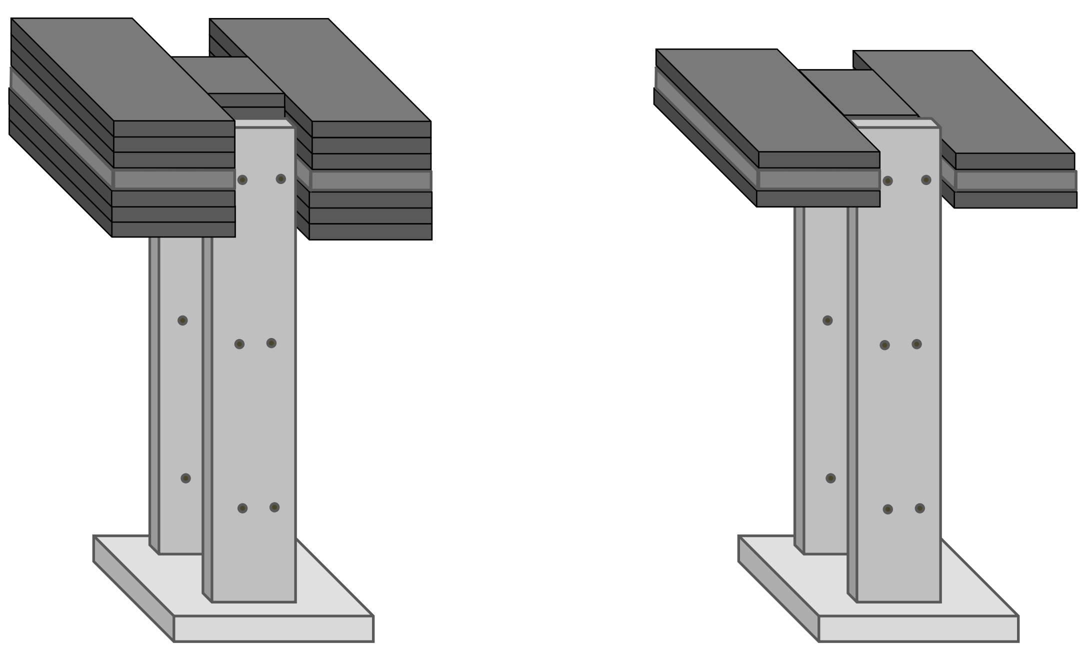

Figure 4. Schematic illustration of systems with different FS_V values achieved through adjusting the superstructure mass.

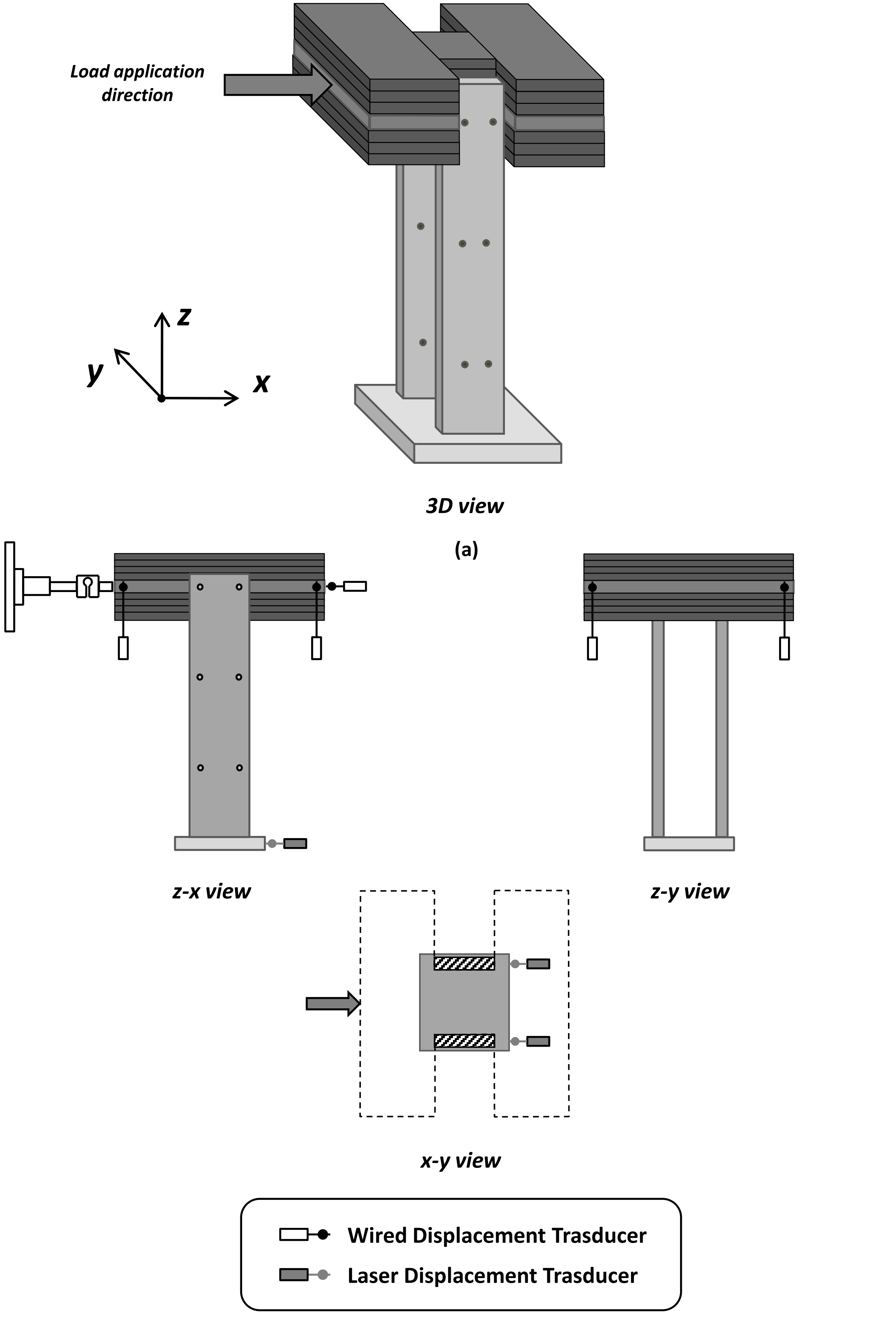

(b)

Figure 5. Instrumentation adopted throughout the whole series of experiments : **(a)** 3d view of the system and the load application direction, **(b)** *z-x*, *z-y* and *x-y* views of the system and configuration of load application direction, wired and laser displacement transducers.

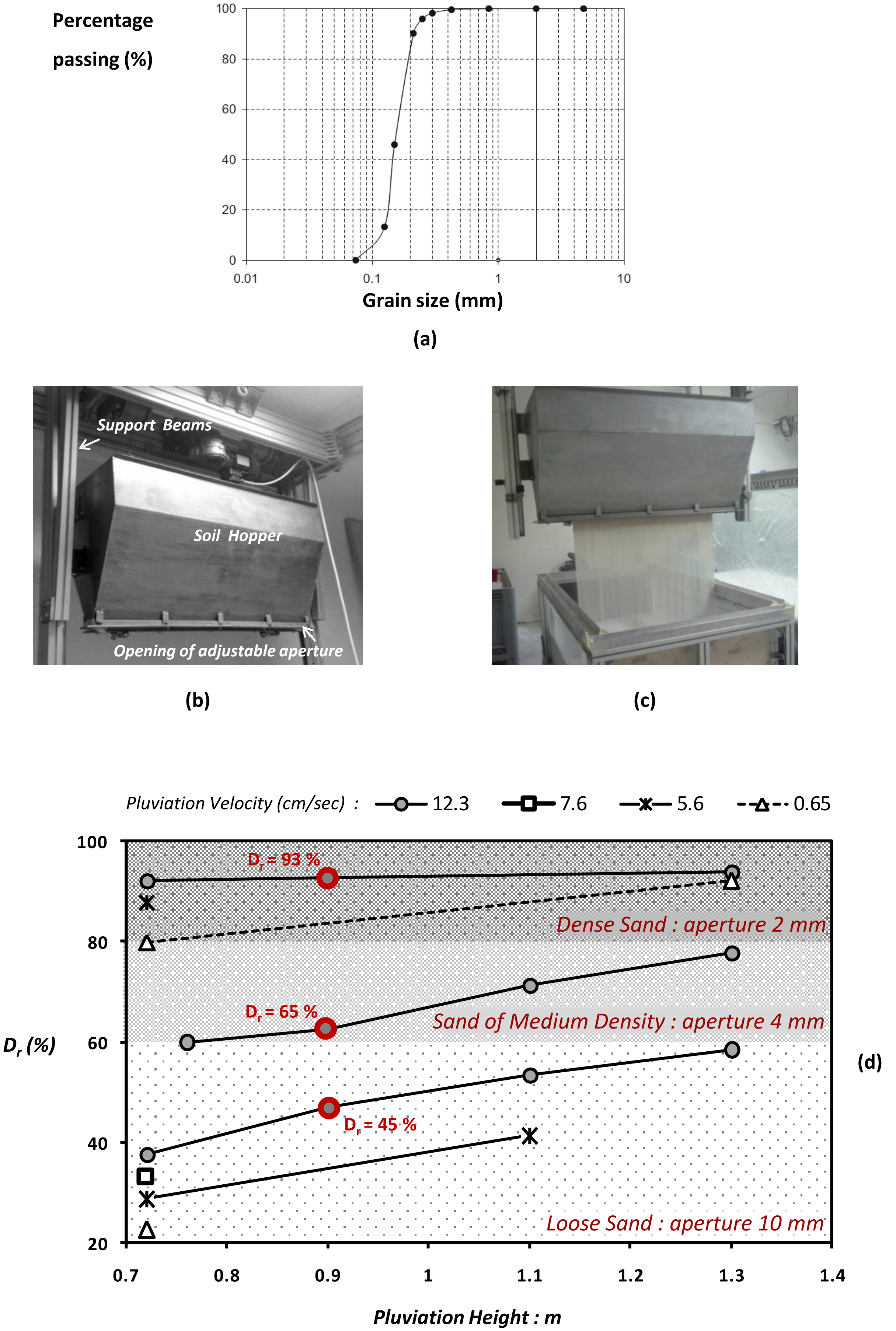

Figure 6. **(a)** Gradation curve of Longstone sand. **(b)** Electronically controlled sand raining system. **(c)** Sand raining in the sandbox. **(d)** Summary of pluviation results : relative density D_r versus pluviation height, raining speed and opening aperture size.

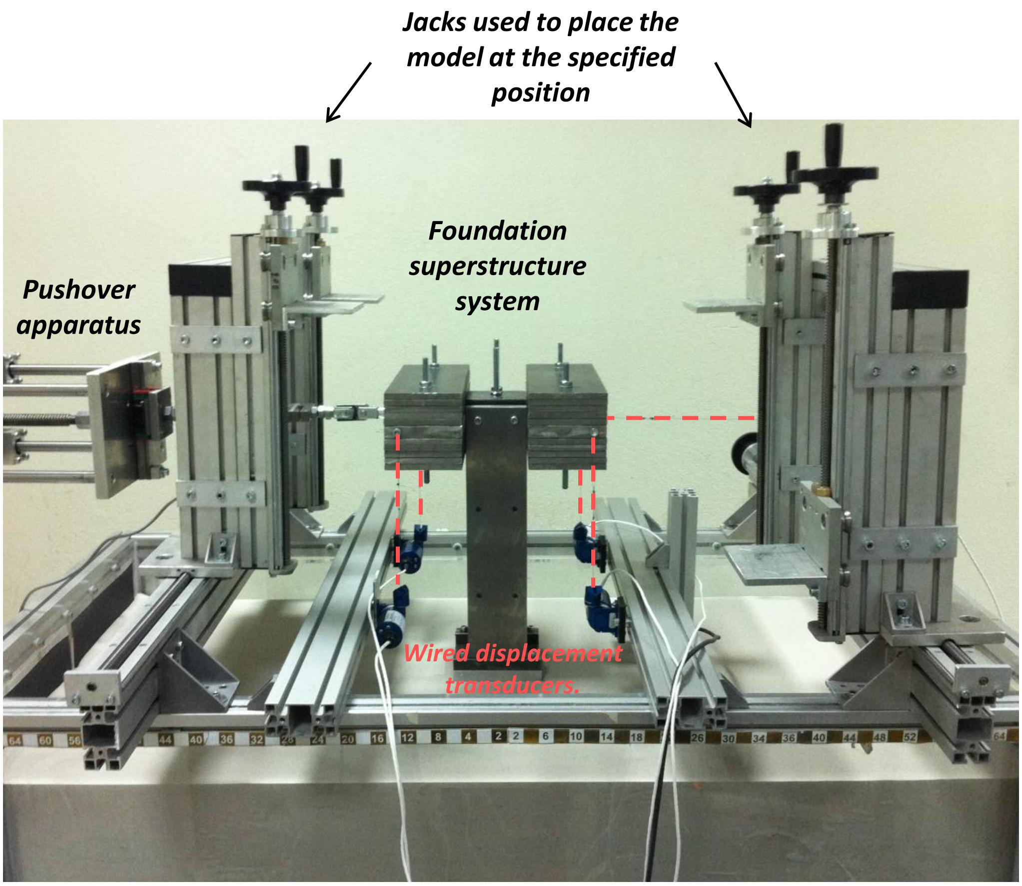

Figure 7. Photograph of a superstructure–foundation system tested placed at the specified position for the horizontal pushover test.

Stuctural Mass	*FS_V*	*Soil Properties*	*Lateral Pushover Loading*	*Experiment*
100 kg	5	Dense Sand	Monotonic	P2011SQF2 - 001
			Cyclic TYPE I	P2011SQF2 - 030
			Cyclic TYPE II	P2011SQF2 - 010
			Cyclic TYPE III	P2011SQF2 - 011
	2.6	Sand of Medium Density	Monotonic	P2011SQF2 - 004
			Cyclic TYPE I	P2011SQF2 - 012
			Cyclic TYPE III	P2011SQF2 - 031
	Soil Improvement on Sand of Medium Density			
	4.1	z/B = 1	Monotonic	P2011SQF2 - 032
			Cyclic TYPE I	P2011SQF2 - 014
			Cyclic TYPE III	P2011SQF2 - 033
	3.1	z/B = 0.5	Monotonic	P2011SQF2 - 029
			Cyclic TYPE I	P2011SQF2 - 013
			Cyclic TYPE III	P2011SQF2 - 028
70 kg	7	Dense Sand	Monotonic	P2011SQF2 - 007
			Cyclic TYPE I	P2011SQF2 - 006
35 kg	14	Dense Sand	Monotonic	P2011SQF2 - 009
			Cyclic TYPE I	P2011SQF2 - 008
			Cyclic TYPE III	P2011SQF2 - 022
	5	Loose Sand	Monotonic	P2011SQF2 - 025
			Cyclic TYPE I	P2011SQF2 - 015
			Cyclic TYPE III	P2011SQF2 - 019
	Soil Improvement on Loose Sand			
	9.8	z/B = 1	Monotonic	P2011SQF2 - 034
			Cyclic TYPE I	P2011SQF2 - 016
			Cyclic TYPE III	P2011SQF2 - 023
	7.1	z/B = 0.5	Monotonic	P2011SQF2 - 026
			Cyclic TYPE I	P2011SQF2 - 017
			Cyclic TYPE III	P2011SQF2 - 018
	5.6	z/B = 0.25	Monotonic	P2011SQF2 - 027
			Cyclic TYPE I	P2011SQF2 - 020
			Cyclic TYPE III	P2011SQF2 - 021

Table 3. Table of experiments with respect to structural systems investigated .

Experimental Project **P2011SQF2**

Experiment **P2011SQF2 - 009**

Date **20/4/2011**

Foundation – Superstructure System

Foundation Width **B = 15 cm**

Aspect Ratio **h/B = 3**

Mass **35 kg**

FS_V **14**

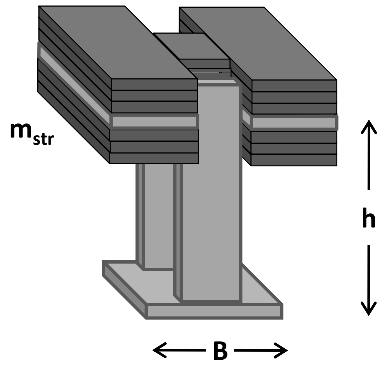

Soil Properties

Homogeneous Soil Deposit

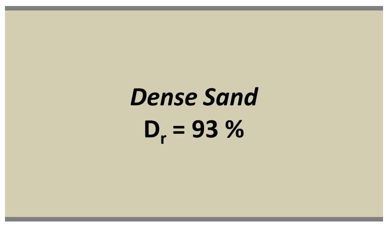

Loading Protocol

Monotonic Loading
(till toppling)

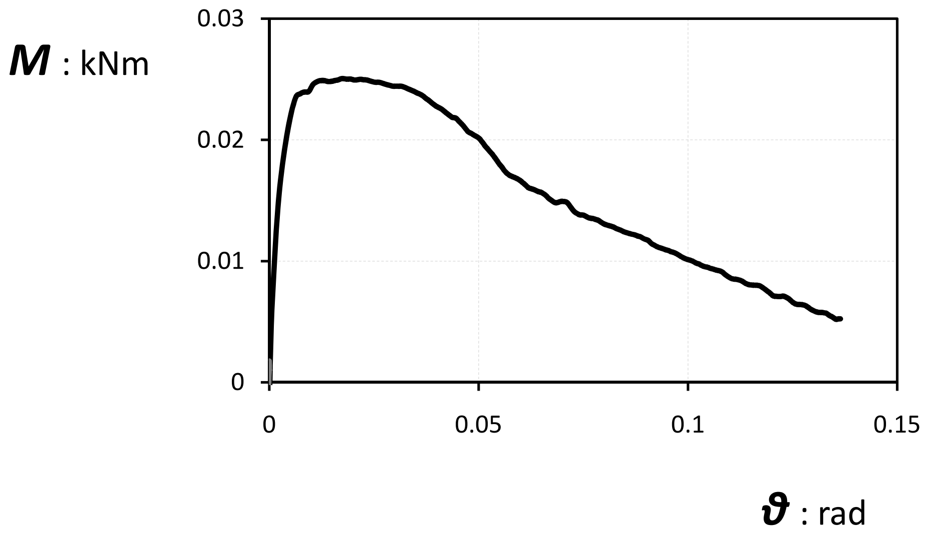

0.03
M : kNm
0.02
0.01
0
0
0.05
0.1
0.15
ϑ : rad

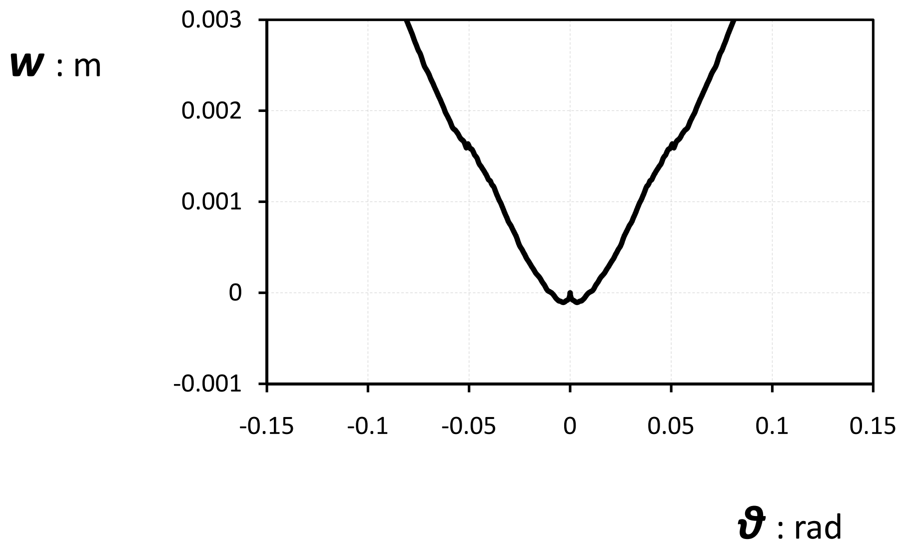

0.003
w : m
0.002
0.001
0
-0.001
-0.15
-0.1
-0.05
0
0.05
0.1
0.15
ϑ : rad

National Technical University of Athens
Laboratory of Soil Mechanics

Experimental Project **P2011SQF2**

Experiment **P2011SQF2 - 008**

Date **19/5/2011**

Foundation – Superstructure System

Foundation Width **B = 15 cm**

Aspect Ratio **h/B = 3**

Mass **35 kg**

FS_V **14**

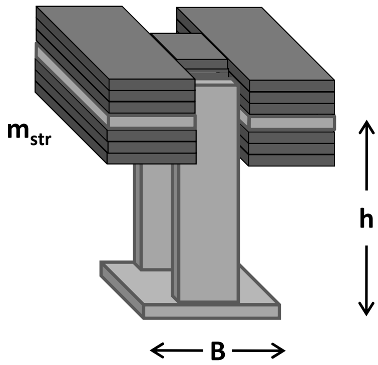

Soil Properties

Homogeneous Soil Deposit

Dense Sand
D_r = 93 %

Loading Protocol

Cyclic Loading
TYPE I

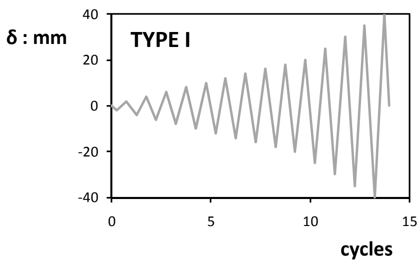

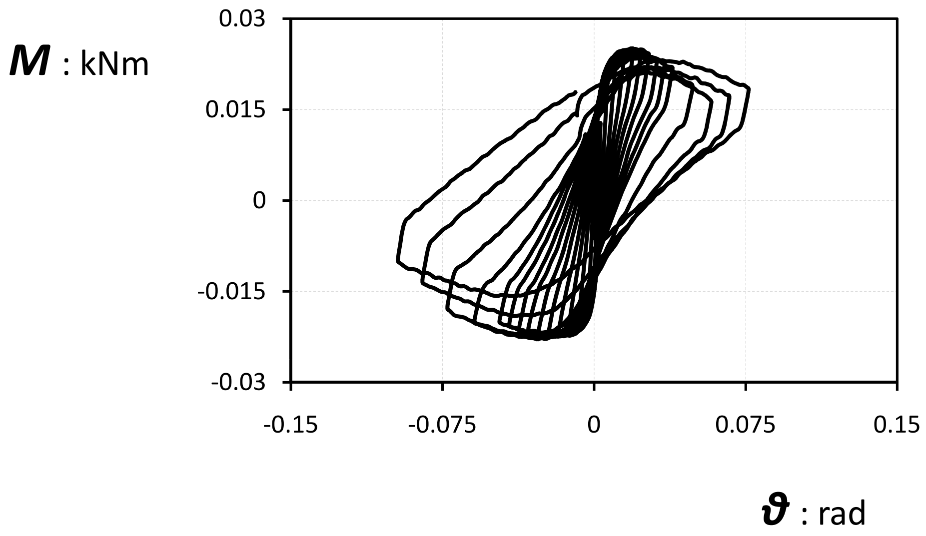

M : kNm
0.03
0.015
0
-0.015
-0.03
-0.15
-0.075
0
0.075
0.15
ϑ : rad

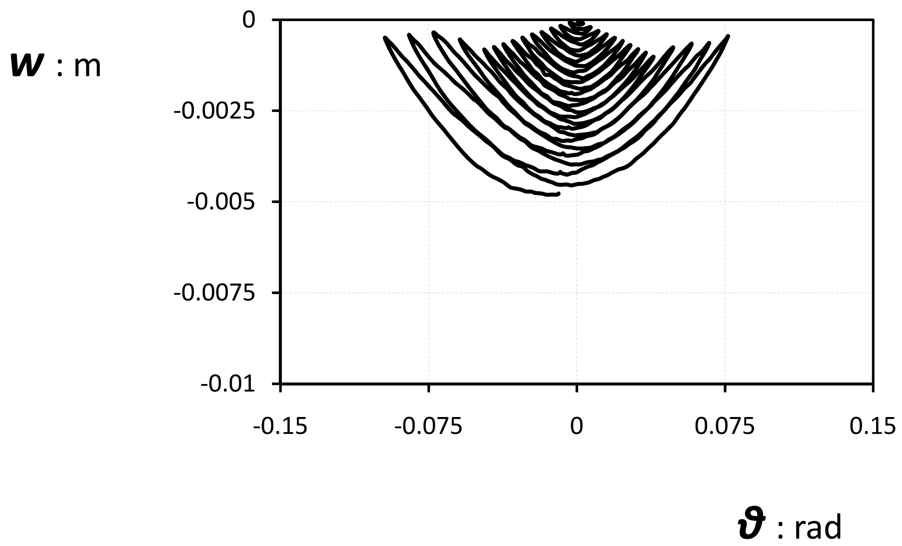

w : m
0
-0.0025
-0.005
-0.0075
-0.01
-0.15
-0.075
0
0.075
0.15
ϑ : rad

Experimental Project **P2011SQF2**

Experiment **P2011SQF2 - 022**

Date **10/5/2011**

Foundation – Superstructure System

Foundation Width **B = 15 cm**

Aspect Ratio **h/B = 3**

Mass **35 kg**

FS_V **14**

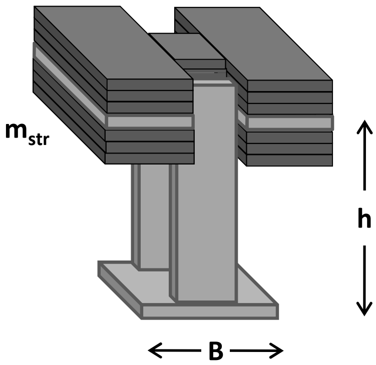

Soil Properties

Homogeneous
Soil Deposit

Dense Sand
D_r = 93 %

Loading Protocol

Cyclic Loading
TYPE III

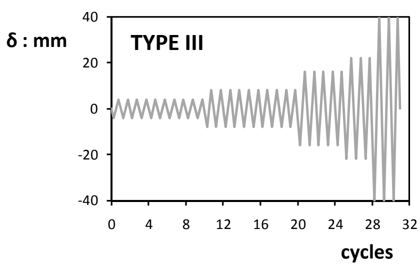

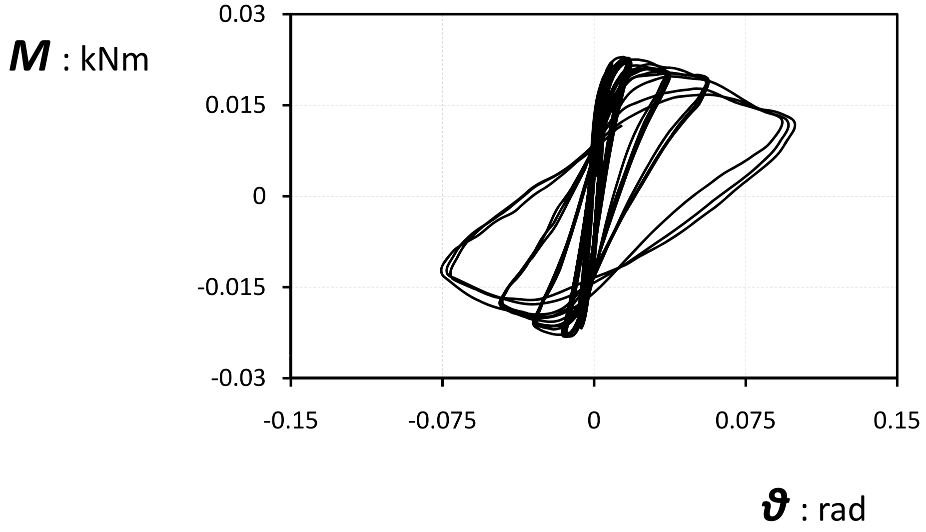
M : kNm
0.03
0.015
0
-0.015
-0.03
-0.15
-0.075
0
0.075
0.15
ϑ : rad

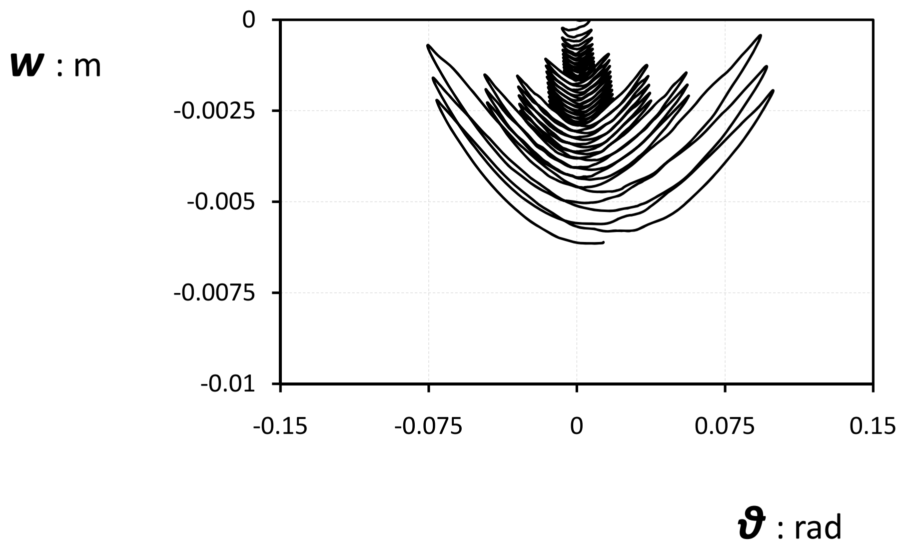
w : m
0
-0.0025
-0.005
-0.0075
-0.01
-0.15
-0.075
0
0.075
0.15
ϑ : rad

National Technical University of Athens
Laboratory of Soil Mechanics

Experimental Project **P2011SQF2**

Experiment **P2011SQF2 - 025**

Date **13/5/2011**

Foundation – Superstructure System

Foundation Width **B = 15 cm**

Aspect Ratio **h/B = 3**

Mass **35 kg**

FS_V **5**

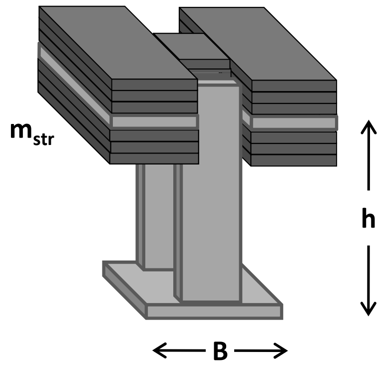

Soil Properties

Homogeneous Soil Deposit

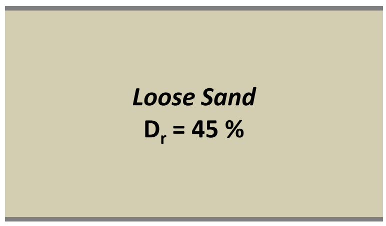

Loading Protocol

Monotonic Loading (till toppling)

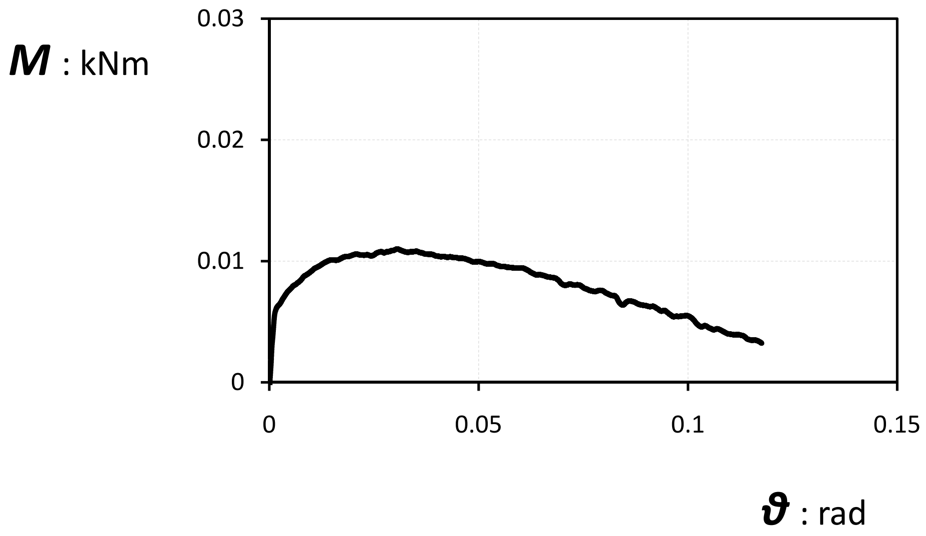

M : kNm
0.03
0.02
0.01
0
0
0.05
0.1
0.15
ϑ : rad

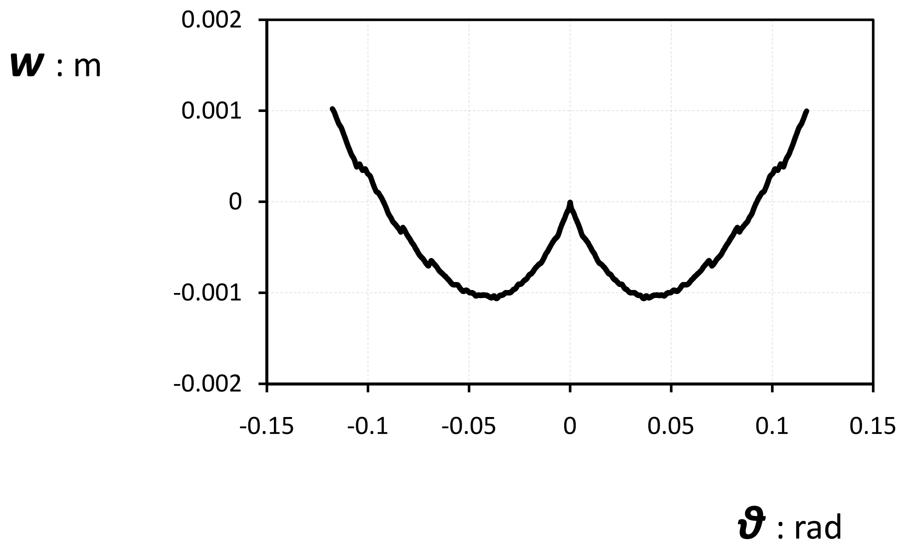

w : m
0.002
0.001
0
-0.001
-0.002
-0.15
-0.1
-0.05
0
0.05
0.1
0.15
ϑ : rad

National Technical University of Athens
Laboratory of Soil Mechanics

Experimental Project **P2011SQF2**

Experiment **P2011SQF2 - 015**

Date **3/5/2011**

Foundation – Superstructure System

Foundation Width **B = 15 cm**

Aspect Ratio **h/B = 3**

Mass **35 kg**

FS_V **5**

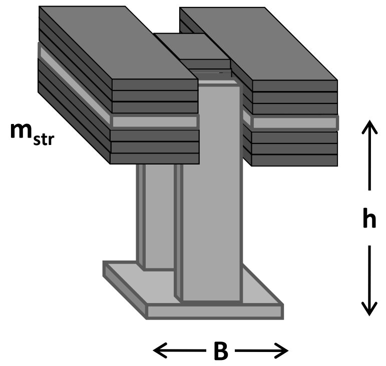

Soil Properties

Homogeneous Soil Deposit

Loose Sand
D_r = 45 %

Loading Protocol

Cyclic Loading
TYPE I

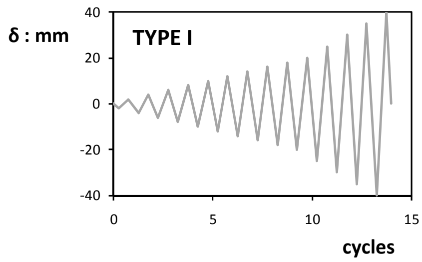

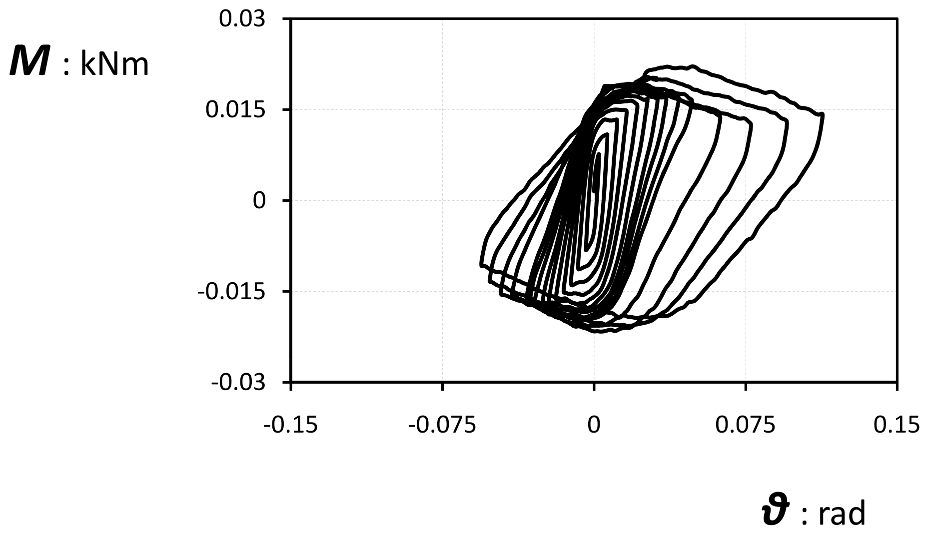

M : kNm
0.03
0.015
0
-0.015
-0.03
-0.15
-0.075
0
0.075
0.15
ϑ : rad

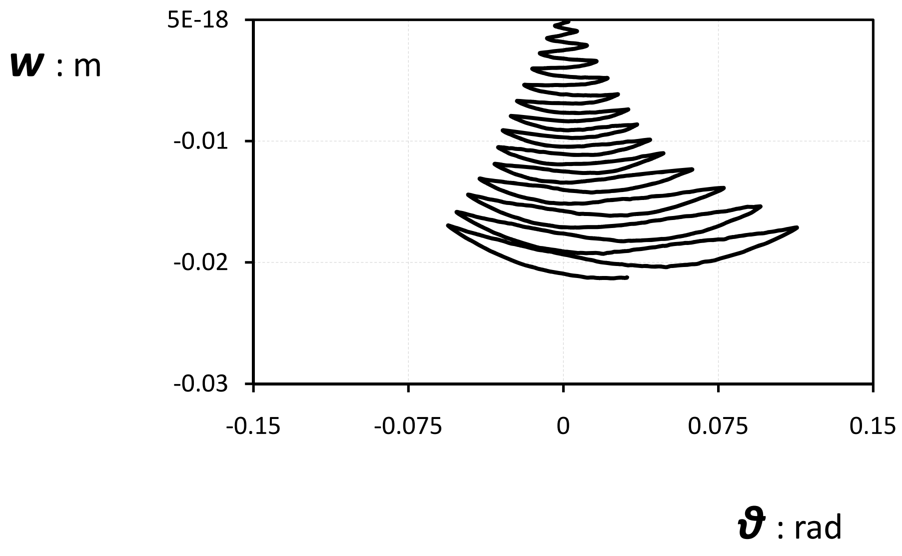

w : m
5E-18
-0.01
-0.02
-0.03
-0.15
-0.075
0
0.075
0.15
ϑ : rad

National Technical University of Athens
Laboratory of Soil Mechanics

Experimental Project **P2011SQF2**

Experiment **P2011SQF2 - 019**

Date **5/5/2011**

Foundation – Superstructure System

Foundation Width **B = 15 cm**

Aspect Ratio **h/B = 3**

Mass **35 kg**

FS_V **5**

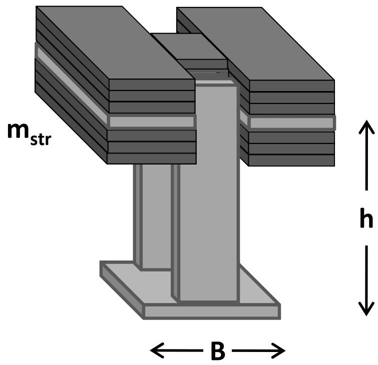

Soil Properties

Homogeneous
Soil Deposit

Loose Sand
D_r = 45 %

Loading Protocol

Cyclic Loading
TYPE III

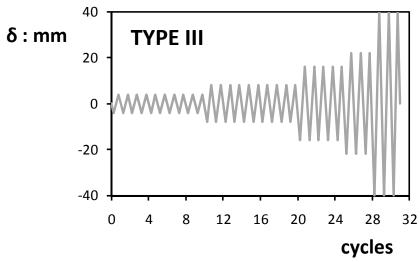

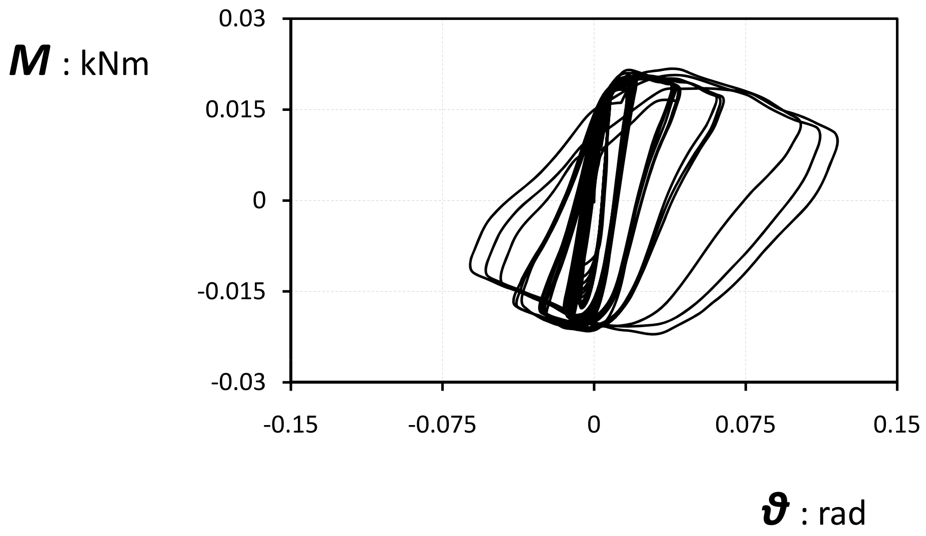
M : kNm
0.03
0.015
0
-0.015
-0.03
-0.15
-0.075
0
0.075
0.15
ϑ : rad

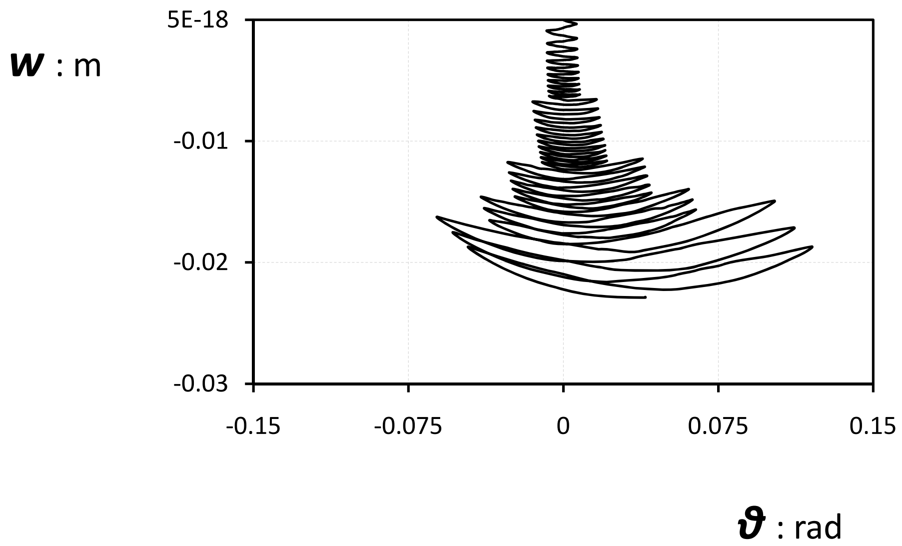
w : m
5E-18
-0.01
-0.02
-0.03
-0.15
-0.075
0
0.075
0.15
ϑ : rad

National Technical University of Athens
Laboratory of Soil Mechanics

Experimental Project **P2011SQF2**

Experiment **P2011SQF2 - 034**

Date **30/5/2011**

Foundation – Superstructure System

Foundation Width **B = 15 cm**

Aspect Ratio **h/B = 3**

Mass **35 kg**

FS_V **9.8**

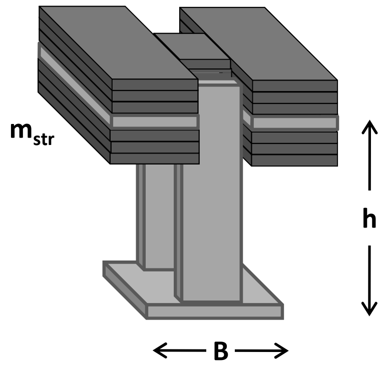

Soil Properties

Two–layered
Soil Deposit
z/B = 1

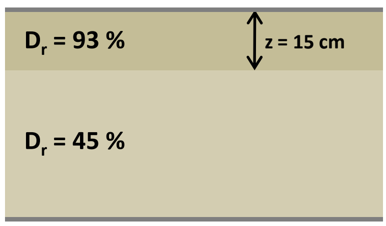

Loading Protocol

Monotonic Loading
(till toppling)

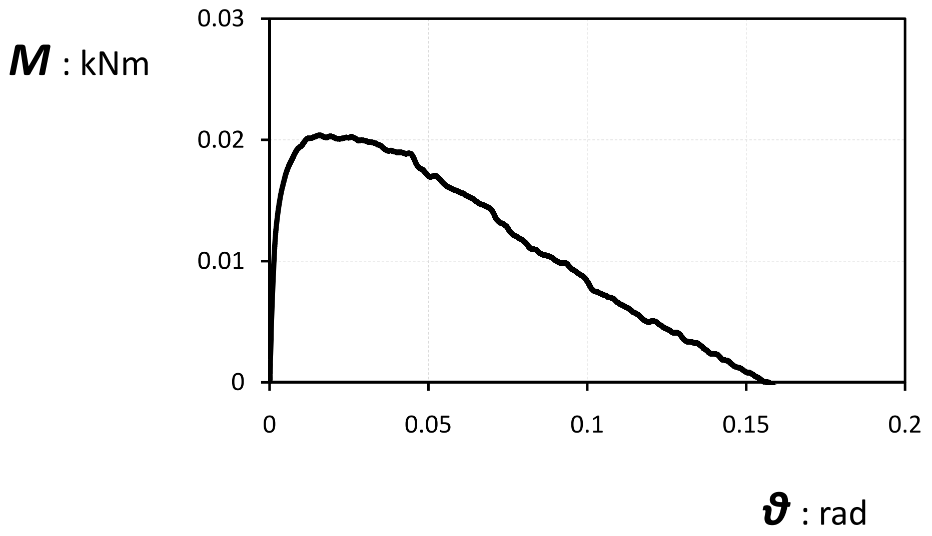
M : kNm
0.03
0.02
0.01
0
0
0.05
0.1
0.15
0.2
ϑ : rad

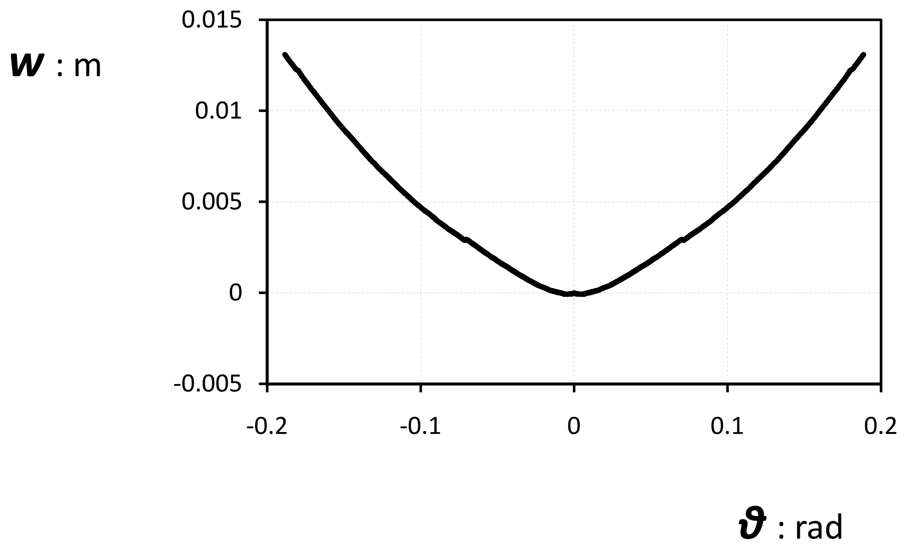
w : m
0.015
0.01
0.005
0
-0.005
-0.2
-0.1
0
0.1
0.2
ϑ : rad

National Technical University of Athens
Laboratory of Soil Mechanics

Experimental Project **P2011SQF2**

Experiment **P2011SQF2 - 016**

Date **4/5/2011**

Foundation – Superstructure System

Foundation Width **B = 15 cm**

Aspect Ratio **h/B = 3**

Mass **35 kg**

FS_V **9.8**

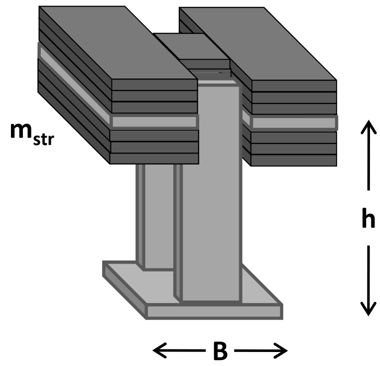

Soil Properties

Two–layered
Soil Deposit
z/B = 1

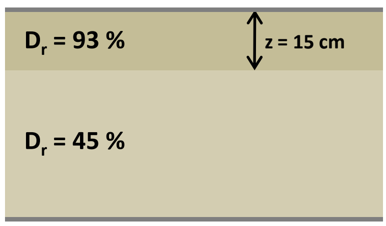

Loading Protocol

Cyclic Loading
TYPE I

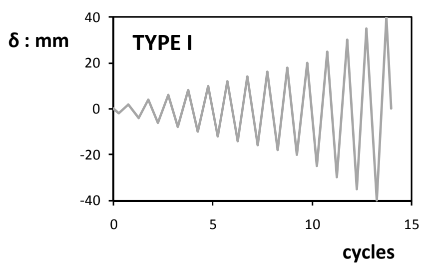

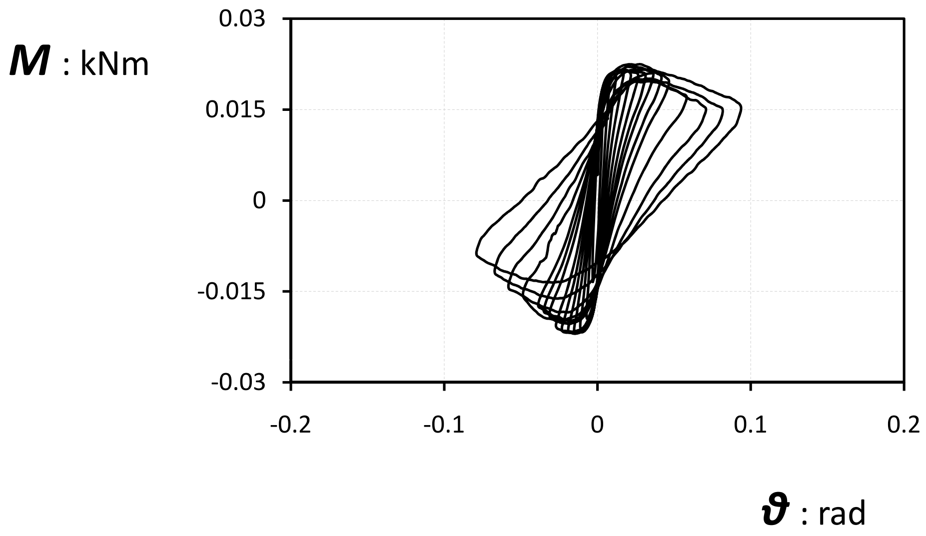

M : kNm
0.03
0.015
0
-0.015
-0.03
-0.2
-0.1
0
0.1
0.2
ϑ : rad

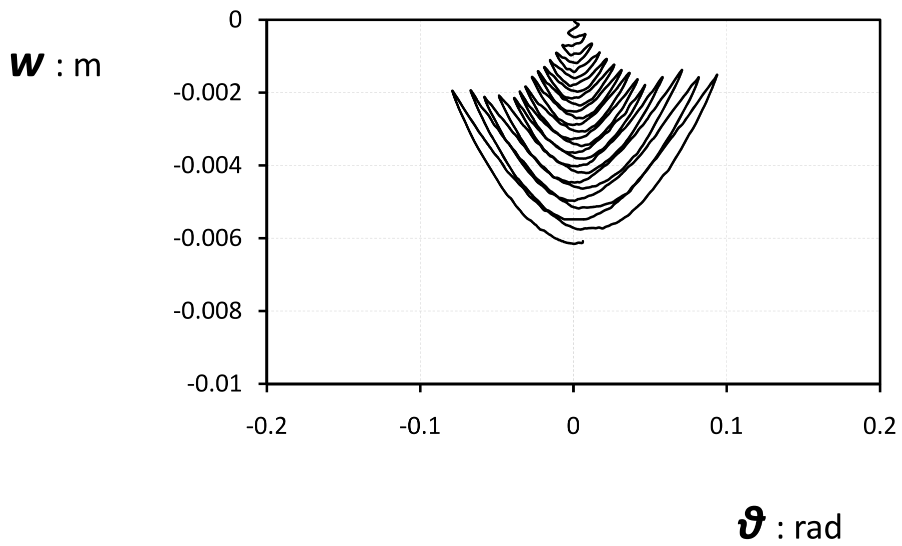

w : m
0
-0.002
-0.004
-0.006
-0.008
-0.01
-0.2
-0.1
0
0.1
0.2
ϑ : rad

National Technical University of Athens

Laboratory of Soil Mechanics

Experimental Project **P2011SQF2**

Experiment **P2011SQF2 - 023**

Date **11/5/2011**

Foundation – Superstructure System

Foundation Width **B = 15 cm**

Aspect Ratio **h/B = 3**

Mass **35 kg**

FS_V **9.8**

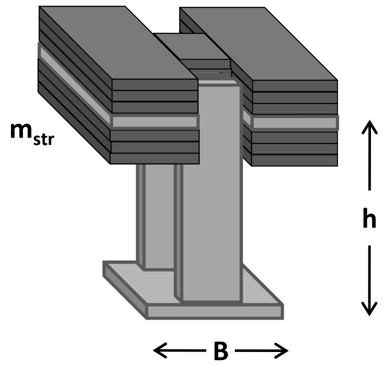

Soil Properties

Two–layered
Soil Deposit
z/B = 1

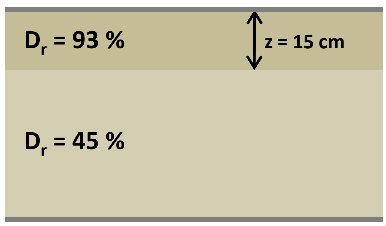

Loading Protocol

Cyclic Loading
TYPE III

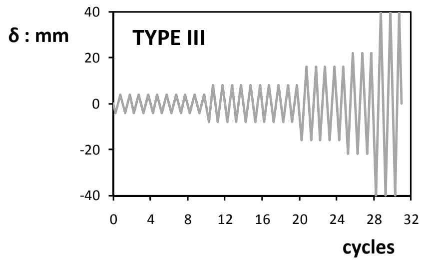

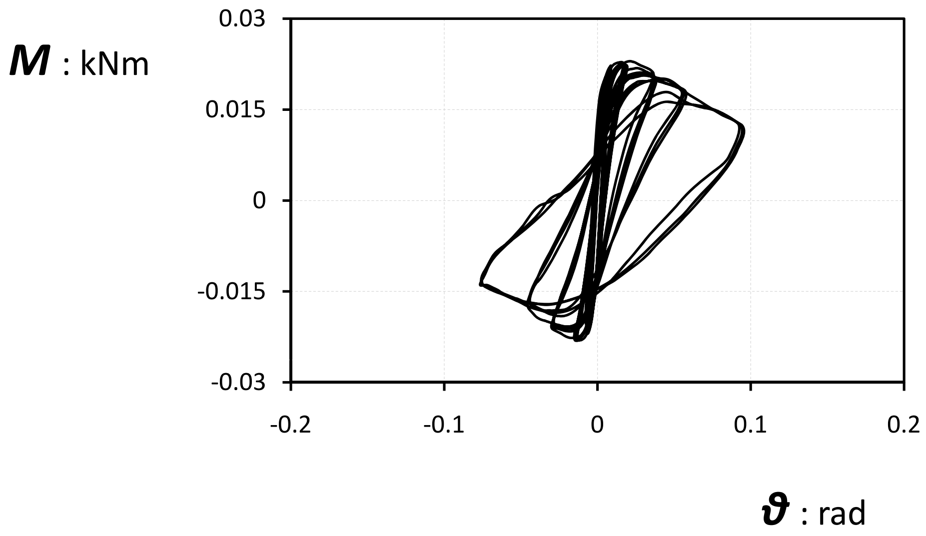
M : kNm
0.03
0.015
0
-0.015
-0.03
-0.2
-0.1
0
0.1
0.2
ϑ : rad

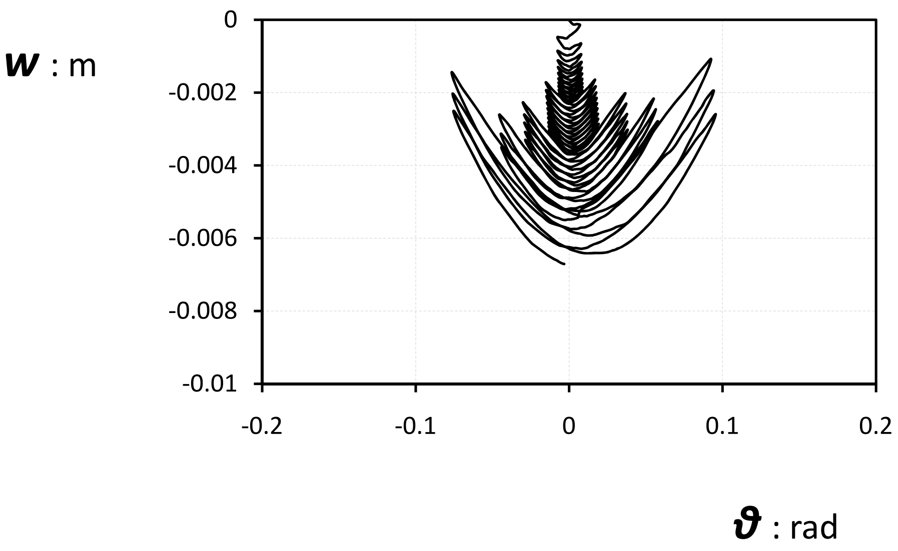
w : m
0
-0.002
-0.004
-0.006
-0.008
-0.01
-0.2
-0.1
0
0.1
0.2
ϑ : rad

National Technical University of Athens
Laboratory of Soil Mechanics

Experimental Project **P2011SQF2**

Experiment **P2011SQF2 - 026**

Date **16/5/2011**

Foundation – Superstructure System

Foundation Width **B = 15 cm**

Aspect Ratio **h/B = 3**

Mass **35 kg**

FS_V **7.1**

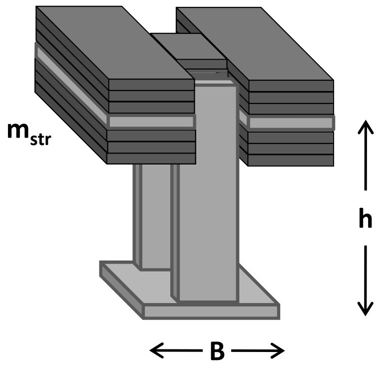

Soil Properties

Two–layered
Soil Deposit
z/B = 0.5

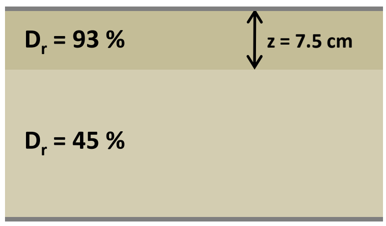

Loading Protocol

Monotonic Loading
(till toppling)

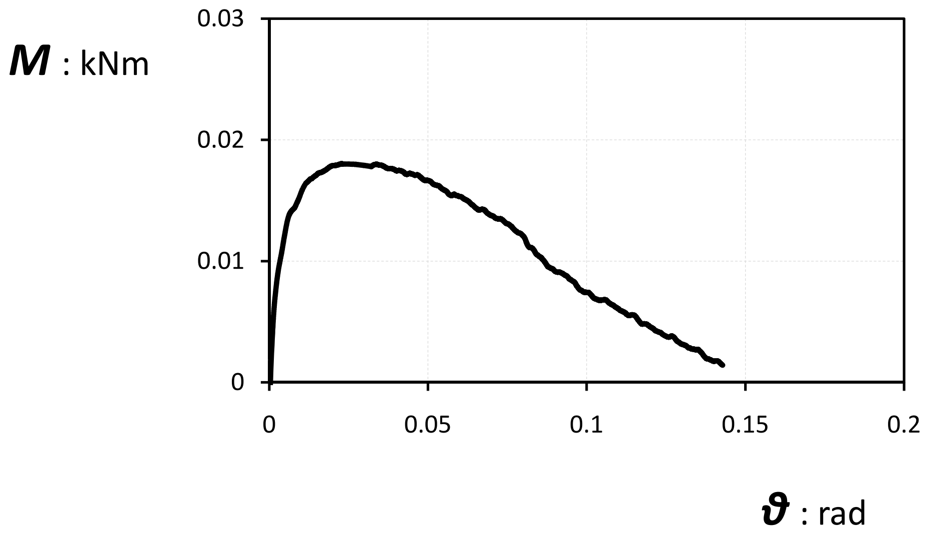

M : kNm
0.03
0.02
0.01
0
0
0.05
0.1
0.15
0.2
ϑ : rad

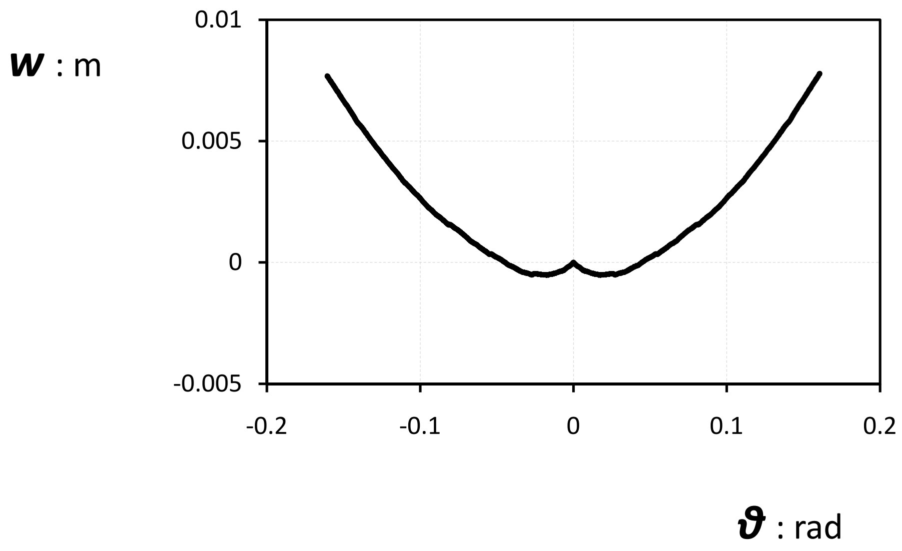

w : m
0.01
0.005
0
-0.005
-0.2
-0.1
0
0.1
0.2
ϑ : rad

National Technical University of Athens
Laboratory of Soil Mechanics

Experimental Project **P2011SQF2**

Experiment **P2011SQF2 - 017**

Date **4/5/2011**

Foundation – Superstructure System

Foundation Width **B = 15 cm**

Aspect Ratio **h/B = 3**

Mass **35 kg**

FS_V **7.1**

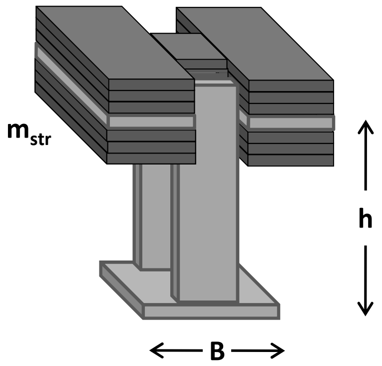

Soil Properties

Two–layered
Soil Deposit
z/B = 0.5

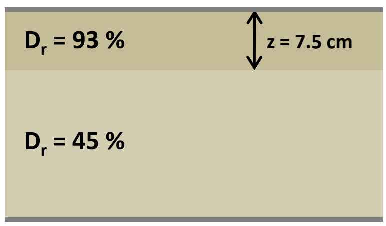

Loading Protocol

Cyclic Loading
TYPE I

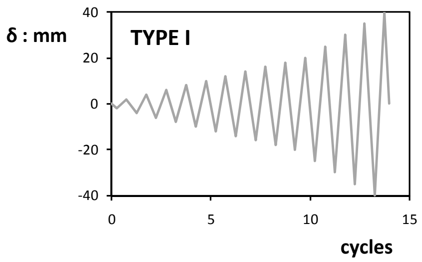

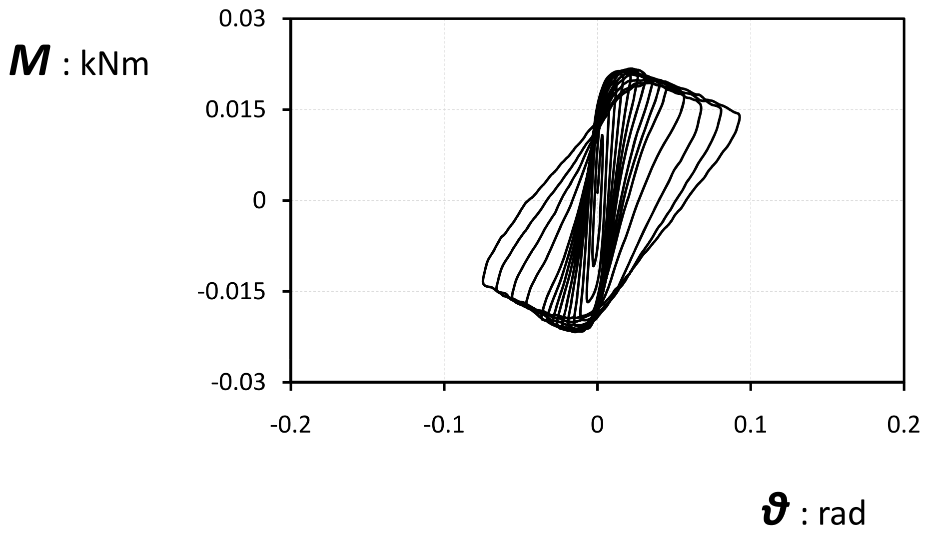
M : kNm
0.03
0.015
0
-0.015
-0.03
-0.2
-0.1
0
0.1
0.2
ϑ : rad

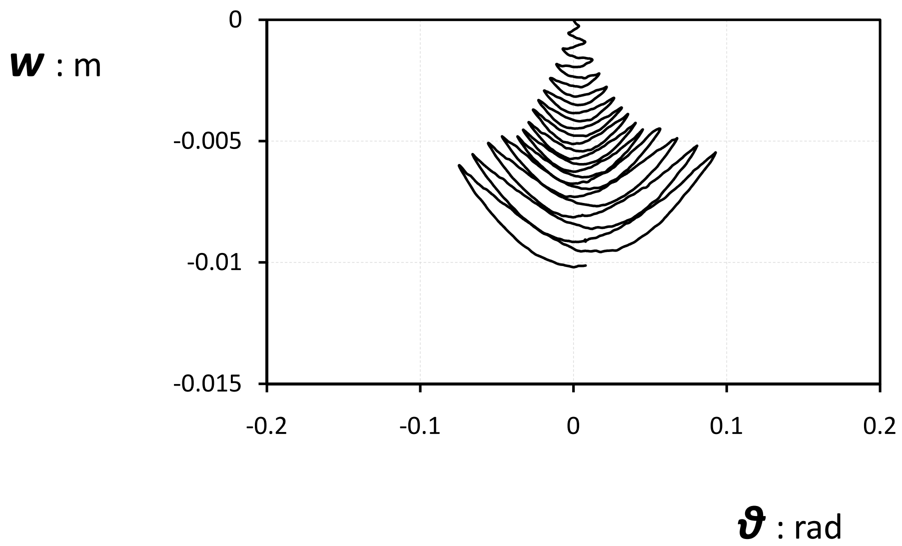
w : m
0
-0.005
-0.01
-0.015
-0.2
-0.1
0
0.1
0.2
ϑ : rad

National Technical University of Athens
Laboratory of Soil Mechanics

Experimental Project **P2011SQF2**

Experiment **P2011SQF2 - 018**

Date **5/5/2011**

Foundation – Superstructure System

Foundation Width **B = 15 cm**

Aspect Ratio **h/B = 3**

Mass **35 kg**

FS_V **7.1**

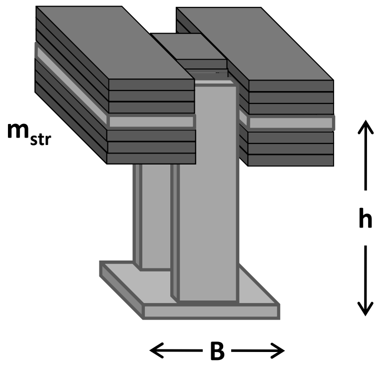

Soil Properties

Two–layered
Soil Deposit
z/B = 0.5

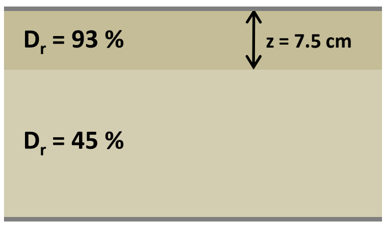

Loading Protocol

Cyclic Loading
TYPE III

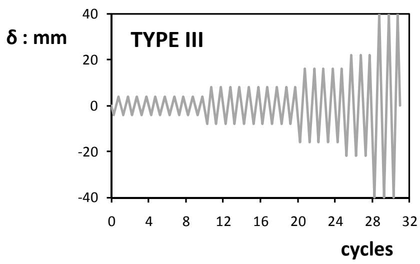

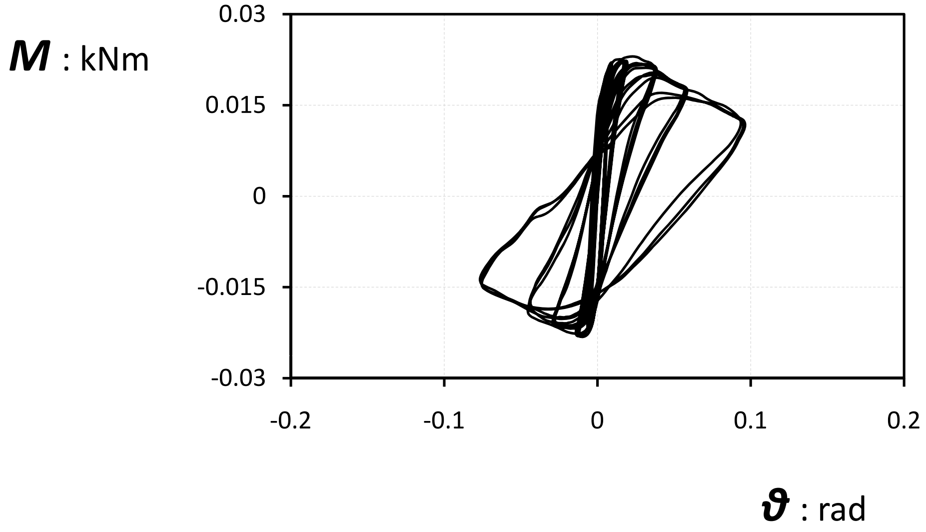

M : kNm
0.03
0.015
0
-0.015
-0.03
-0.2
-0.1
0
0.1
0.2
ϑ : rad

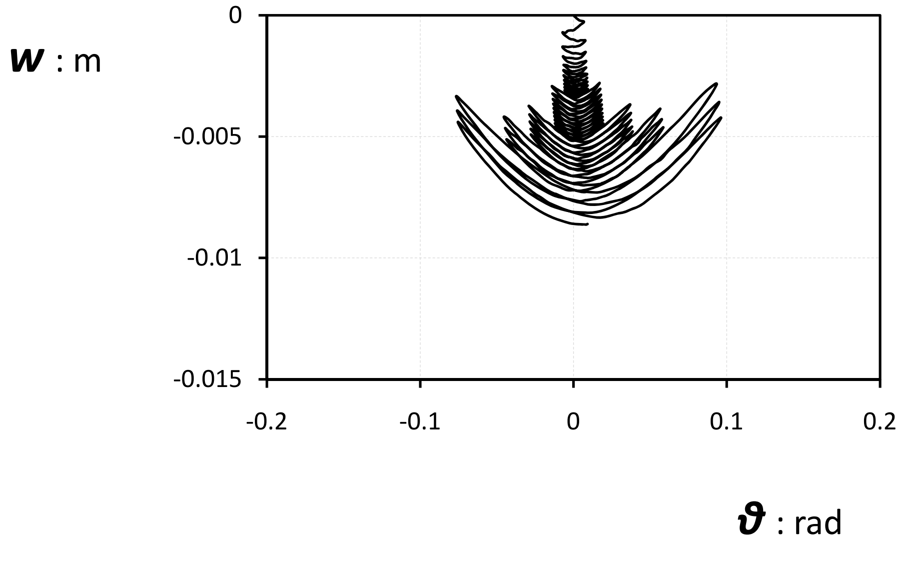

w : m
0
-0.005
-0.01
-0.015
-0.2
-0.1
0
0.1
0.2
ϑ : rad

National Technical University of Athens
Laboratory of Soil Mechanics

Experimental Project **P2011SQF2**

Experiment **P2011SQF2 - 027**

Date **17/5/2011**

Foundation – Superstructure System

Foundation Width **B = 15 cm**

Aspect Ratio **h/B = 3**

Mass **35 kg**

FS_V **5.6**

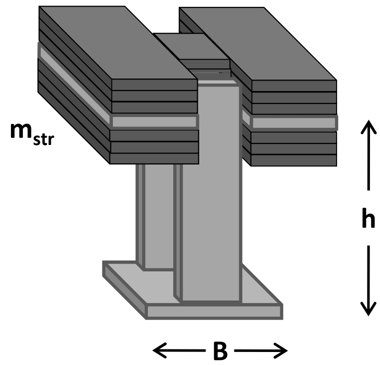

Soil Properties

Two–layered
Soil Deposit
z/B = 0.25

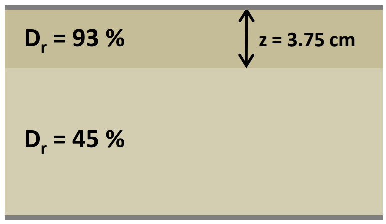

Loading Protocol

Monotonic Loading
(till toppling)

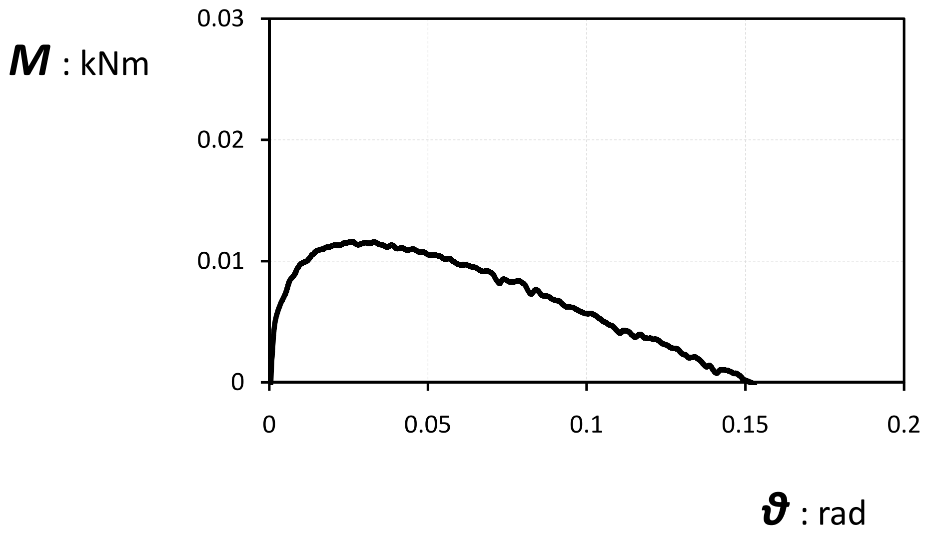

0.03
M : kNm
0.02
0.01
0
0
0.05
0.1
0.15
0.2
ϑ : rad

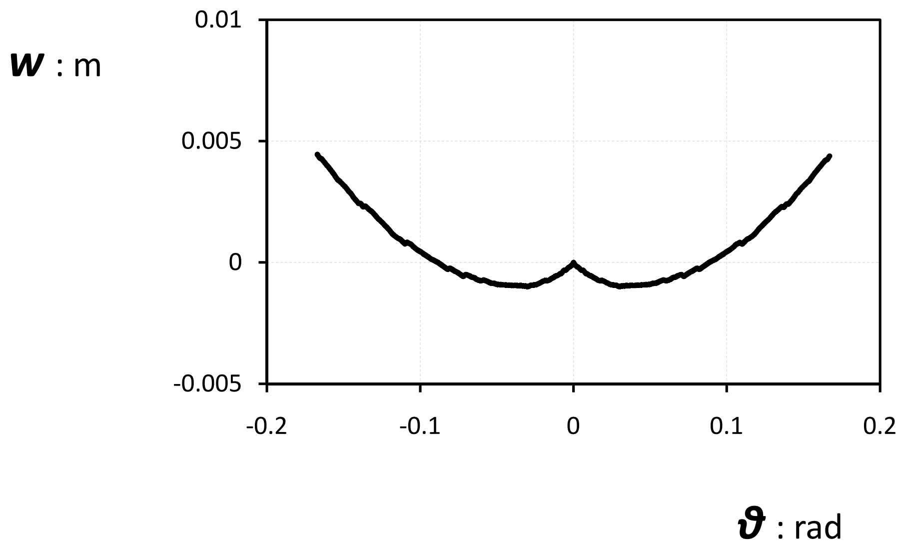

0.01
w : m
0.005
0
-0.005
-0.2
-0.1
0
0.1
0.2
ϑ : rad

National Technical University of Athens
Laboratory of Soil Mechanics

Experimental Project **P2011SQF2**

Experiment **P2011SQF2 - 020**

Date **6/5/2011**

Foundation – Superstructure System

Foundation Width **B = 15 cm**

Aspect Ratio **h/B = 3**

Mass **35 kg**

FS_V **5.6**

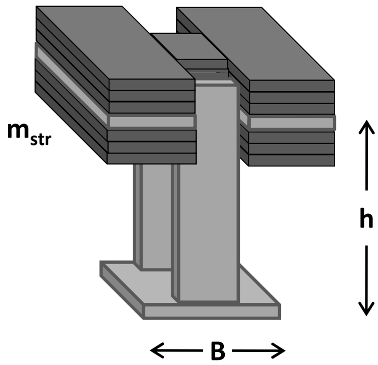

Soil Properties

Two–layered
Soil Deposit
z/B = 0.25

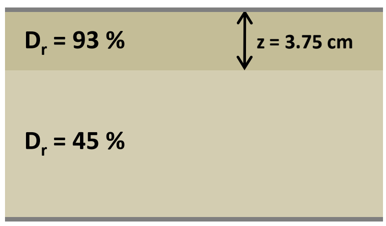

Loading Protocol

Cyclic Loading
TYPE I

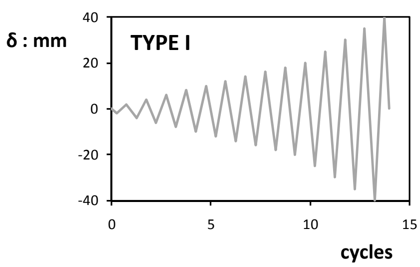

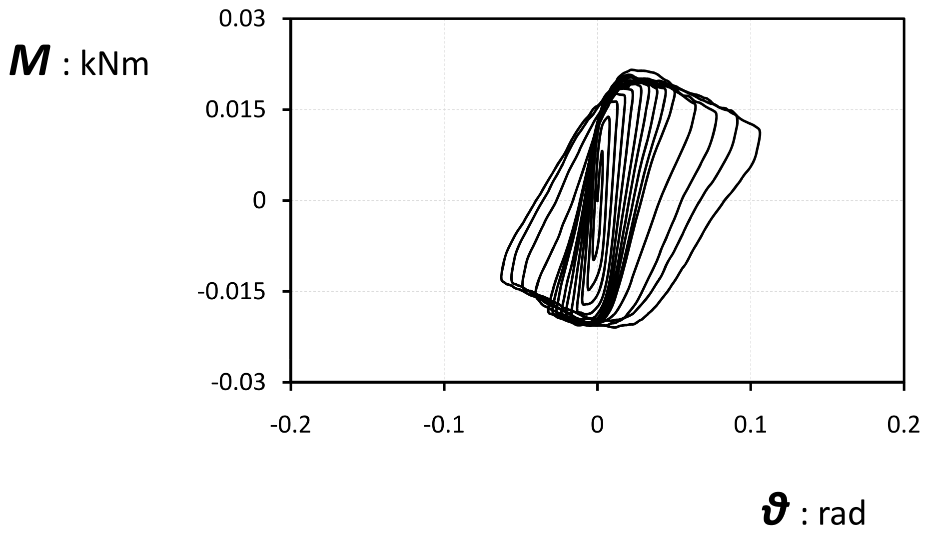

M : kNm
0.03
0.015
0
-0.015
-0.03
-0.2
-0.1
0
0.1
0.2
ϑ : rad

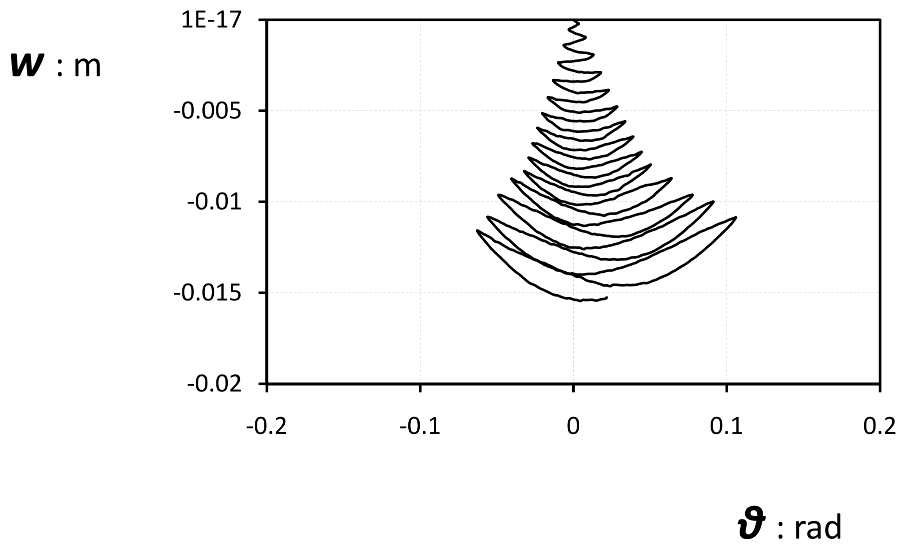

w : m
1E-17
-0.005
-0.01
-0.015
-0.02
-0.2
-0.1
0
0.1
0.2
ϑ : rad

Experimental Project	**P2011SQF2**
Experiment	**P2011SQF2 - 021**
Date	**6/5/2011**

Foundation – Superstructure System

Foundation Width	**B = 15 cm**
Aspect Ratio	**h/B = 3**
Mass	**35 kg**
FS_V	**5.6**

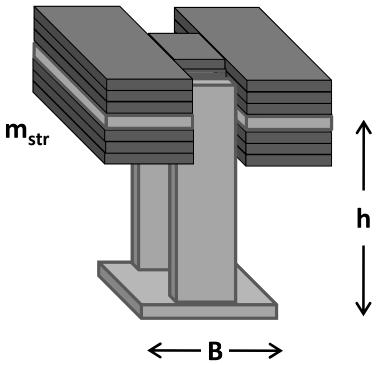

Soil Properties

Two–layered
Soil Deposit
z/B = 0.25

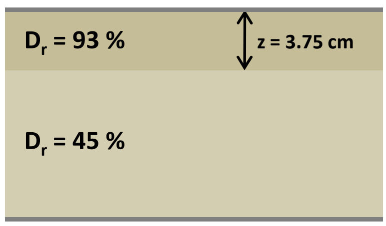

Loading Protocol

Cyclic Loading
TYPE III

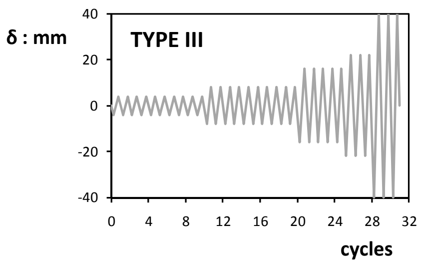

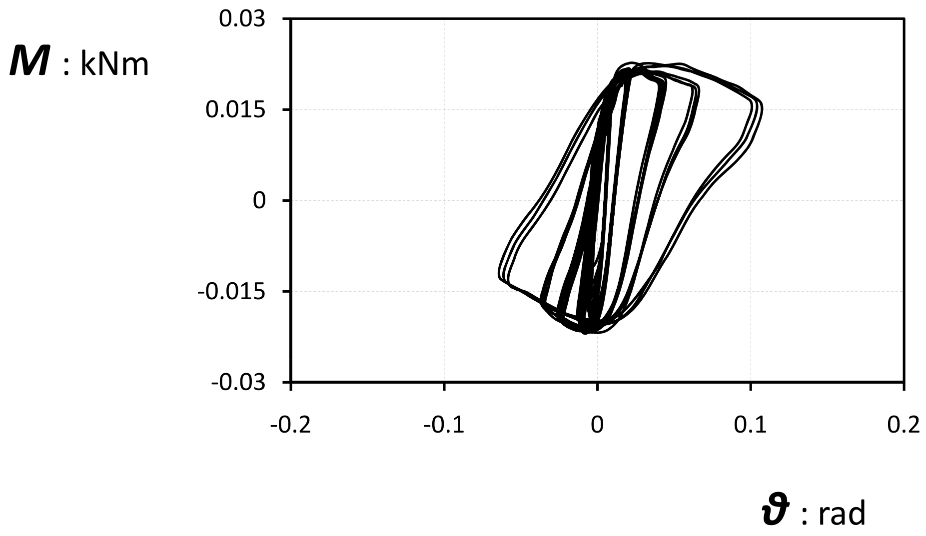

M : kNm
0.03
0.015
0
-0.015
-0.03
-0.2
-0.1
0
0.1
0.2
ϑ : rad

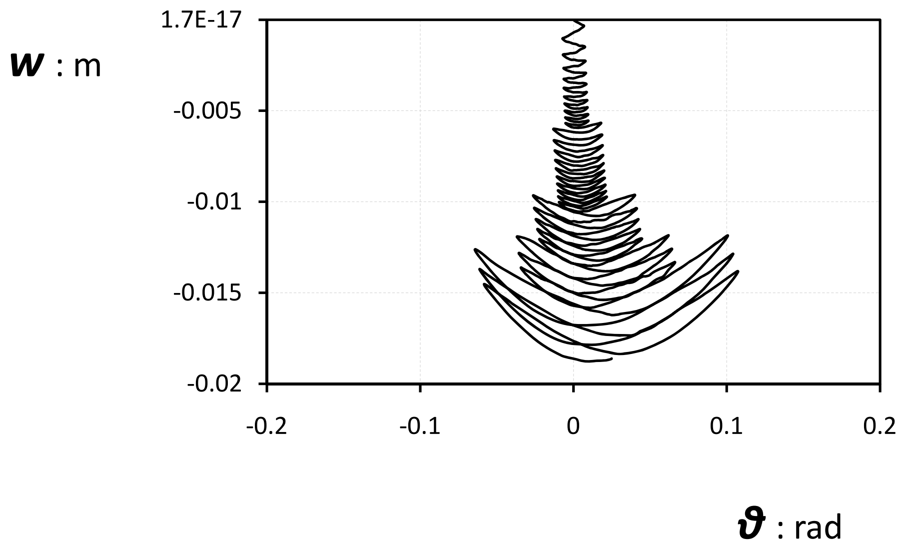

w : m
1.7E-17
-0.005
-0.01
-0.015
-0.02
-0.2
-0.1
0
0.1
0.2
ϑ : rad

National Technical University of Athens
Laboratory of Soil Mechanics

Experimental Project **P2011SQF2**

Experiment **P2011SQF2 - 007**

Date **18/4/2011**

Foundation – Superstructure System

Foundation Width **B = 15 cm**

Aspect Ratio **h/B = 3**

Mass **70 kg**

FS_V **7**

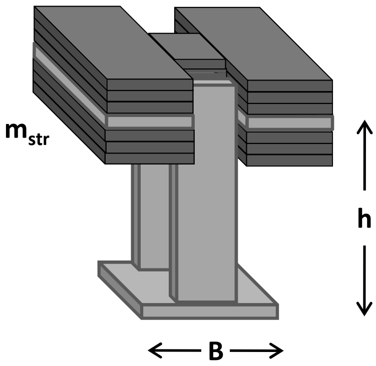

Soil Properties

Homogeneous
Soil Deposit

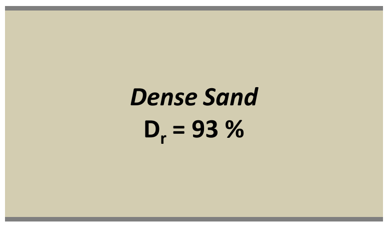

Loading Protocol

Monotonic Loading
(till toppling)

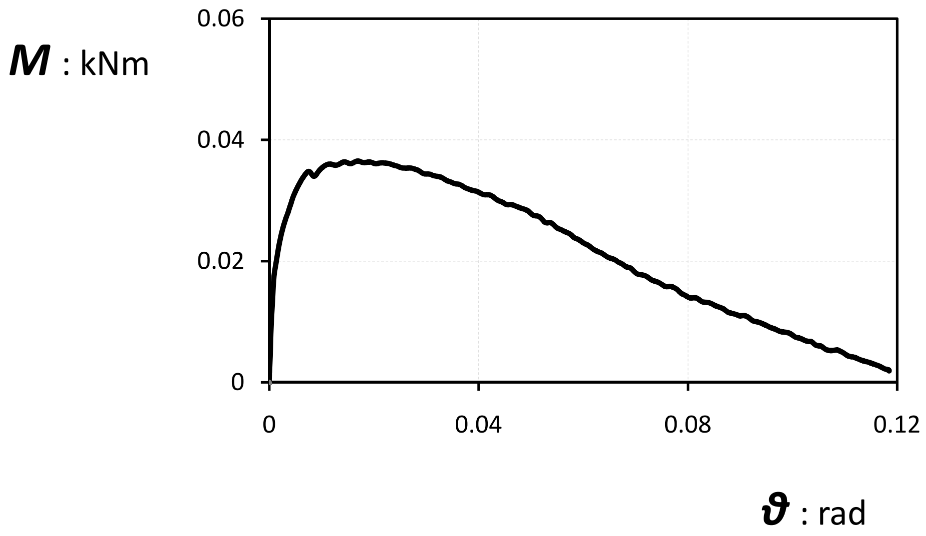

M : kNm
0.06
0.04
0.02
0
0
0.04
0.08
0.12
ϑ : rad

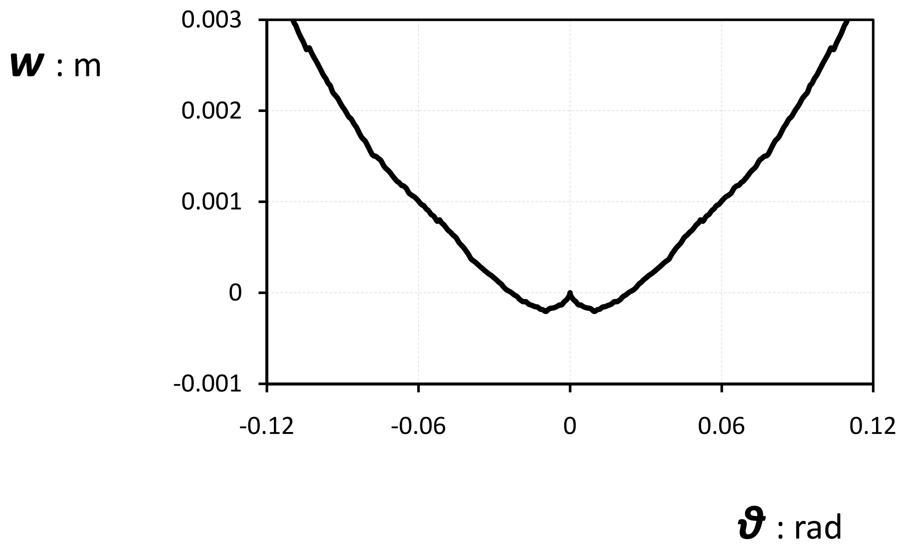

w : m
0.003
0.002
0.001
0
-0.001
-0.12
-0.06
0
0.06
0.12
ϑ : rad

National Technical University of Athens
Laboratory of Soil Mechanics

Experimental Project **P2011SQF2**

Experiment **P2011SQF2 - 006**

Date **15/4/2011**

Foundation – Superstructure System

Foundation Width **B = 15 cm**

Aspect Ratio **h/B = 3**

Mass **70 kg**

FS_V **7**

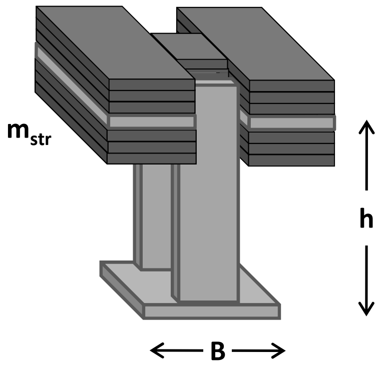

Soil Properties

Homogeneous
Soil Deposit

Dense Sand
D_r = 93 %

Loading Protocol

Cyclic Loading
TYPE I

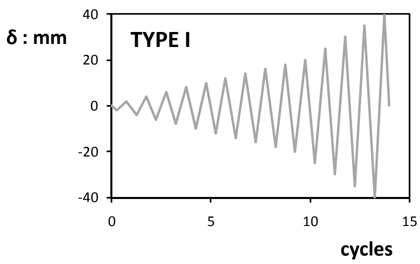

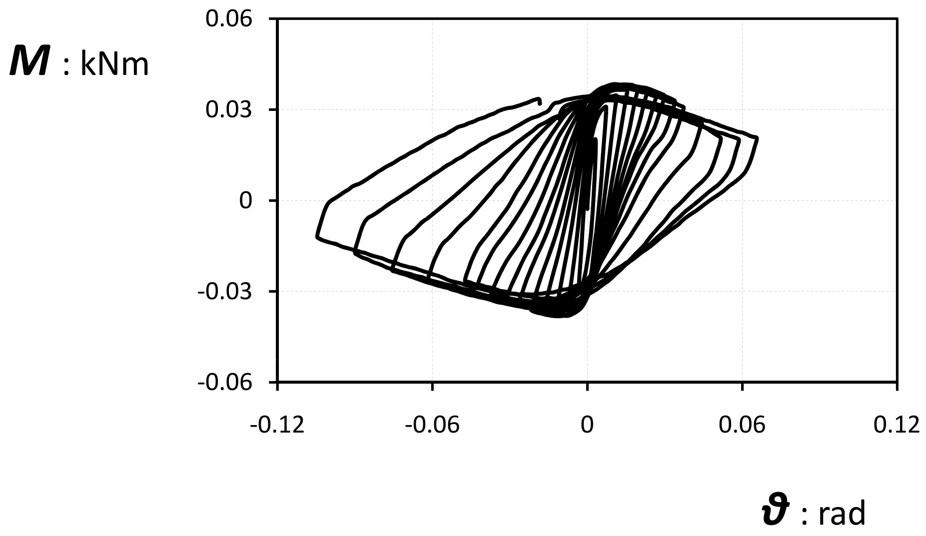
M : kNm
0.06
0.03
0
-0.03
-0.06
-0.12
-0.06
0
0.06
0.12
ϑ : rad

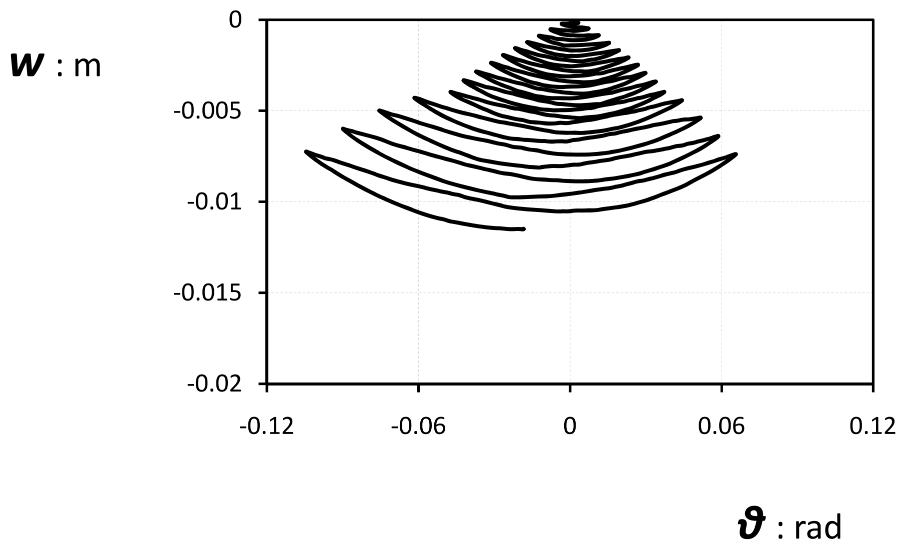
w : m
0
-0.005
-0.01
-0.015
-0.02
-0.12
-0.06
0
0.06
0.12
ϑ : rad

Experimental Project **P2011SQF2**

Experiment **P2011SQF2 - 001**

Date **7/4/2011**

Foundation – Superstructure System

Foundation Width **B = 15 cm**

Aspect Ratio **h/B = 3**

Mass **100 kg**

FS_V **5**

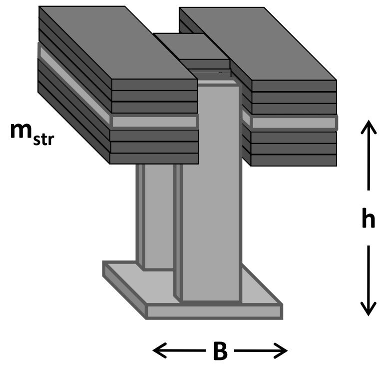

Soil Properties

Homogeneous Soil Deposit

Dense Sand
D_r = 93 %

Loading Protocol

Monotonic Loading (till toppling)

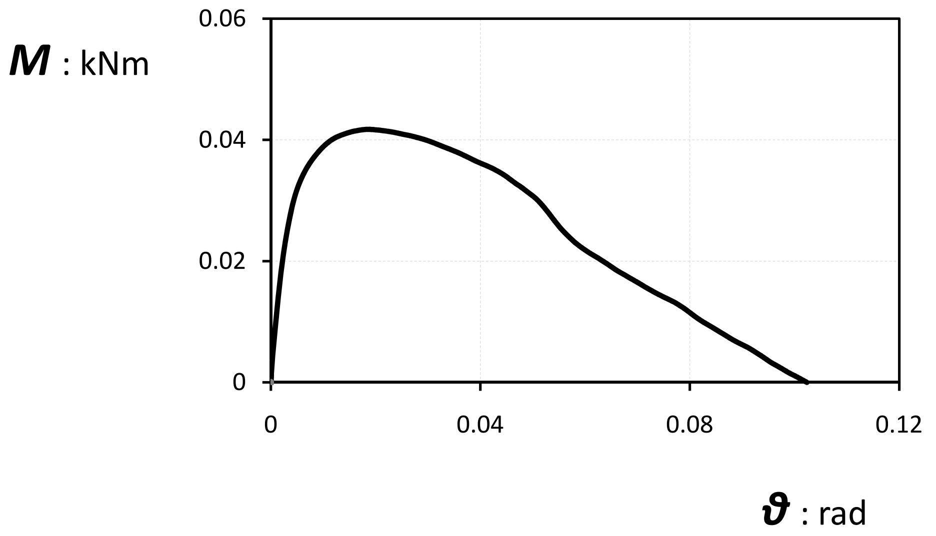
M : kNm
0.06
0.04
0.02
0
0
0.04
0.08
0.12
ϑ : rad

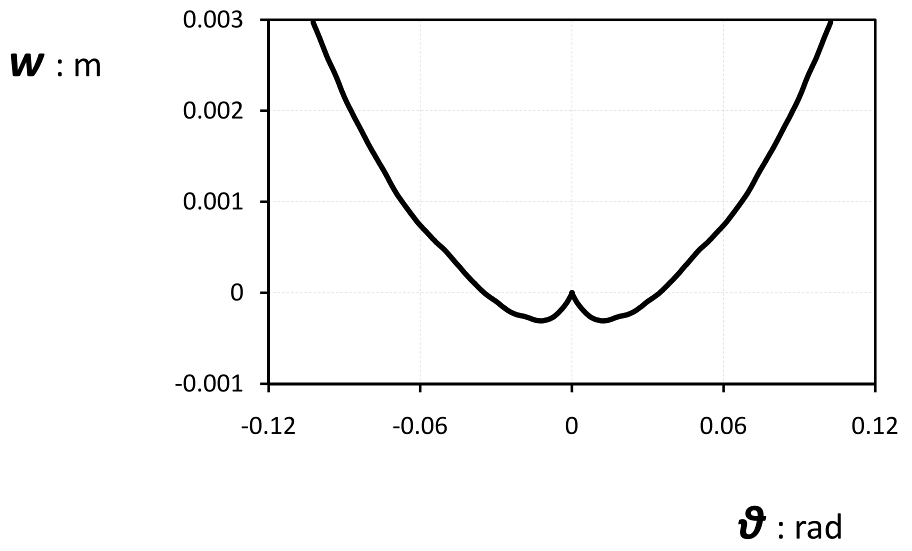
w : m
0.003
0.002
0.001
0
-0.001
-0.12
-0.06
0
0.06
0.12
ϑ : rad

National Technical University of Athens
Laboratory of Soil Mechanics

Experimental Project **P2011SQF2**

Experiment **P2011SQF2 - 030**

Date **20/5/2011**

Foundation – Superstructure System

Foundation Width **B = 15 cm**

Aspect Ratio **h/B = 3**

Mass **100 kg**

FS_V **5**

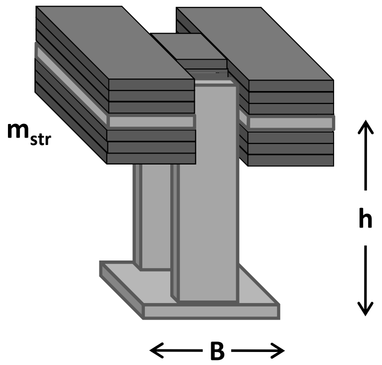

Soil Properties

Homogeneous
Soil Deposit

Dense Sand
D_r = 93 %

Loading Protocol

Cyclic Loading
TYPE I

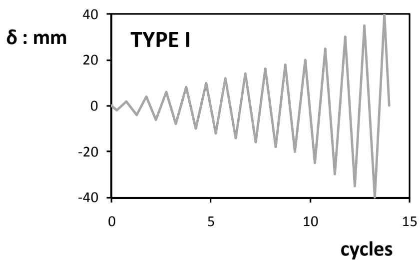

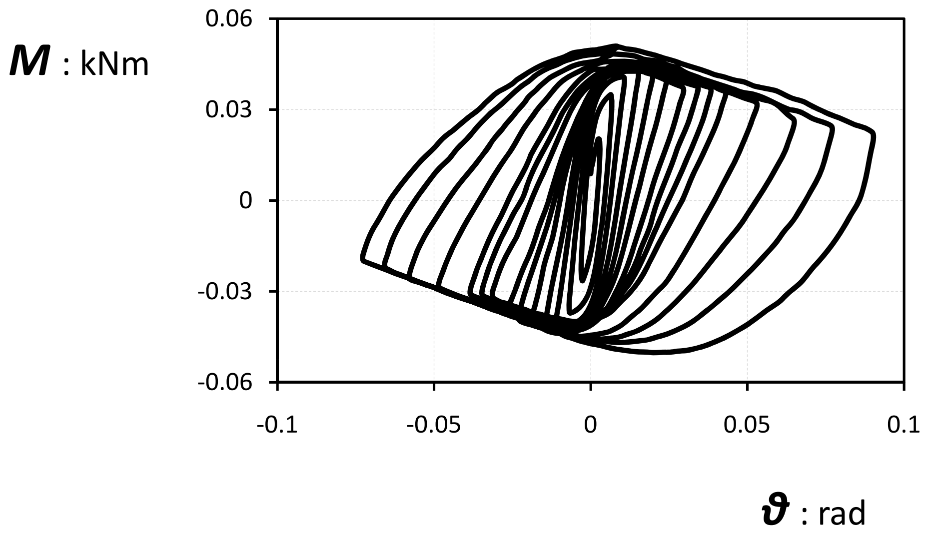
M : kNm
0.06
0.03
0
-0.03
-0.06
-0.1
-0.05
0
0.05
0.1
ϑ : rad

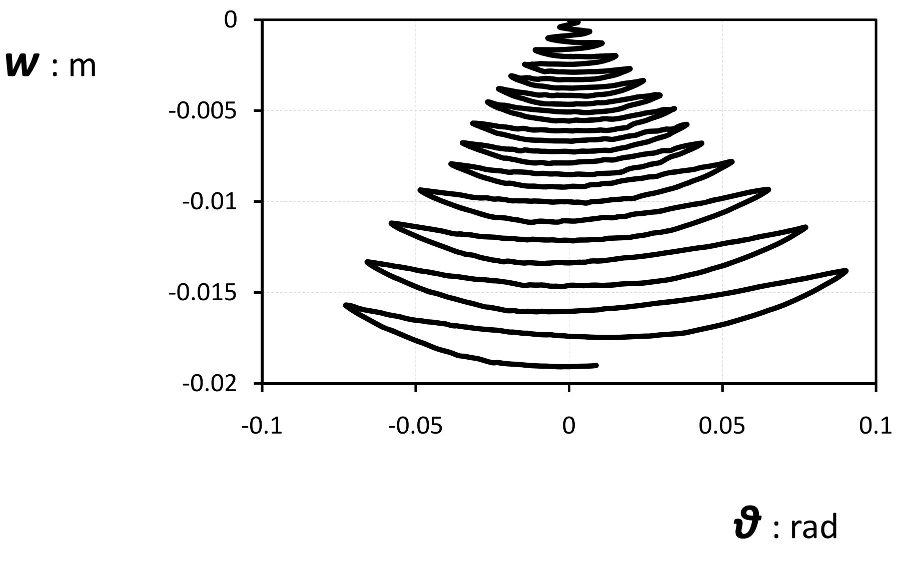
w : m
0
-0.005
-0.01
-0.015
-0.02
-0.1
-0.05
0
0.05
0.1
ϑ : rad

National Technical University of Athens
Laboratory of Soil Mechanics

Experimental Project **P2011SQF2**

Experiment **P2011SQF2 - 010**

Date **21/4/2011**

Foundation – Superstructure System

Foundation Width **B = 15 cm**

Aspect Ratio **h/B = 3**

Mass **100 kg**

FS_V **5**

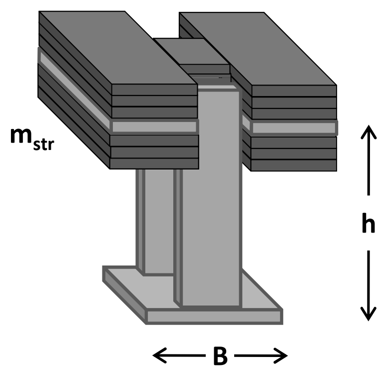

Soil Properties

Homogeneous Soil Deposit

Dense Sand
D_r = 93 %

Loading Protocol

Cyclic Loading
TYPE II

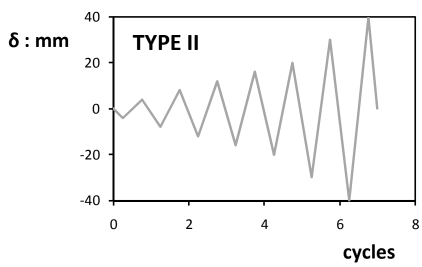

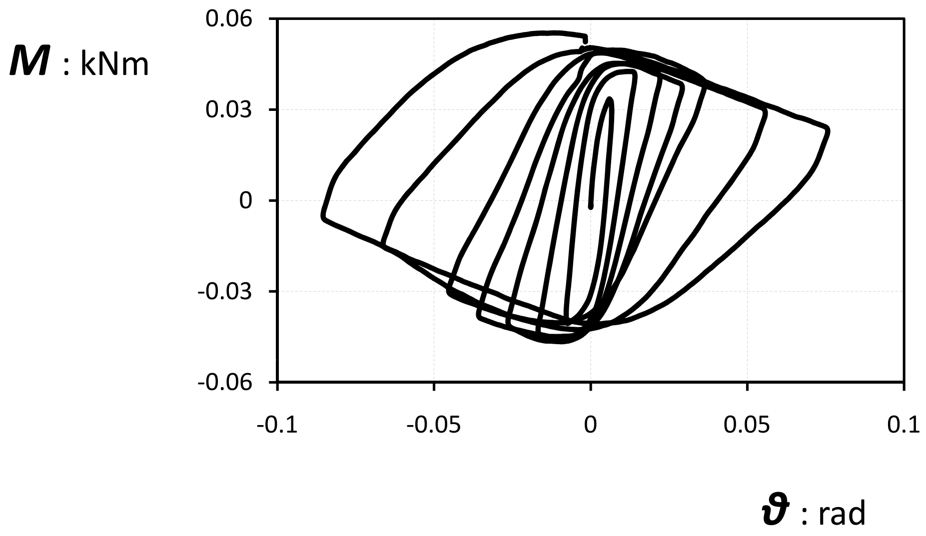

M : kNm
0.06
0.03
0
-0.03
-0.06
-0.1
-0.05
0
0.05
0.1
ϑ : rad

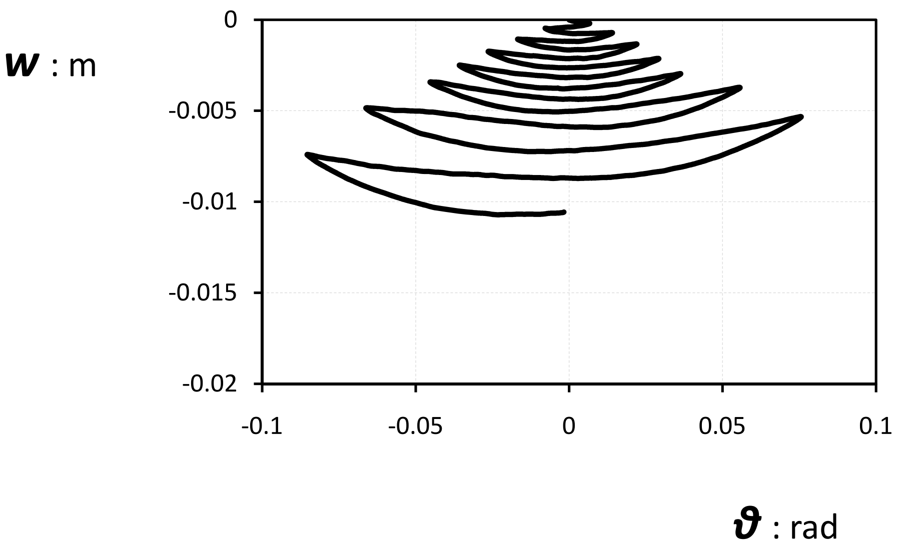

w : m
0
-0.005
-0.01
-0.015
-0.02
-0.1
-0.05
0
0.05
0.1
ϑ : rad

National Technical University of Athens
Laboratory of Soil Mechanics

Experimental Project **P2011SQF2**

Experiment **P2011SQF2 - 011**

Date **26/4/2011**

Foundation – Superstructure System

Foundation Width **B = 15 cm**

Aspect Ratio **h/B = 3**

Mass **100 kg**

FS_V **5**

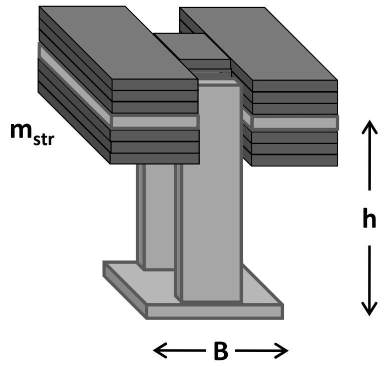

Soil Properties

Homogeneous Soil Deposit

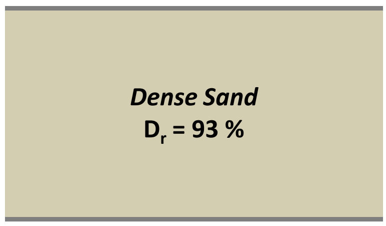

Loading Protocol

Cyclic Loading
TYPE III

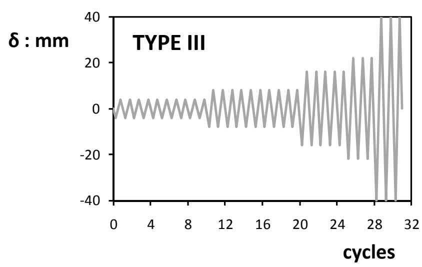

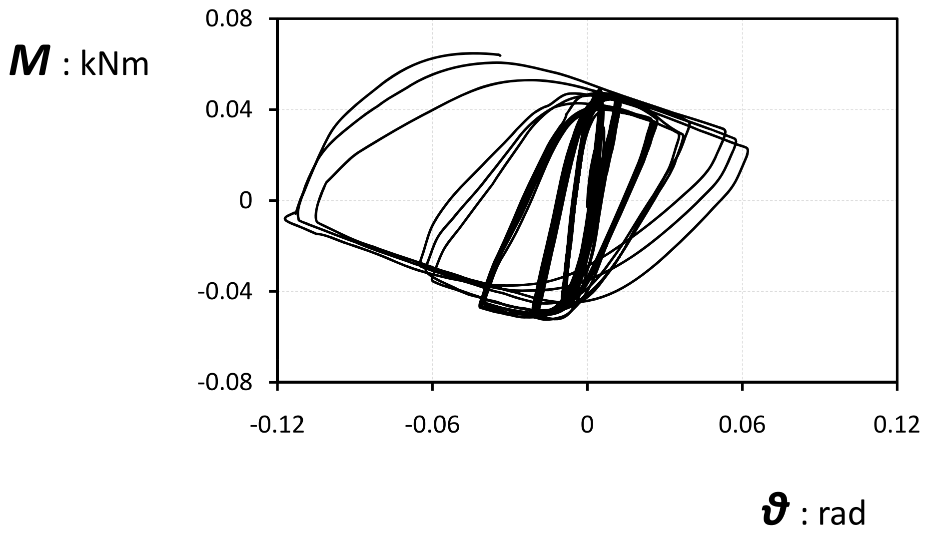

M : kNm
0.08
0.04
0
-0.04
-0.08
-0.12
-0.06
0
0.06
0.12
ϑ : rad

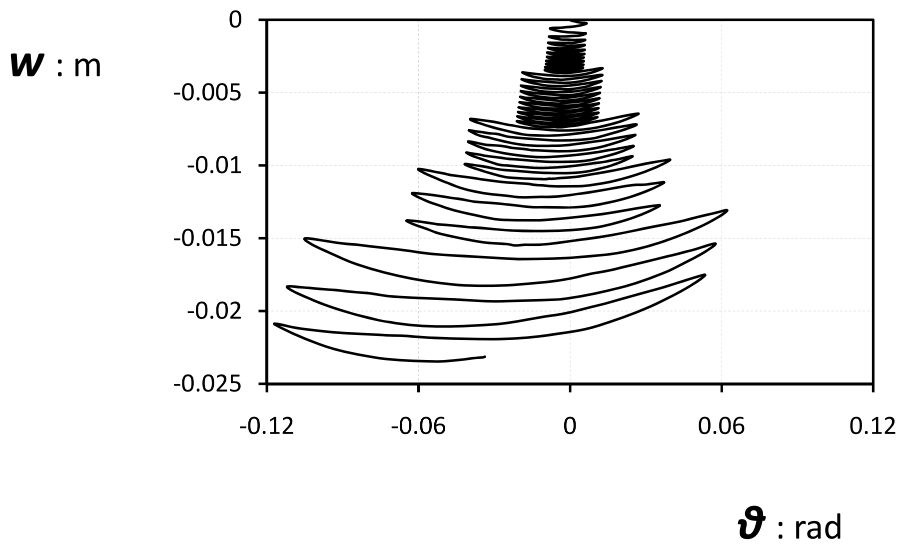

w : m
0
-0.005
-0.01
-0.015
-0.02
-0.025
-0.12
-0.06
0
0.06
0.12
ϑ : rad

National Technical University of Athens
Laboratory of Soil Mechanics

Experimental Project **P2011SQF2**

Experiment **P2011SQF2 - 004**

Date **13/4/2011**

Foundation – Superstructure System

Foundation Width **B = 15 cm**

Aspect Ratio **h/B = 3**

Mass **100 kg**

FS_V **2.6**

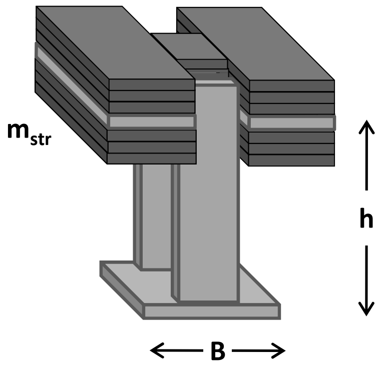

Soil Properties

Homogeneous Soil Deposit

Sand of Medium Density
D_r = 93 %

Loading Protocol

Monotonic Loading (till toppling)

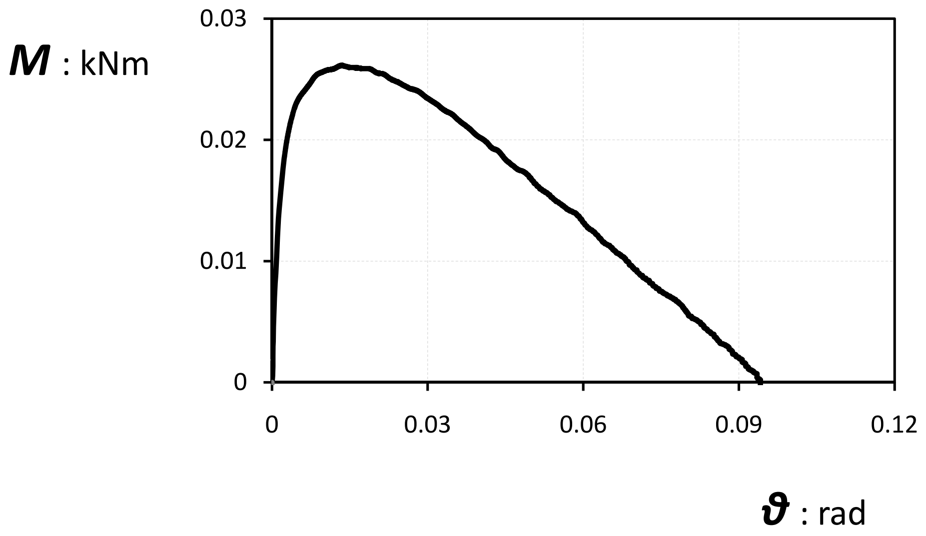
M : kNm
0.03
0.02
0.01
0
0
0.03
0.06
0.09
0.12
ϑ : rad

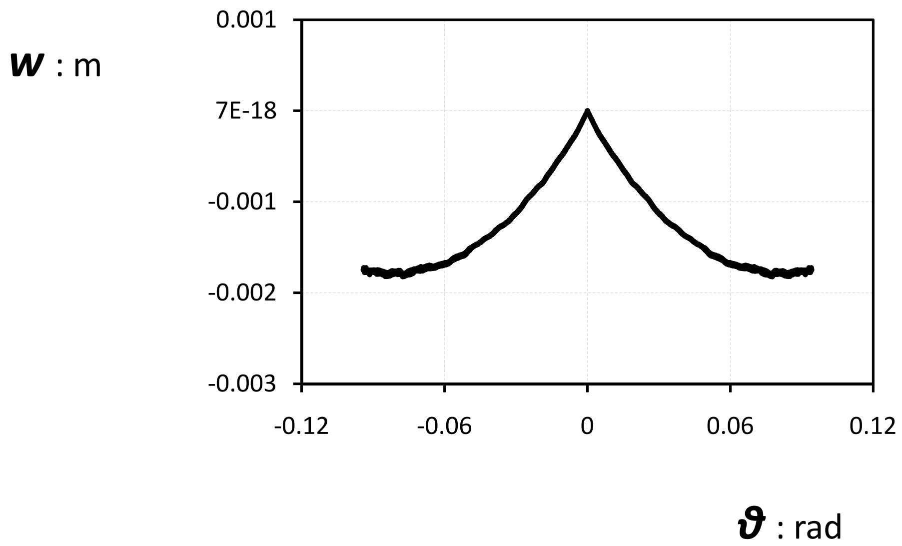
w : m
0.001
7E-18
-0.001
-0.002
-0.003
-0.12
-0.06
0
0.06
0.12
ϑ : rad

National Technical University of Athens
Laboratory of Soil Mechanics

Experimental Project **P2011SQF2**

Experiment **P2011SQF2 - 012**

Date **28/4/2011**

Foundation – Superstructure System

Foundation Width **B = 15 cm**

Aspect Ratio **h/B = 3**

Mass **100 kg**

FS_V **2.6**

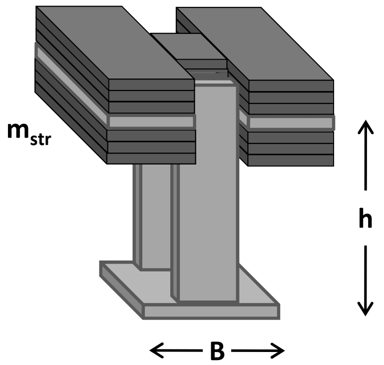

Soil Properties

Homogeneous Soil Deposit

Sand of Medium Density
D_r = 93 %

Loading Protocol

Cyclic Loading
TYPE I

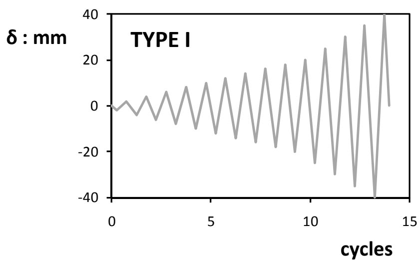

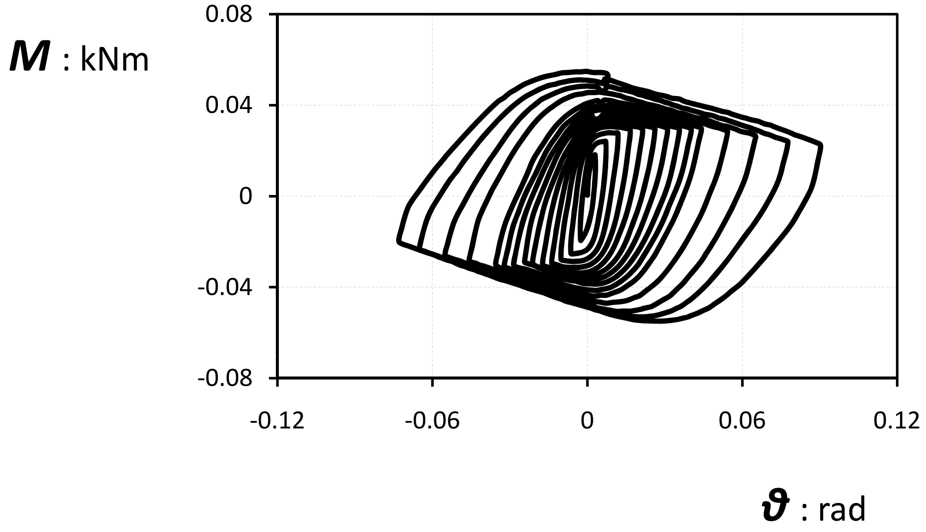

M : kNm
0.08
0.04
0
-0.04
-0.08
-0.12
-0.06
0
0.06
0.12
ϑ : rad

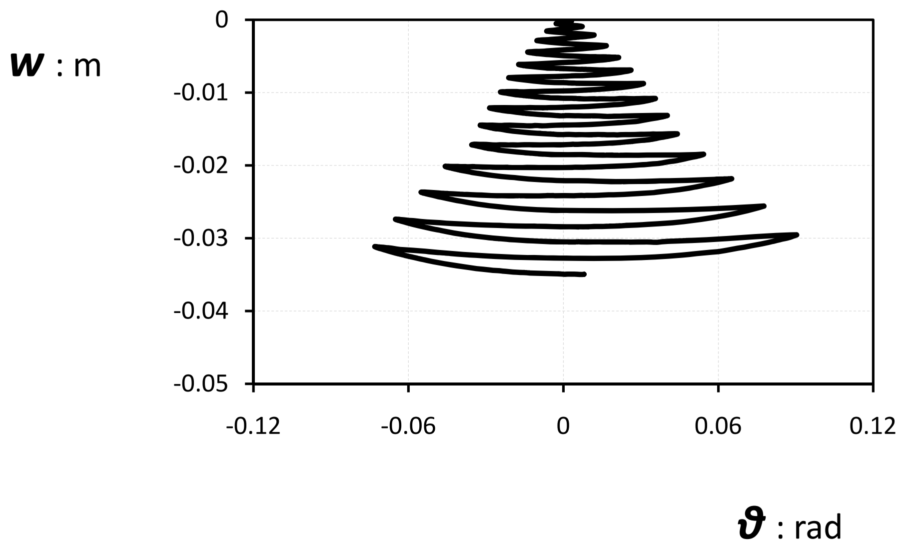

w : m
0
-0.01
-0.02
-0.03
-0.04
-0.05
-0.12
-0.06
0
0.06
0.12
ϑ : rad

National Technical University of Athens
Laboratory of Soil Mechanics

Experimental Project **P2011SQF2**

Experiment **P2011SQF2 - 031**

Date **23/5/2011**

Foundation – Superstructure System

Foundation Width **B = 15 cm**

Aspect Ratio **h/B = 3**

Mass **100 kg**

FS_V **2.6**

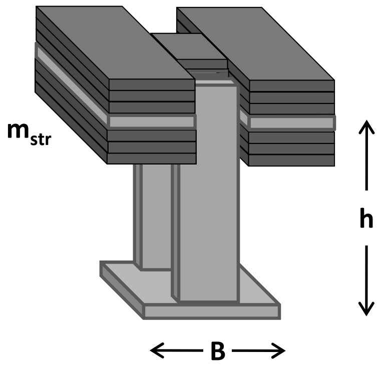

Soil Properties

Homogeneous Soil Deposit

Sand of Medium Density
D_r = 93 %

Loading Protocol

Cyclic Loading
TYPE III

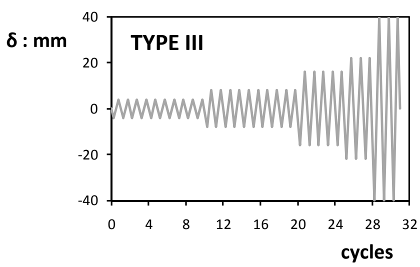

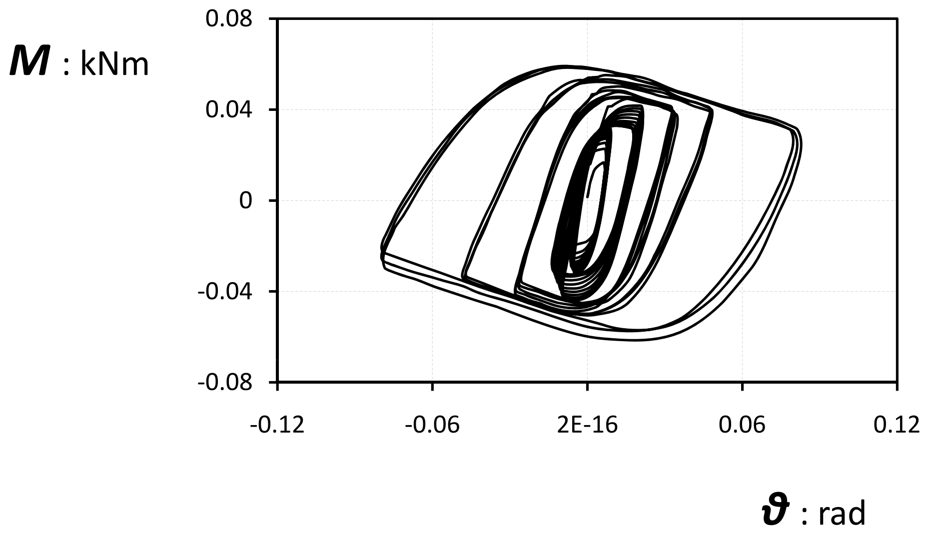

0.08
0.04
0
-0.04
-0.08
-0.12
-0.06
2E-16
0.06
0.12
M : kNm
ϑ : rad

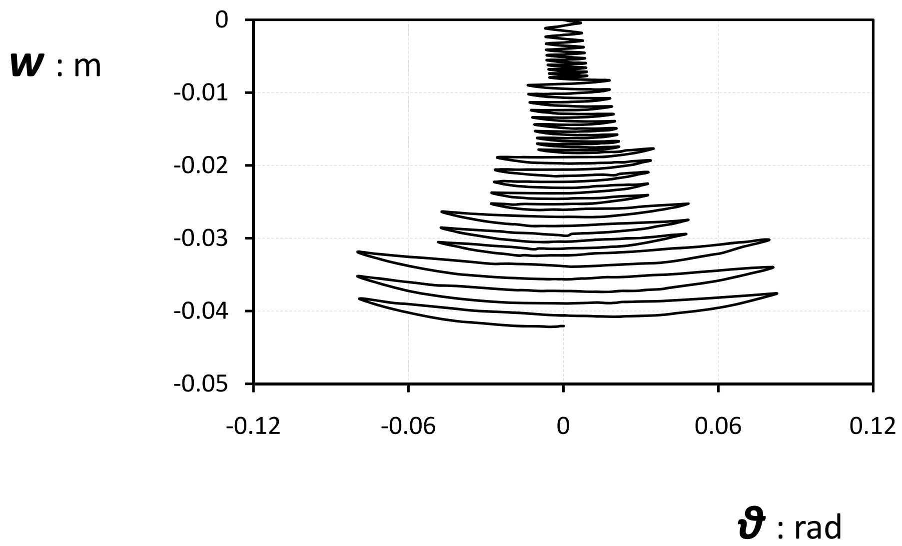

0
-0.01
-0.02
-0.03
-0.04
-0.05
-0.12
-0.06
0
0.06
0.12
w : m
ϑ : rad

National Technical University of Athens
Laboratory of Soil Mechanics

Experimental Project	**P2011SQF2**
Experiment	**P2011SQF2 - 032**
Date	**25/5/2011**

Foundation – Superstructure System

Foundation Width	**B = 15 cm**
Aspect Ratio	**h/B = 3**
Mass	**100 kg**
FS_V	**4.1**

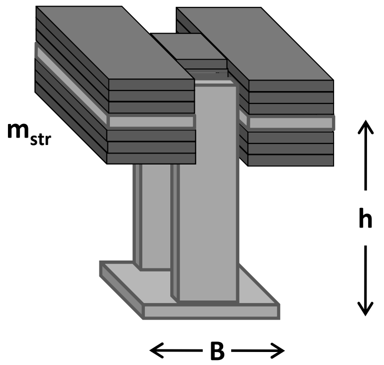

Soil Properties

Two–layered
Soil Deposit
z/B = 1

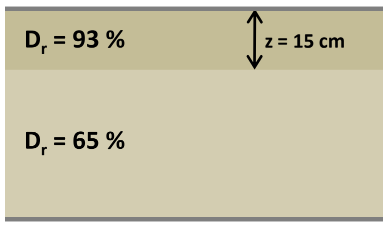

Loading Protocol

Monotonic Loading
(till toppling)

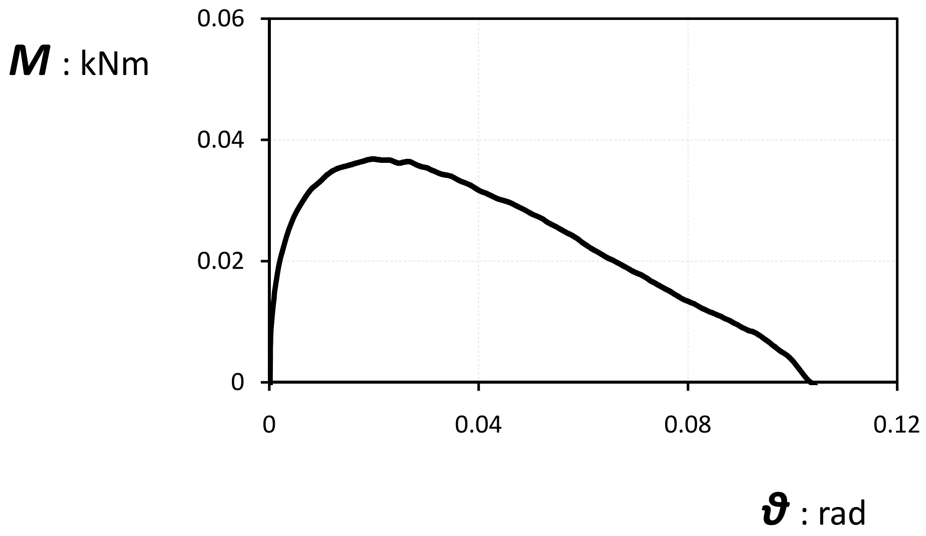

M : kNm
0.06
0.04
0.02
0
0
0.04
0.08
0.12
ϑ : rad

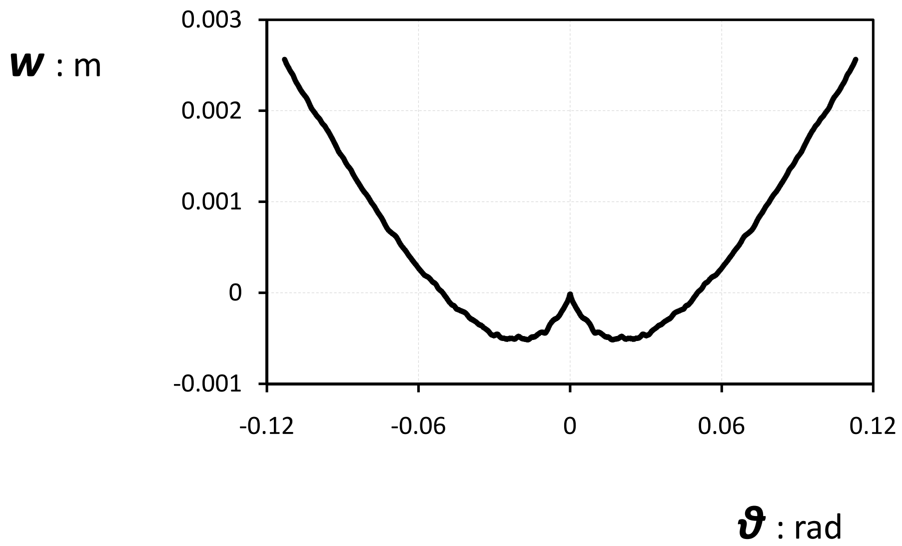

w : m
0.003
0.002
0.001
0
-0.001
-0.12
-0.06
0
0.06
0.12
ϑ : rad

National Technical University of Athens
Laboratory of Soil Mechanics

Experimental Project **P2011SQF2**

Experiment **P2011SQF2 - 014**

Date **2/5/2011**

Foundation – Superstructure System

Foundation Width **B = 15 cm**

Aspect Ratio **h/B = 3**

Mass **100 kg**

FS_V **4.1**

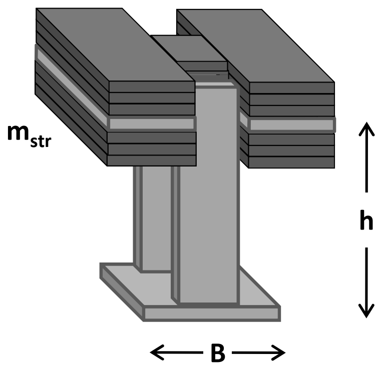

Soil Properties

Two–layered
Soil Deposit
z/B = 1

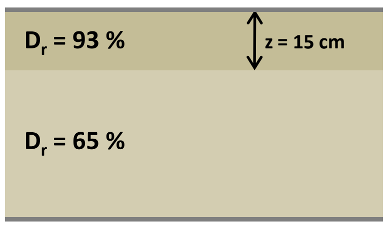

Loading Protocol

Cyclic Loading
TYPE I

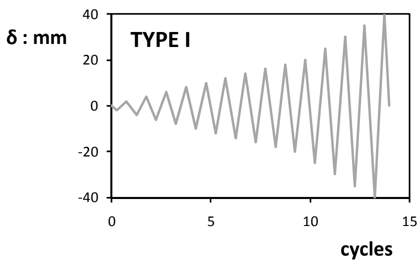

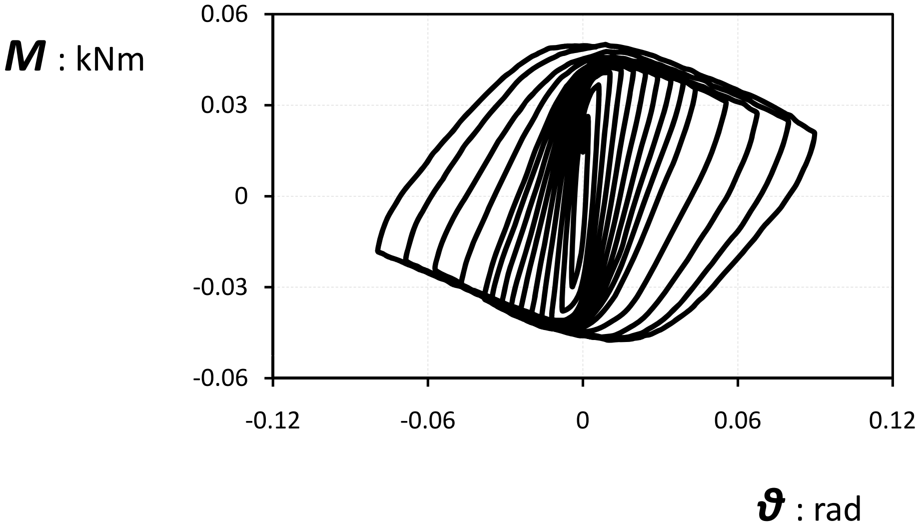

M : kNm
0.06
0.03
0
-0.03
-0.06
-0.12
-0.06
0
0.06
0.12
ϑ : rad

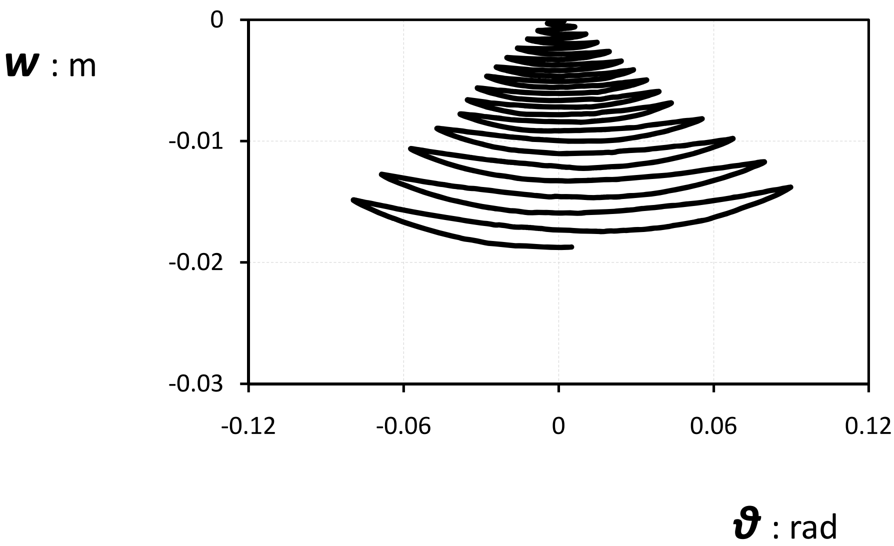

w : m
0
-0.01
-0.02
-0.03
-0.12
-0.06
0
0.06
0.12
ϑ : rad

National Technical University of Athens
Laboratory of Soil Mechanics

Experimental Project	**P2011SQF2**
Experiment	**P2011SQF2 - 033**
Date	**26/5/2011**

Foundation – Superstructure System

Foundation Width	**B = 15 cm**
Aspect Ratio	**h/B = 3**
Mass	**100 kg**
FS_V	**4.1**

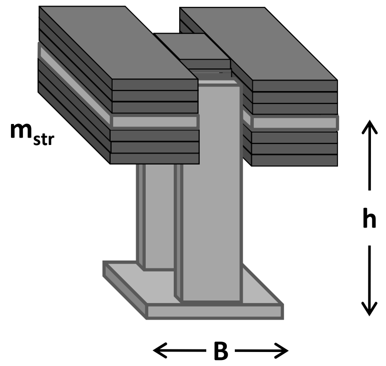

Soil Properties

Two–layered
Soil Deposit
z/B = 1

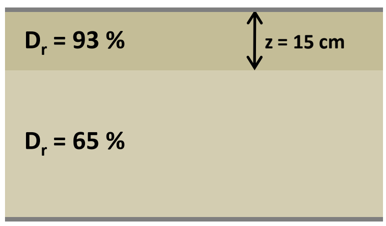

Loading Protocol

Cyclic Loading
TYPE III

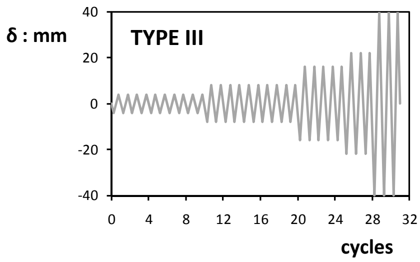

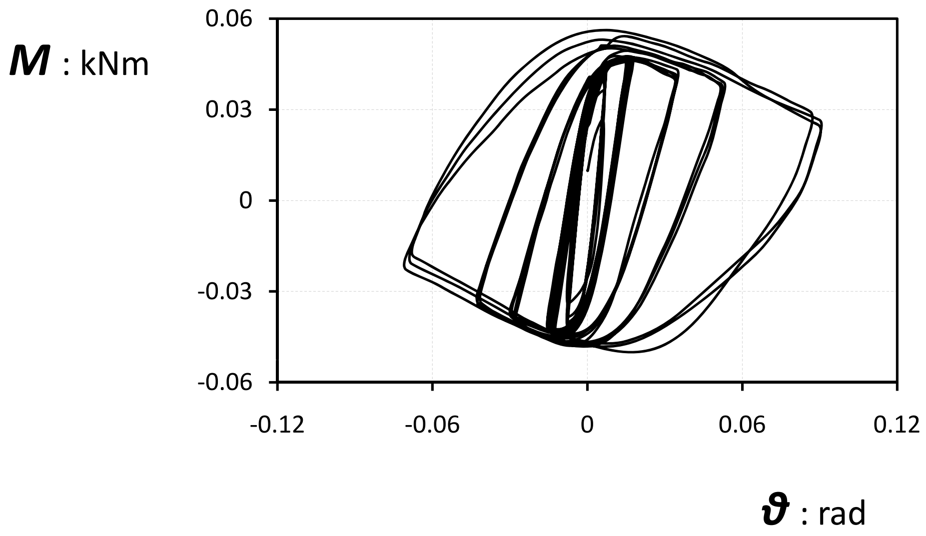

M : kNm
0.06
0.03
0
-0.03
-0.06
-0.12
-0.06
0
0.06
0.12
ϑ : rad

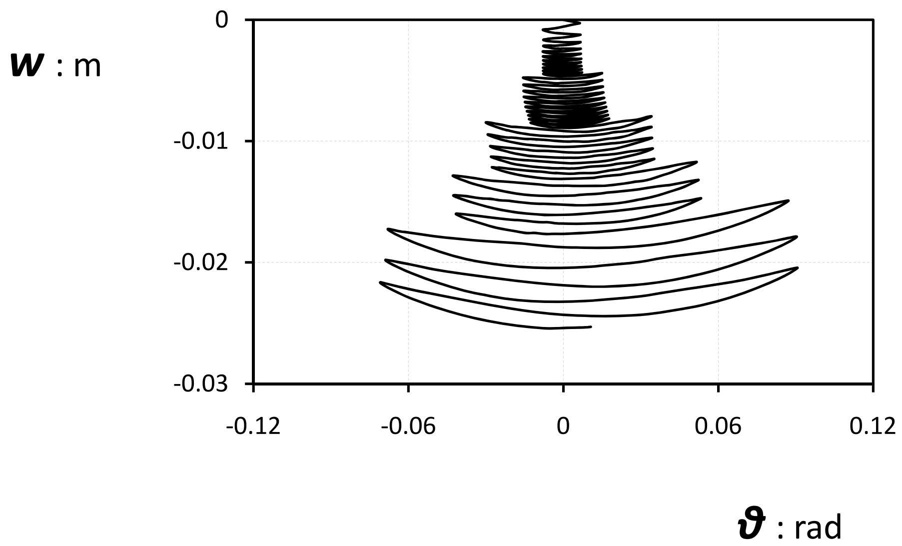

w : m
0
-0.01
-0.02
-0.03
-0.12
-0.06
0
0.06
0.12
ϑ : rad

National Technical University of Athens
Laboratory of Soil Mechanics

Experimental Project **P2011SQF2**

Experiment **P2011SQF2 - 029**

Date **19/5/2011**

Foundation – Superstructure System

Foundation Width **B = 15 cm**

Aspect Ratio **h/B = 3**

Mass **100 kg**

FS_V **3.1**

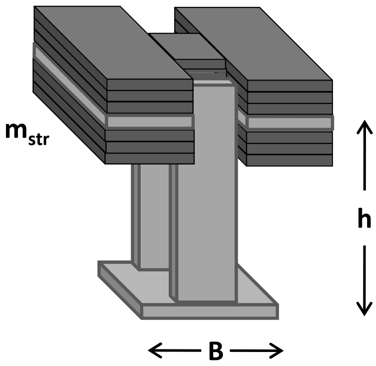

Soil Properties

Two–layered
Soil Deposit
z/B = 0.5

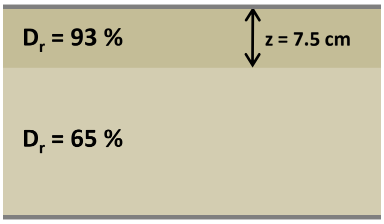

Loading Protocol

Monotonic Loading
(till toppling)

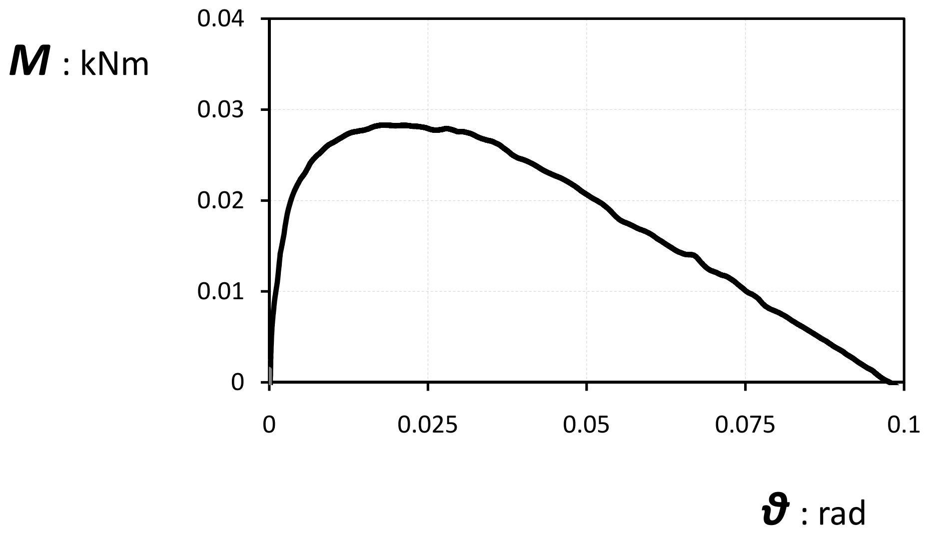

M : kNm
0.04
0.03
0.02
0.01
0
0
0.025
0.05
0.075
0.1
ϑ : rad

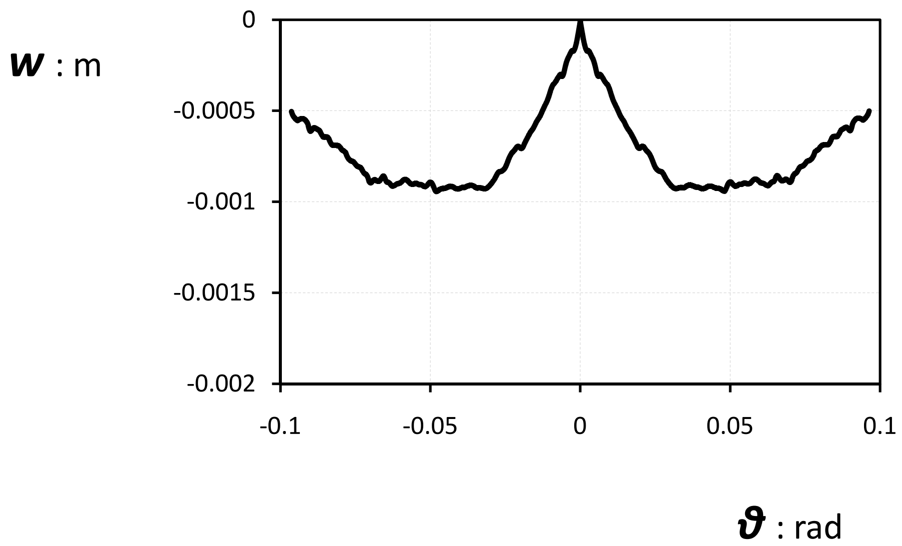

w : m
0
-0.0005
-0.001
-0.0015
-0.002
-0.1
-0.05
0
0.05
0.1
ϑ : rad

National Technical University of Athens
Laboratory of Soil Mechanics

Experimental Project	**P2011SQF2**
Experiment	**P2011SQF2 - 013**
Date	**29/4/2011**

Foundation – Superstructure System

Foundation Width	**B = 15 cm**
Aspect Ratio	**h/B = 3**
Mass	**100 kg**
FS_V	**3.1**

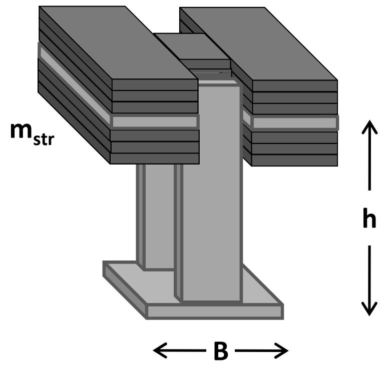

Soil Properties

Two–layered
Soil Deposit
z/B = 0.5

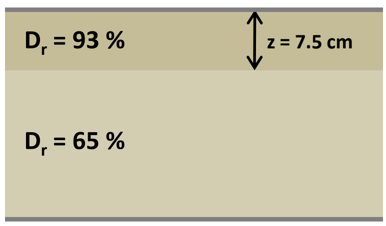

Loading Protocol

Cyclic Loading
TYPE I

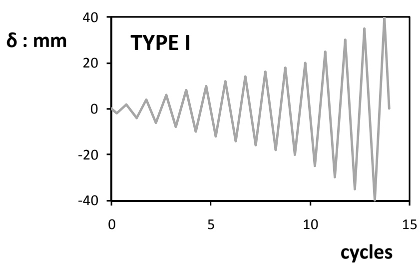

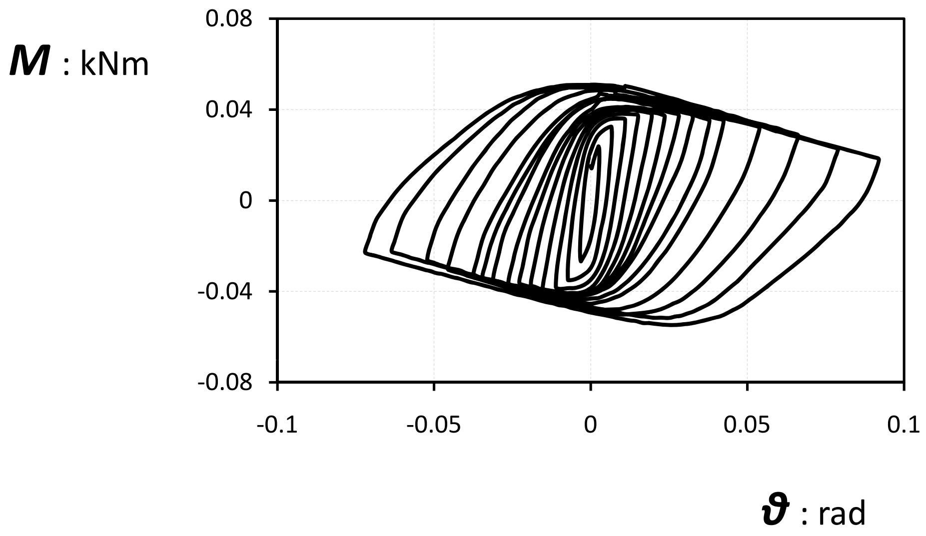

M : kNm
0.08
0.04
0
-0.04
-0.08
-0.1
-0.05
0
0.05
0.1
ϑ : rad

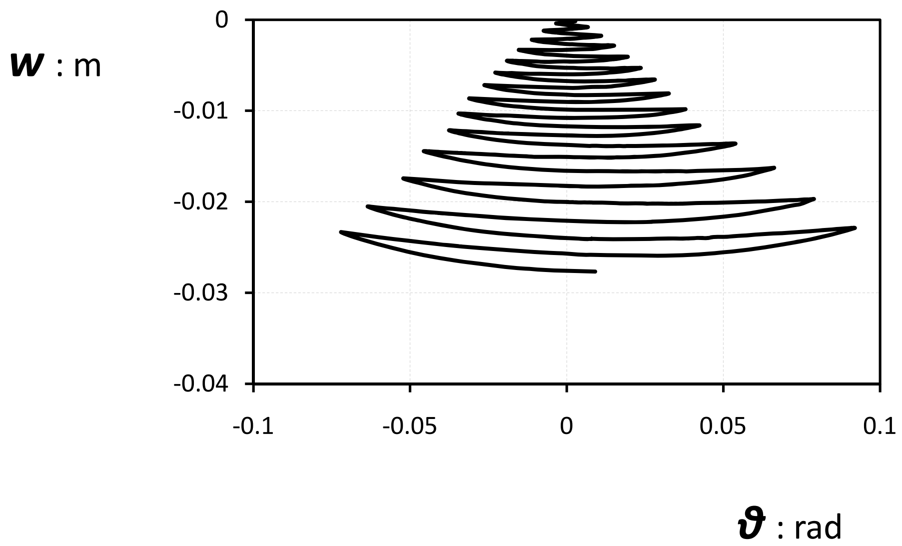

w : m
0
-0.01
-0.02
-0.03
-0.04
-0.1
-0.05
0
0.05
0.1
ϑ : rad

National Technical University of Athens
Laboratory of Soil Mechanics

Experimental Project **P2011SQF2**

Experiment **P2011SQF2 - 028**

Date **18/5/2011**

Foundation – Superstructure System

Foundation Width **B = 15 cm**

Aspect Ratio **h/B = 3**

Mass **100 kg**

FS_V **3.1**

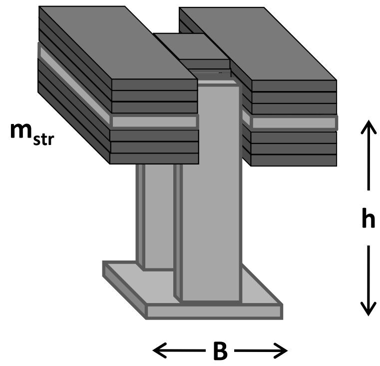

Soil Properties

Two–layered
Soil Deposit
z/B = 0.5

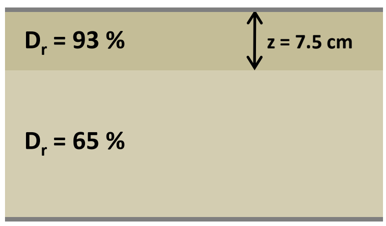

Loading Protocol

Cyclic Loading
TYPE III

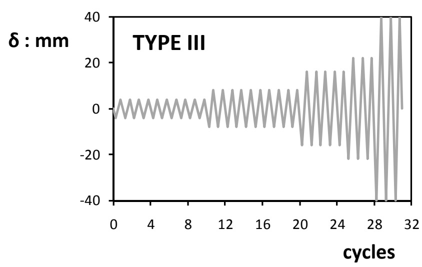

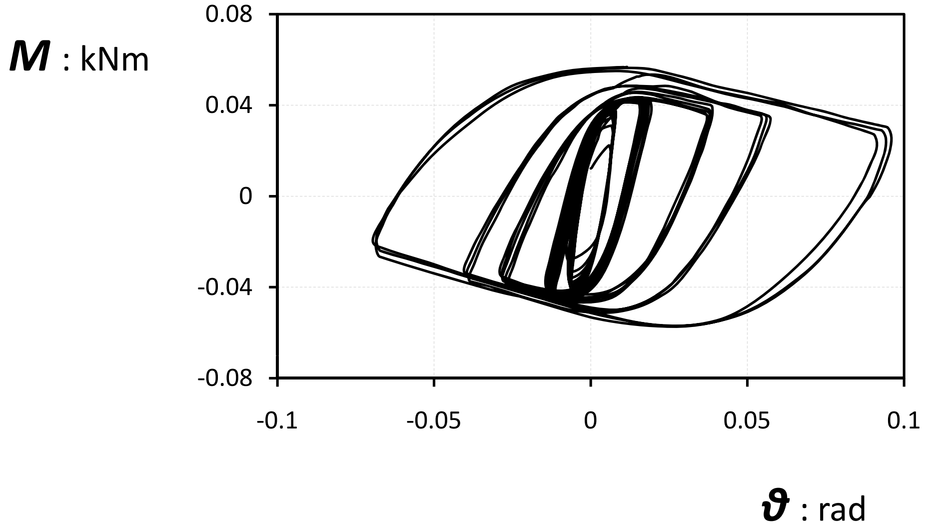
M : kNm
0.08
0.04
0
-0.04
-0.08
-0.1
-0.05
0
0.05
0.1
ϑ : rad

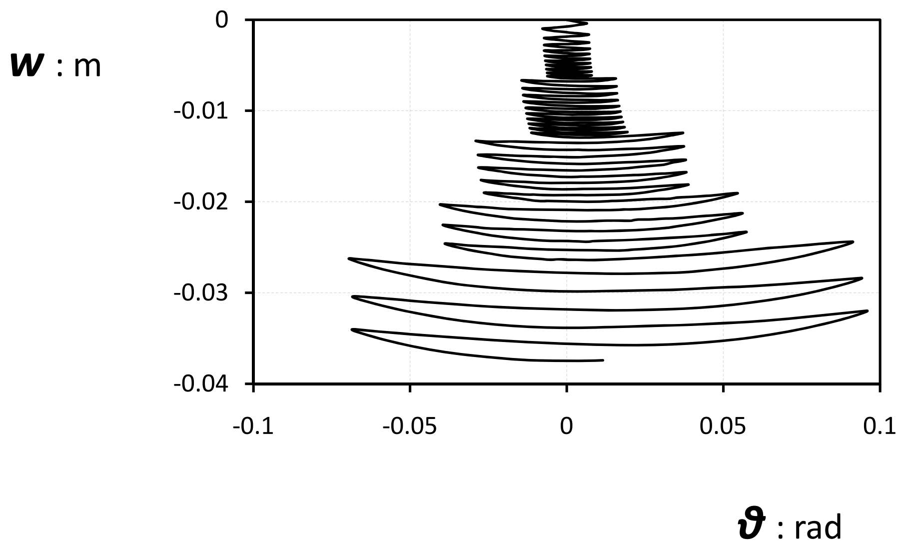
w : m
0
-0.01
-0.02
-0.03
-0.04
-0.1
-0.05
0
0.05
0.1
ϑ : rad

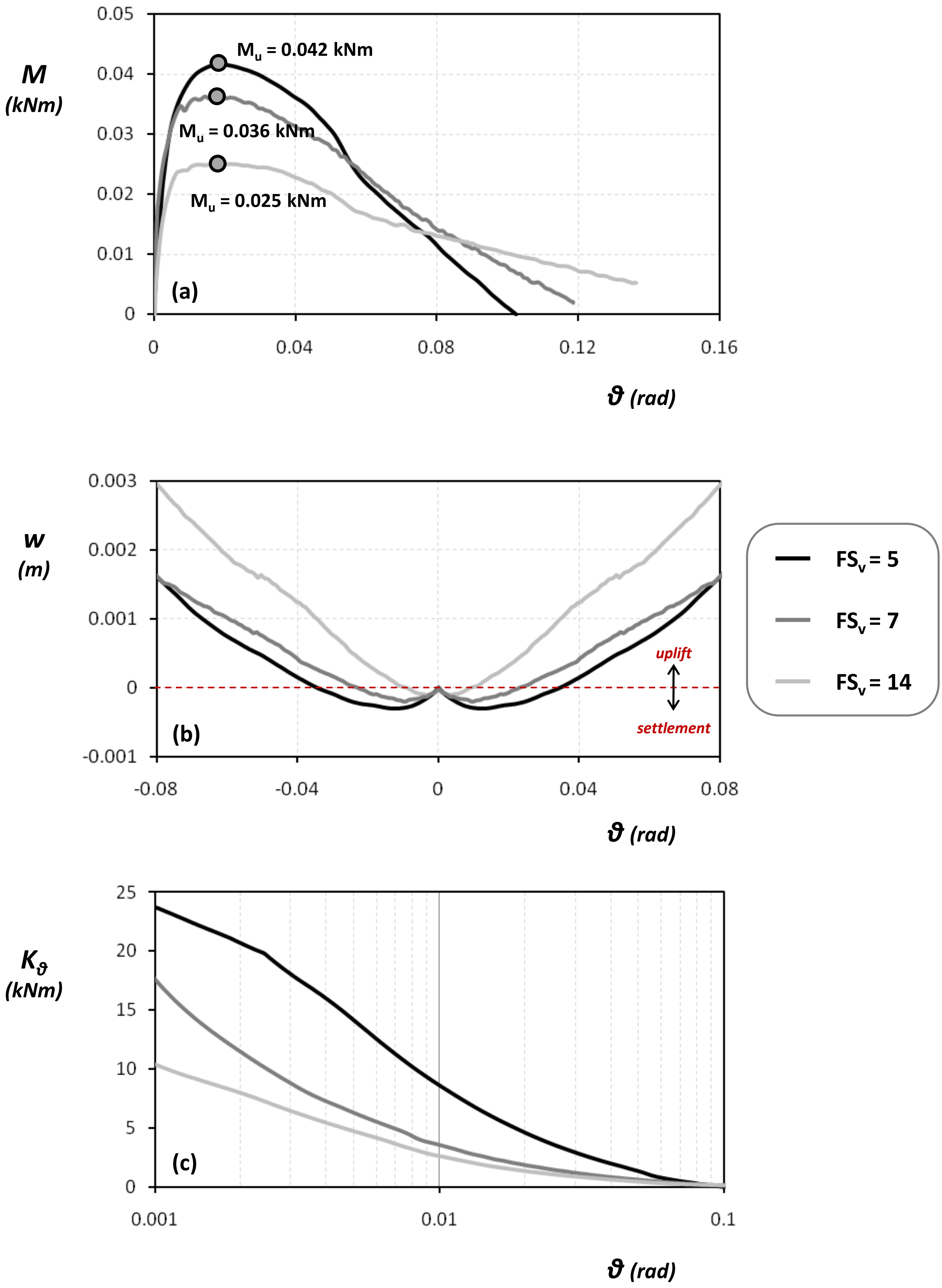

Figure 4.1. **(a)** Moment–rotation curves, **(b)** settlement–rotation curves, **(c)** rotational stiffness curves derived from monotonic pushover tests for systems with FS_v = 5, 7 and 14 (lying on dense sand D_r = 93 %).

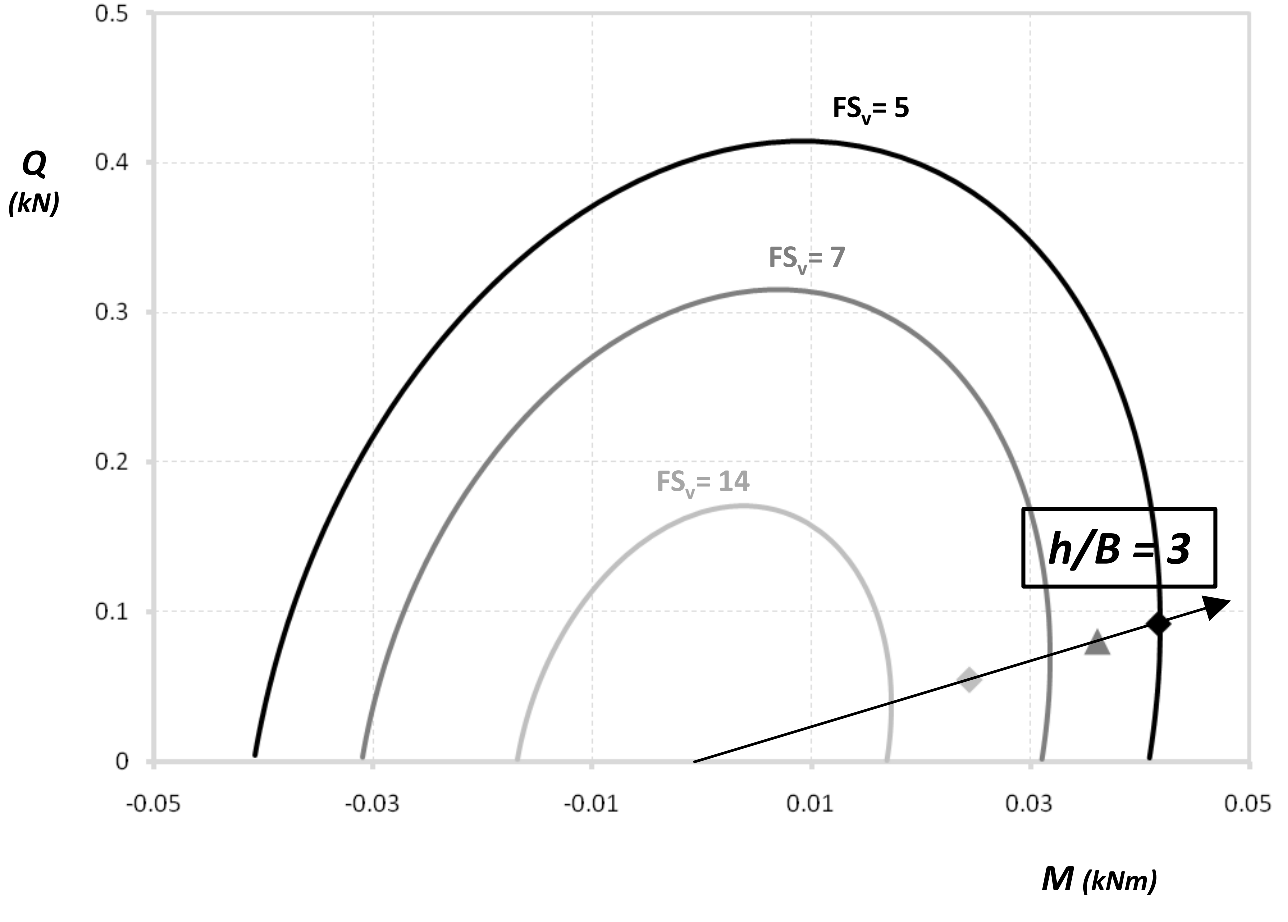

Figure 4.2. Comparison in the *Q : M loading plane* between the failure envelopes derived by Butterfield & Gottardi (1994) and the experimental results for FS_v = 5, 7 and 14.

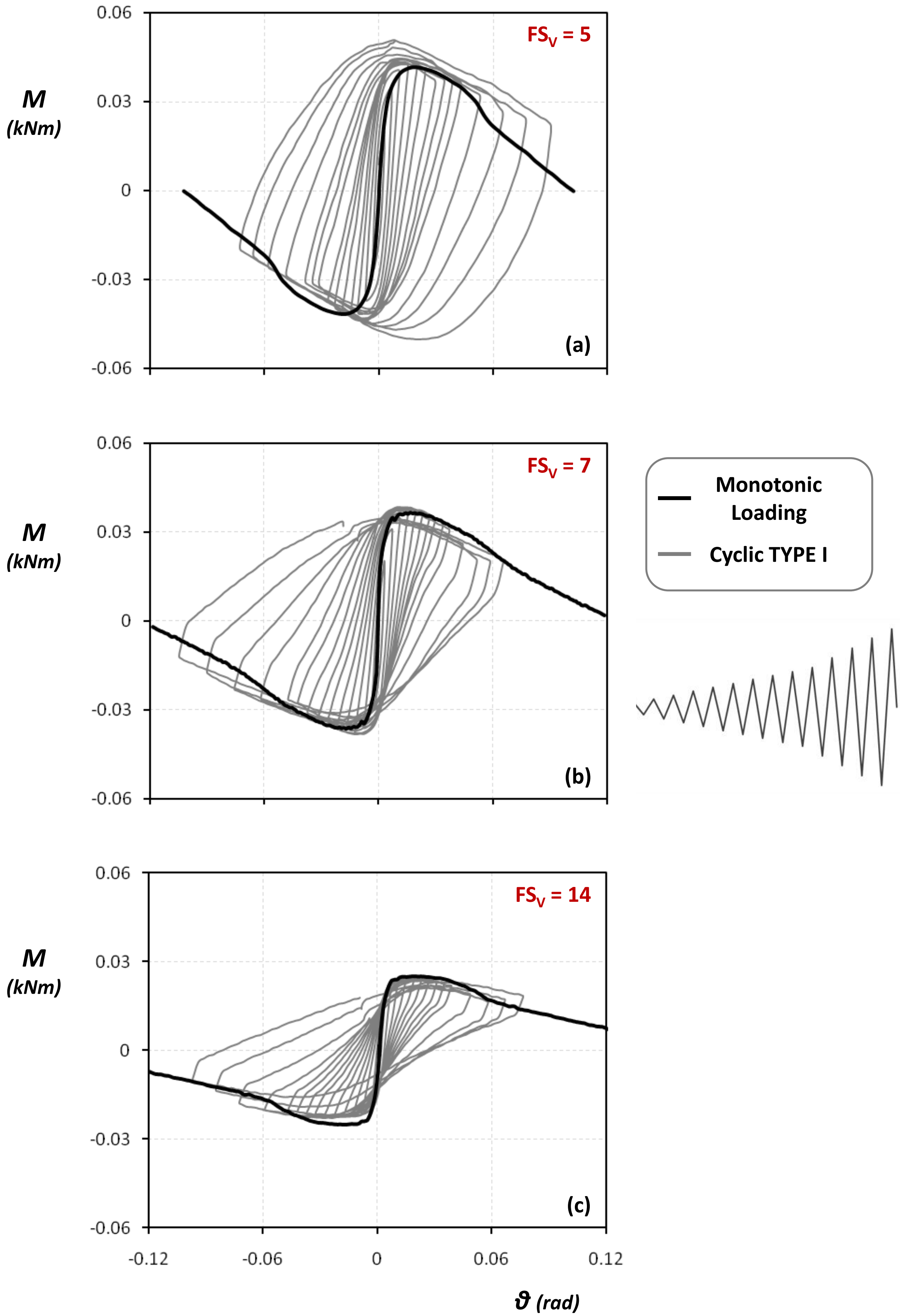

Figure 4.3. Moment–rotation curves derived from slow cyclic pushover tests (**TYPE I**) for systems with FS_V **(a)** 5**, (b)** 7 and **(c)** 14 (lying on dense sand D_r = 93 %). The black lines correspond to the monotonic backbone curves.

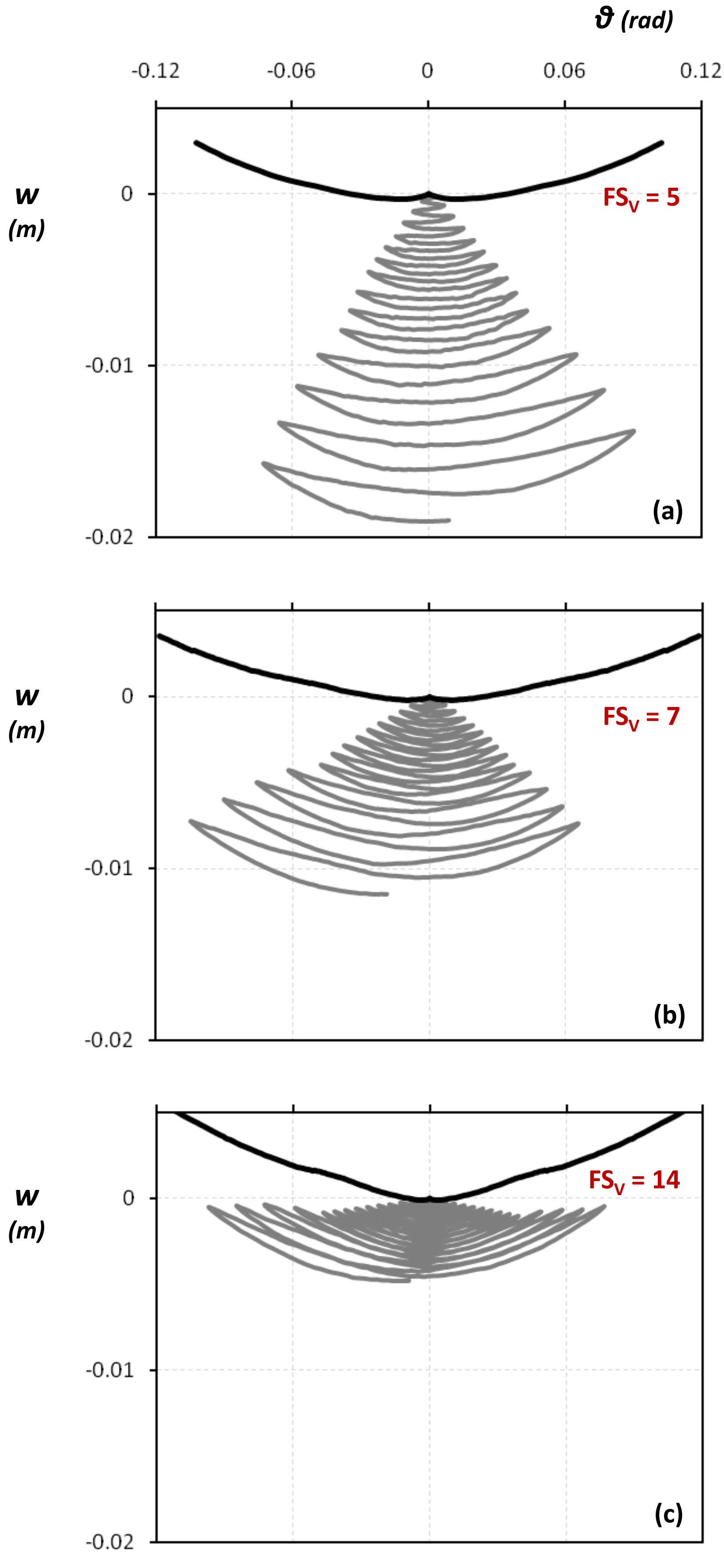

Figure 4.4. Settlement–rotation curves derived from slow cyclic pushover tests (**TYPE I**) for systems with FS_V **(a)** 5**, (b)** 7 and **(c)** 14 (lying on dense sand D_r = 93 %). The black lines correspond to the monotonic backbone curves.

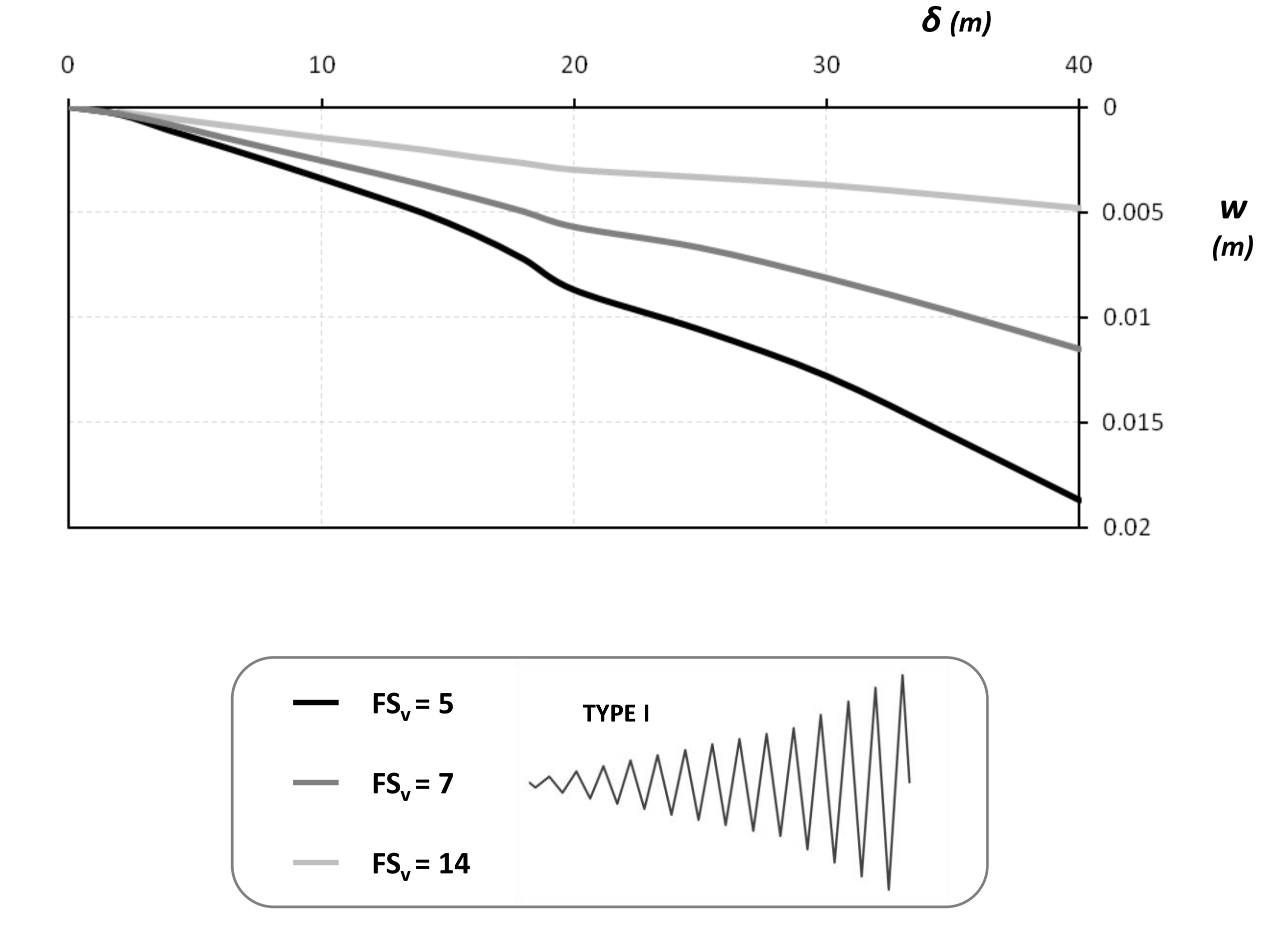

Figure 4.5. Cumulative settlement per imposed horizontal displacement derived from slow cyclic pushover tests (**TYPE I**) for systems with FS_v = 5, 7 and 14 (lying on dense sand D_r = 93 %).

$FS_V = 2.6$

(a)

(b)

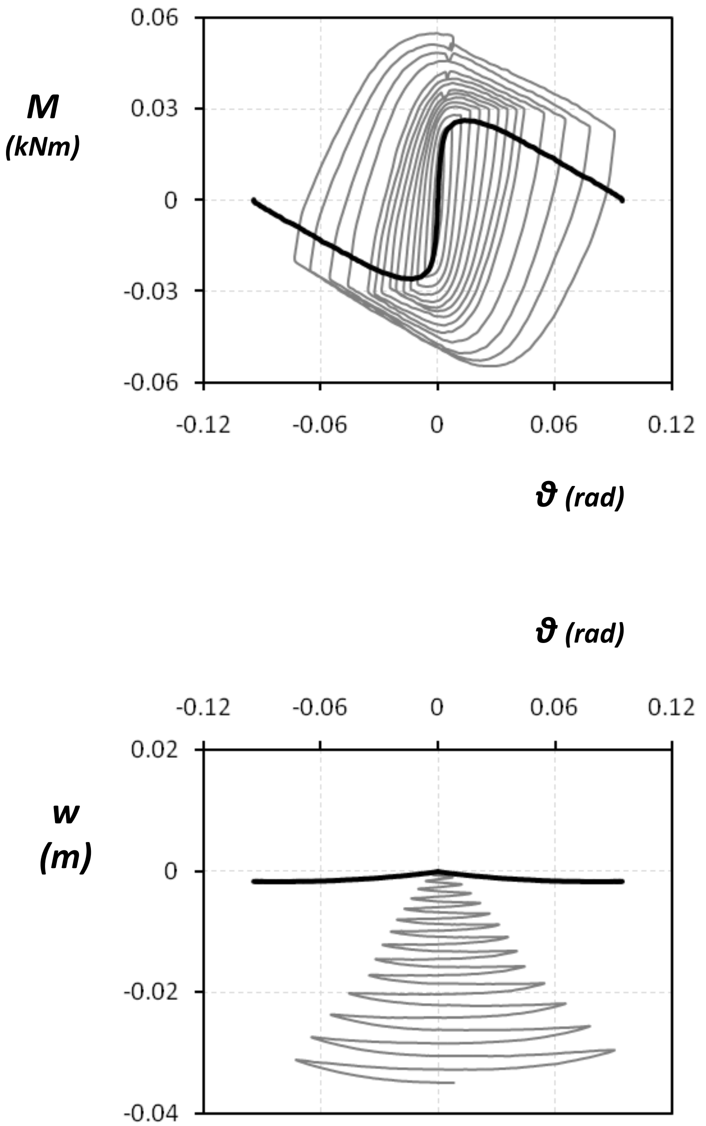

Figure 4.6. (a) Moment–rotation and **(b)** settlement–rotation curves derived from monotonic and slow cyclic pushover tests (**TYPE I**) for the system loaded with mass $\mathbf{m_{str} = 100\ kg}$ lying on sand of relative density D_r = 65% ($\mathbf{FS_V = 2.6}$).

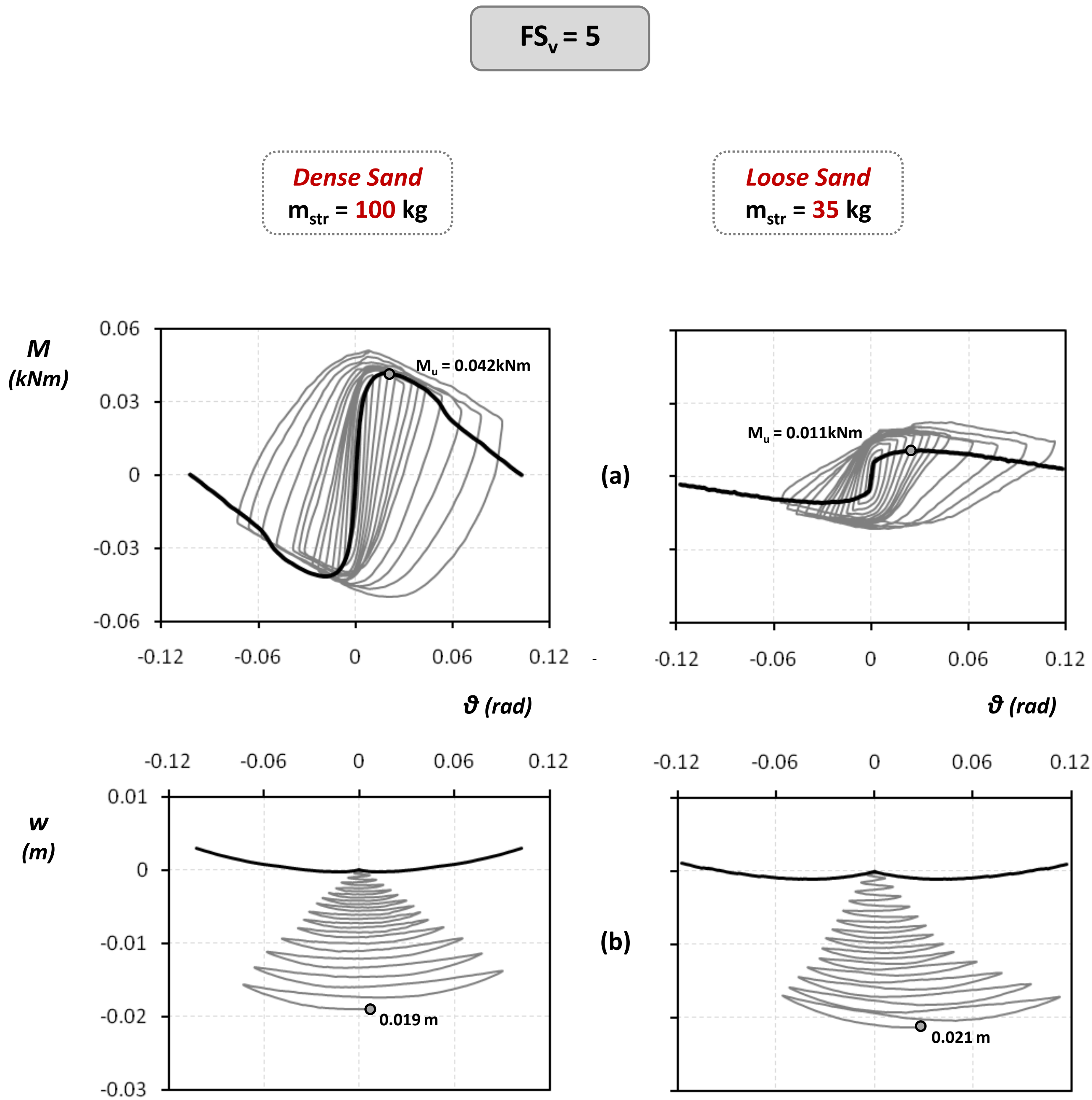

Figure 4.7. (a) Moment–rotation and **(b)** settlement–rotation curves derived from slow cyclic pushover tests (**TYPE I**) for a system with structural mass **m_{str} = 100 kg** lying on sand of relative density D_r = 93 % (**FS_V = 5**) and a system with structural mass **m_{str} = 35 kg** lying on sand of relative density D_r = 45 % (**FS_V = 5**). The static backbone curves derived from the respective monotonic tests are also plotted.

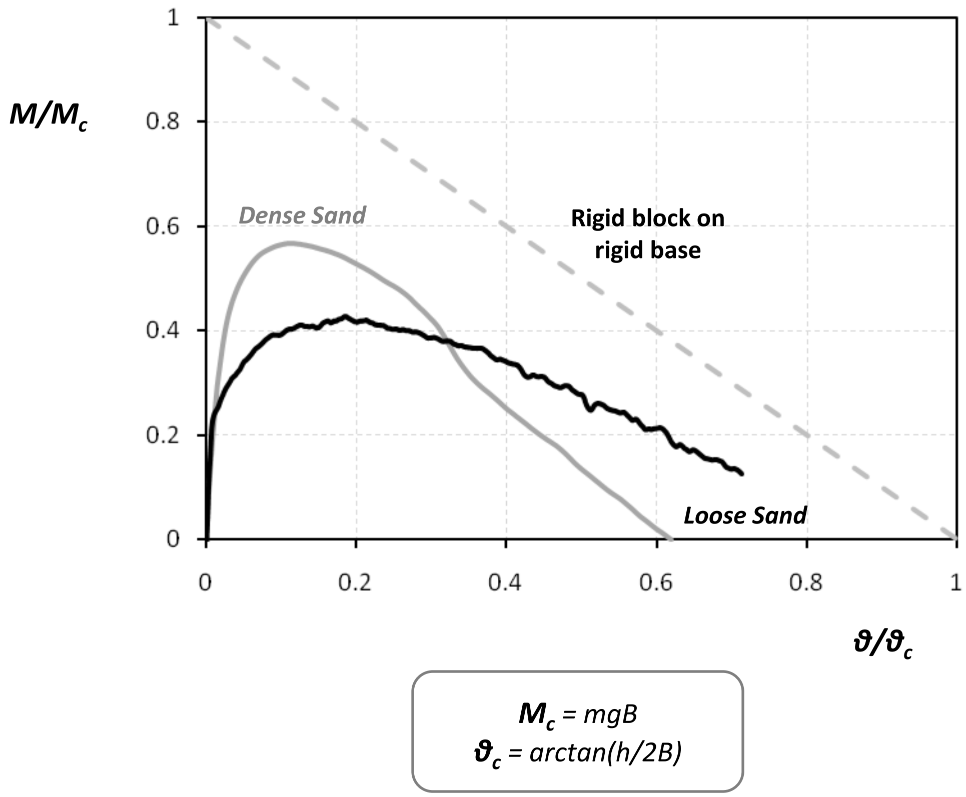

Figure 4.8. Dimensionless moment–rotation curves derived from monotonic pushover tests for the aforementioned systems with **FS_V = 5**.

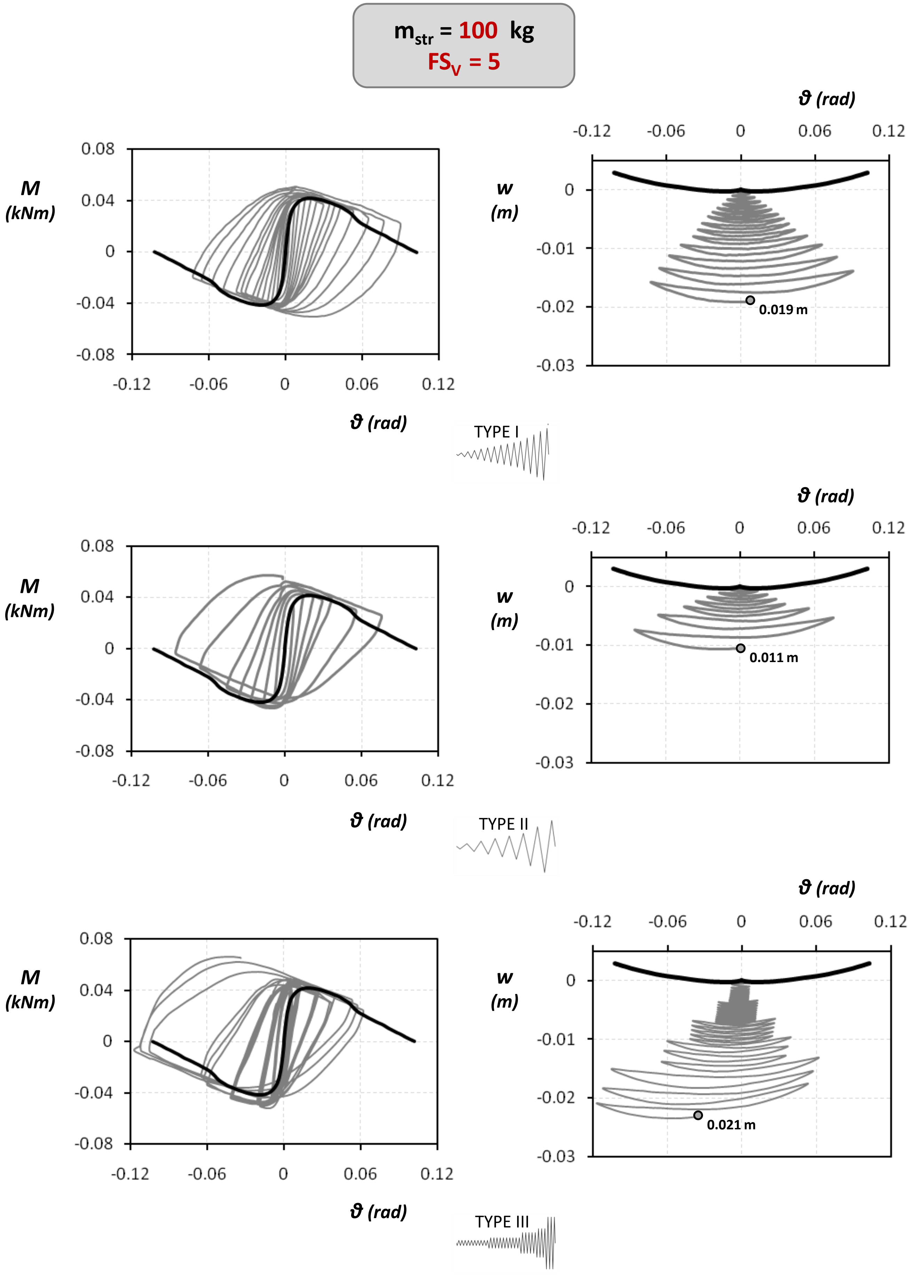

Figure 4.9. **(a)** Moment–rotation and **(b)** settlement–rotation curves derived from slow cyclic pushover tests of different loading protocols. The structural mass is $\mathbf{m_{str} = 100\ kg}$ and the sand relative density $\mathbf{D_r = 93\ \%}$.

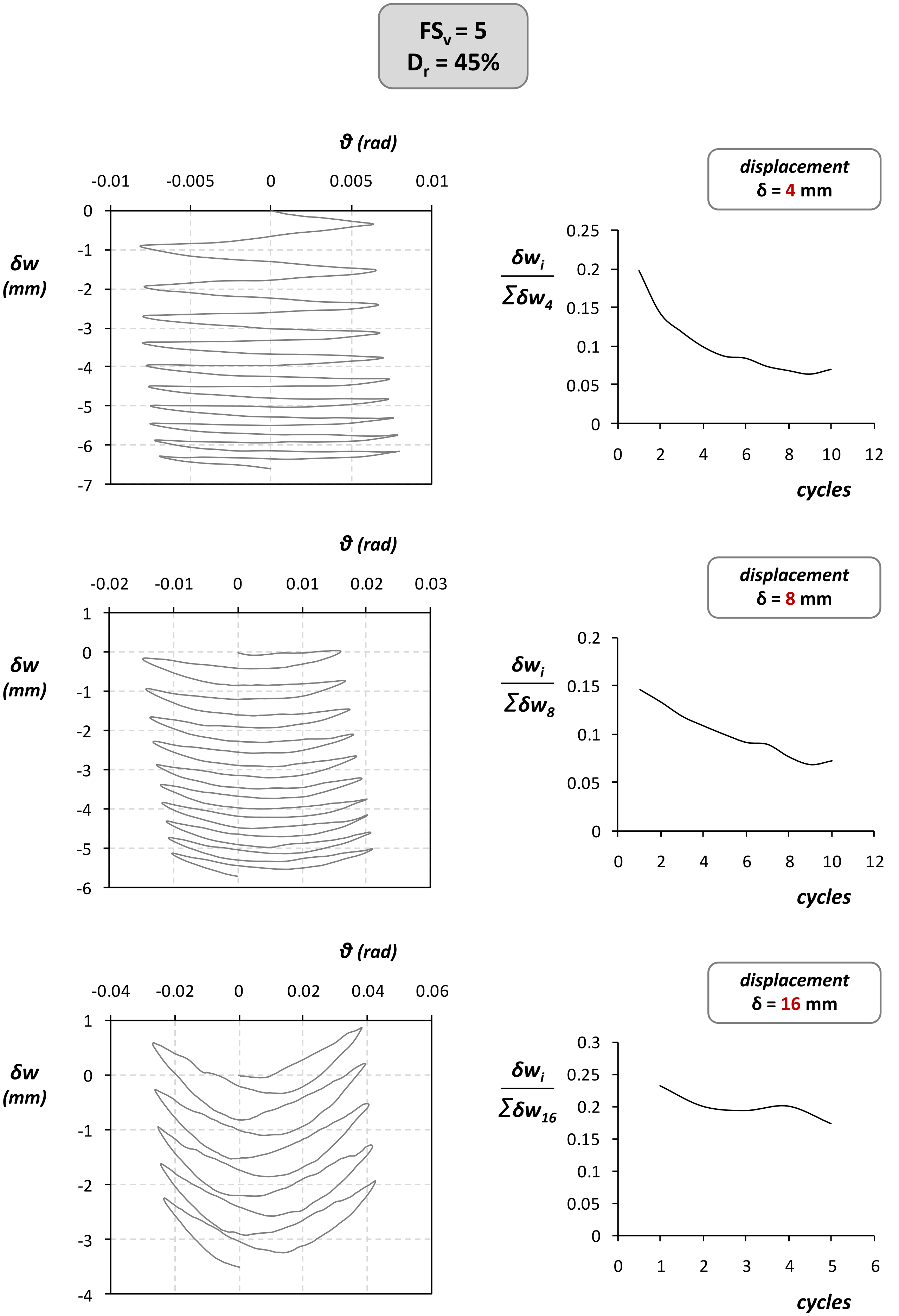

Figure 4.10. (a) Accumulated settlement versus rotation angle for three first load packs of loading protocol Type III. The structural mass is **m_{str} = 35 kg** and the sand relative density is **D_r = 45 %**.

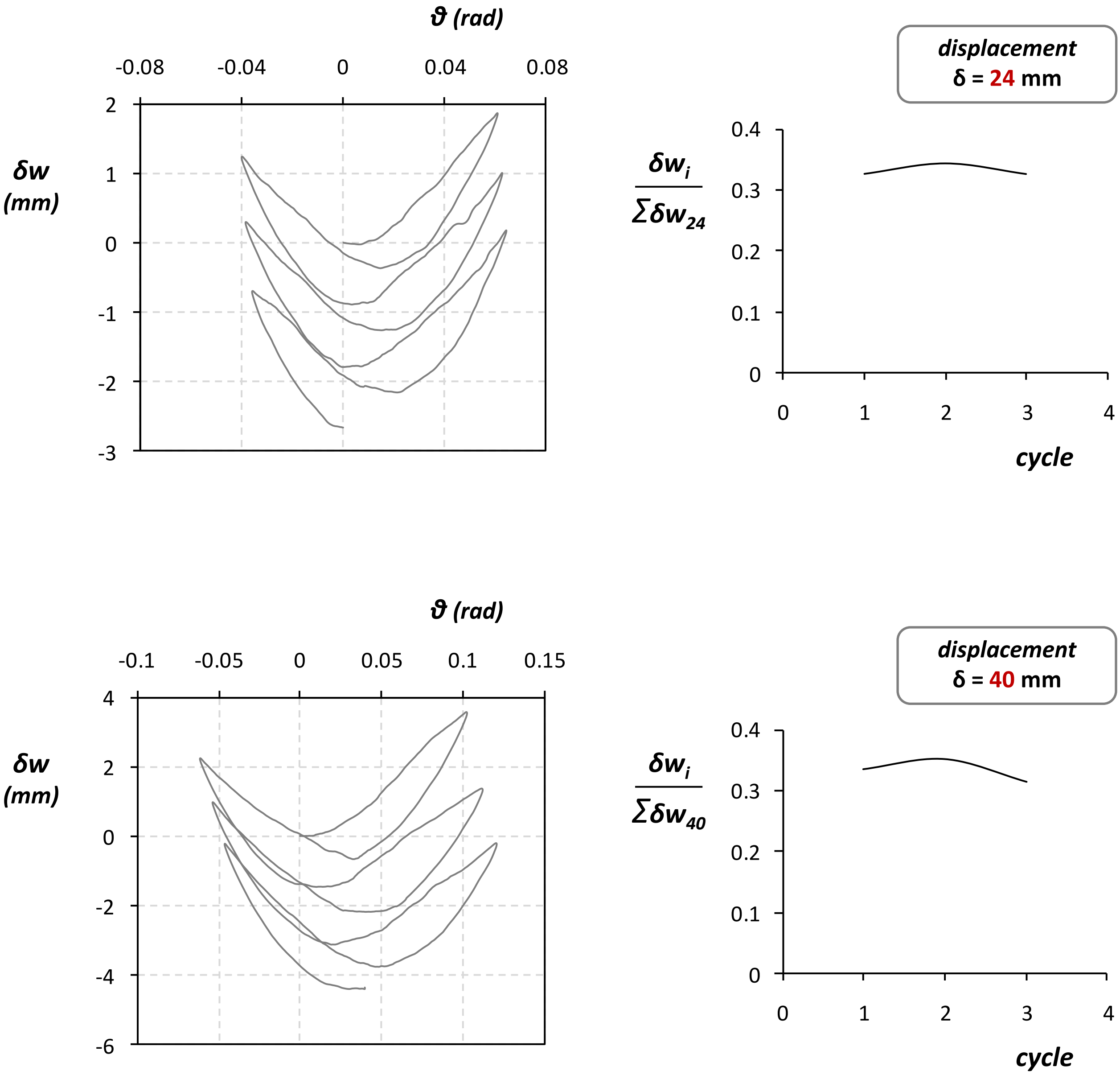

Figure 4.11. (a) Accumulated settlement versus rotation angle for two last load packs of loading protocol Type III. The structural mass is $\mathbf{m_{str} = 35\ kg}$ and the sand relative density is $\mathbf{D_r = 45\ \%}$.

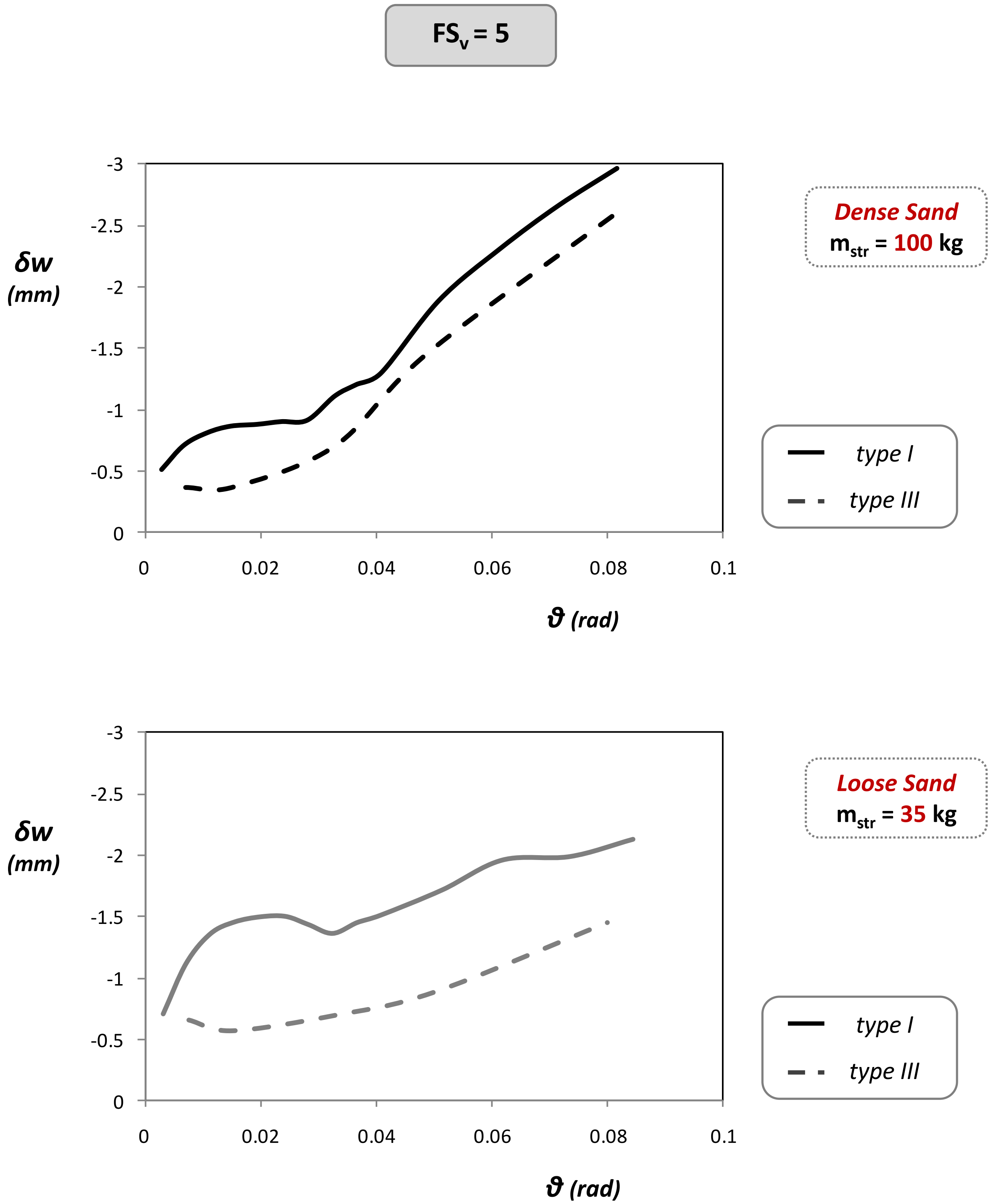

Figure 4.12. Additional settlement per rotation amplitude for the two equivalent systems in terms of FS$_V$ compared before. Comparison between settlement development in load protocol Type I and Type III. The settlement referring to Type III is the final settlement of each load pack divided by the number of the cycles of this specific load pack.

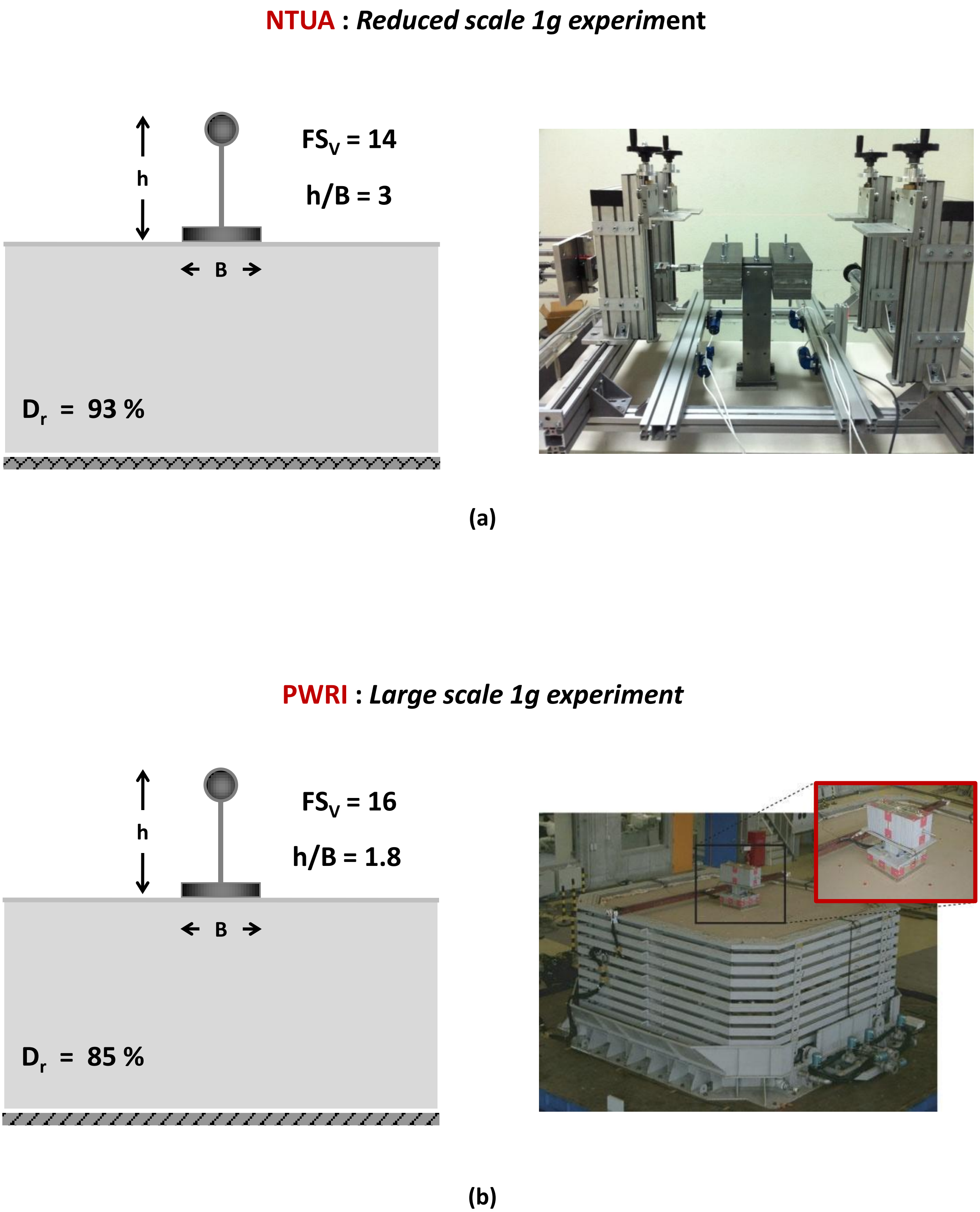

Figure 4.13. Schematic illustration and picture of **(a)** the system investigated herein and **(b)** the system examined at PWRI (photograph from Paolucci et al, 2008).

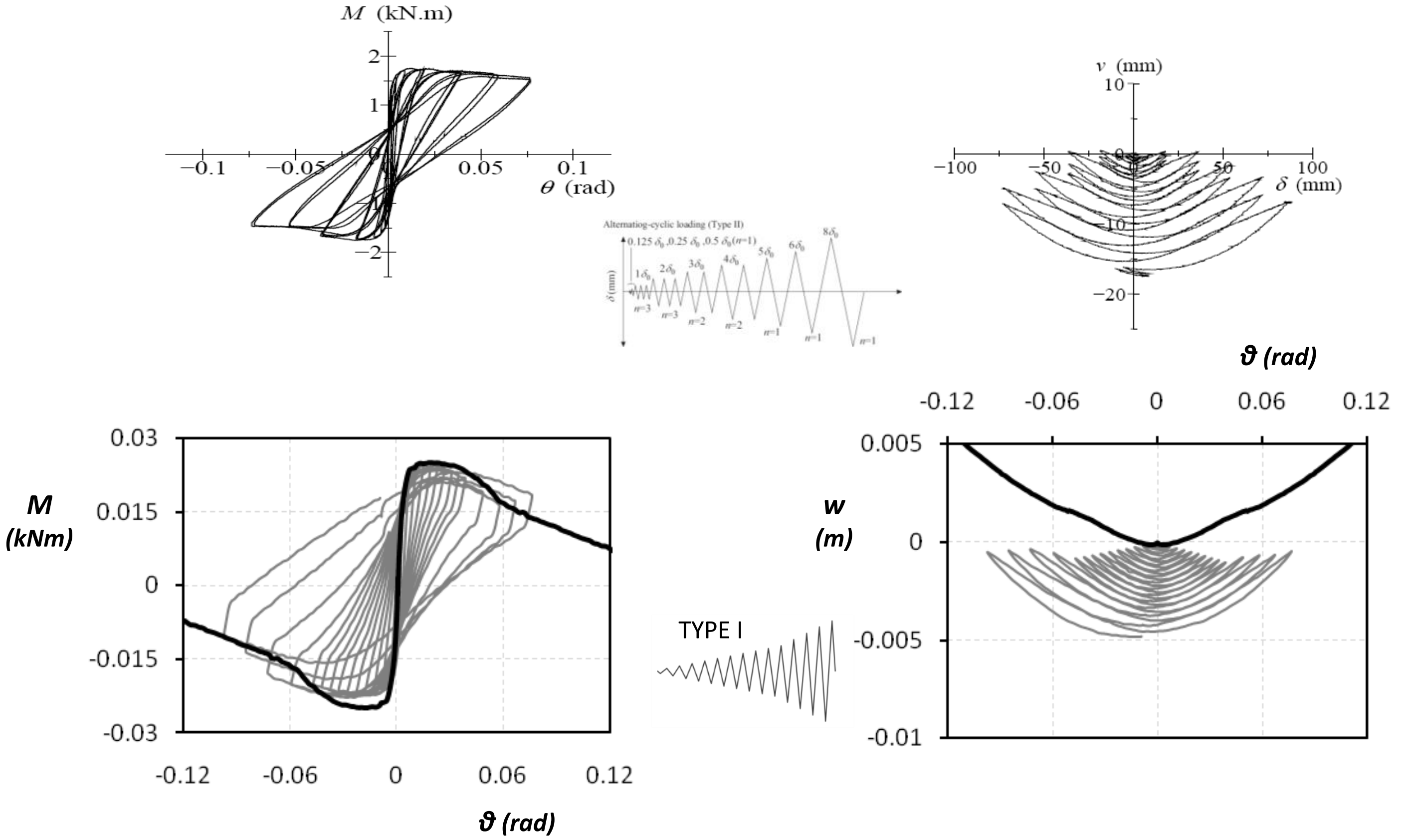

(a)

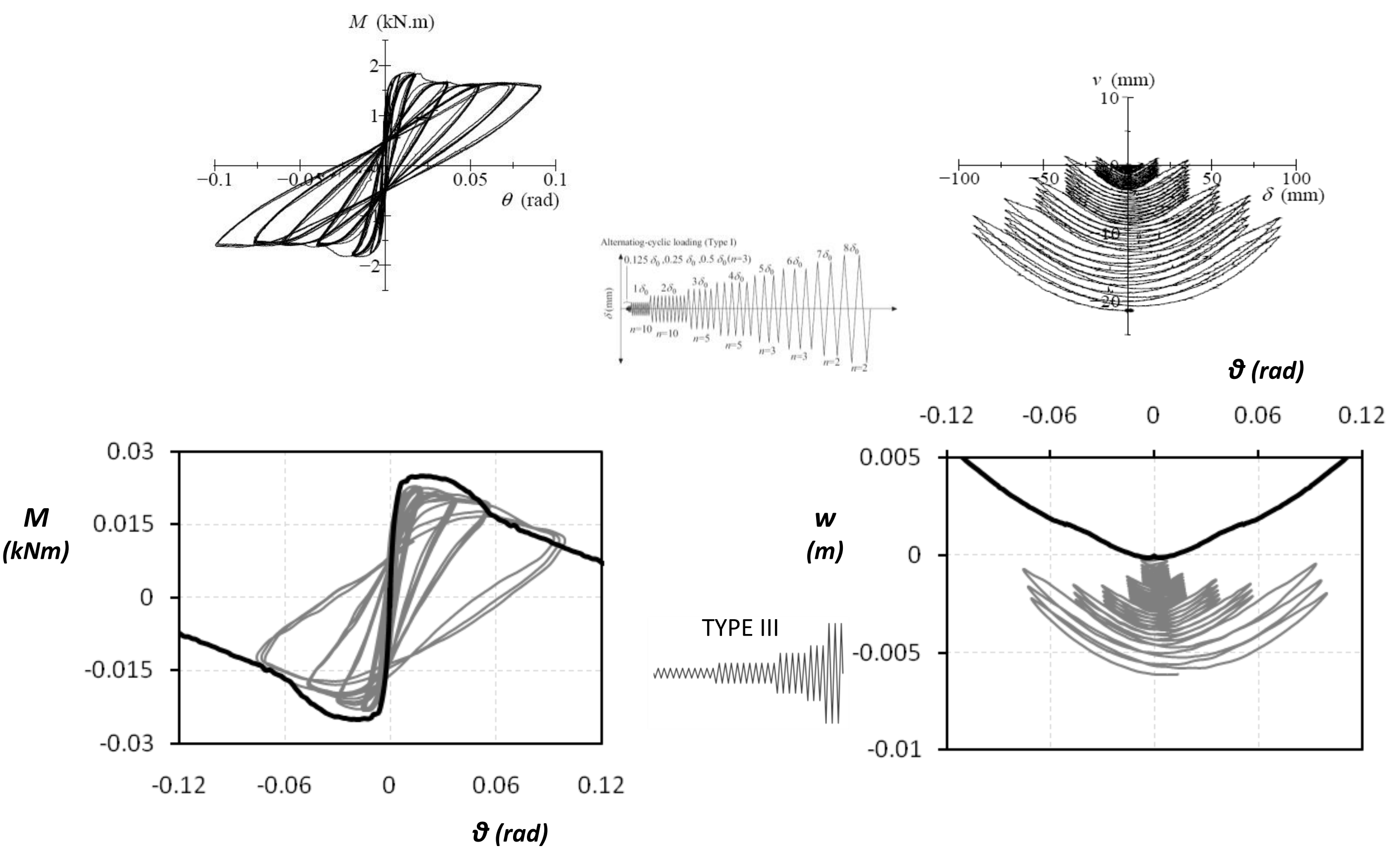

(b)

Figure 4.14. Qualitative comparison between the experiments conducted at **PWRI** and **NTUA** in terms of moment–rotation and settlement–displacement (rotation) curves for **(a)** one cycle per horizontal displacement amplitude and **(b)** many cycles per horizontal displacement amplitude.

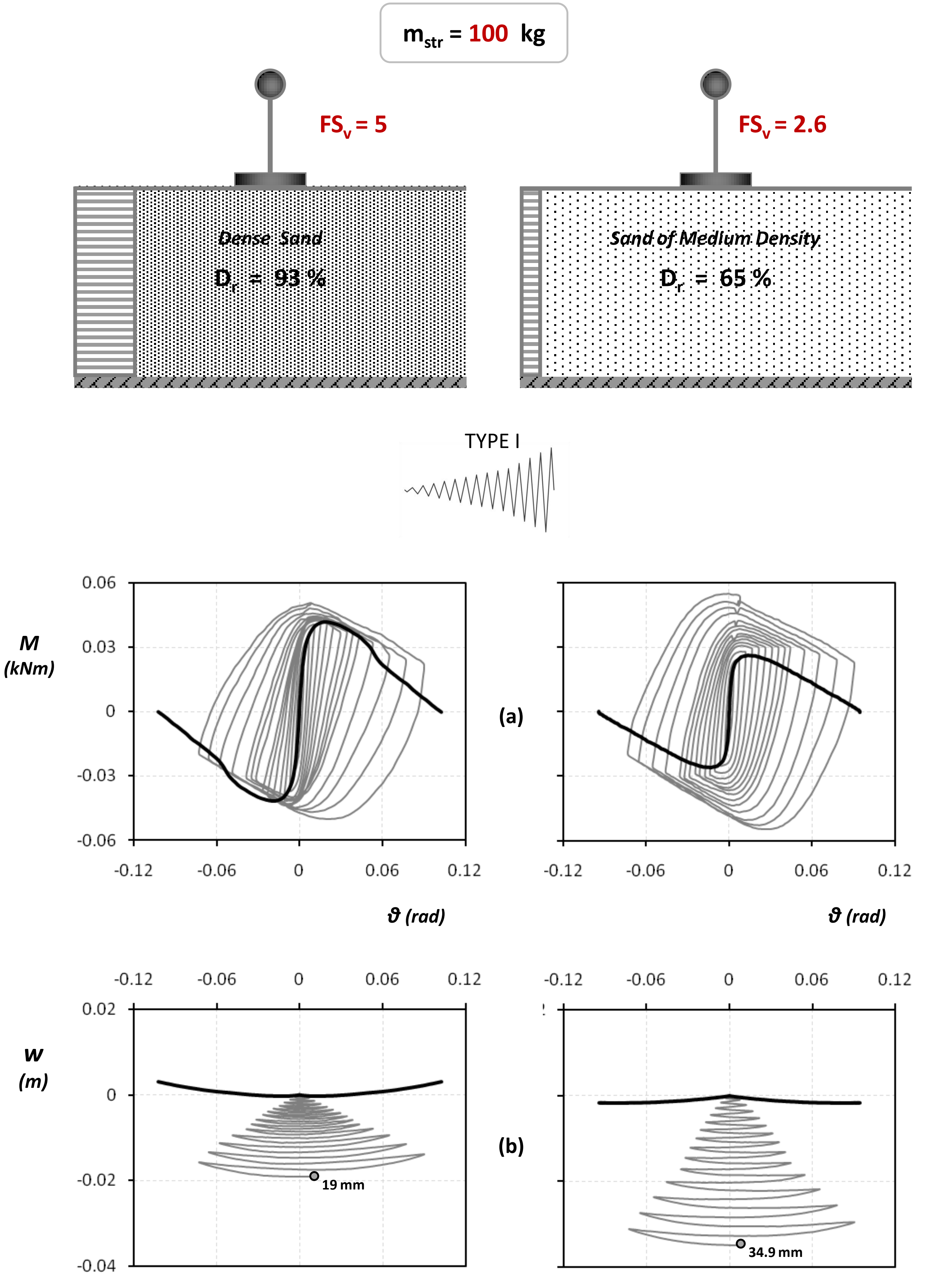

Figure 4.15. (a) Moment–rotation and **(b)** settlement–rotation curves derived from slow cyclic pushover tests (**TYPE I**) for systems with structural mass $\mathbf{m_{str} = 100\ kg}$ lying on sand of relative density D_r = 93 % ($\mathbf{FS_V = 5}$) and D_r = 65 % ($\mathbf{FS_V = 2.6}$).

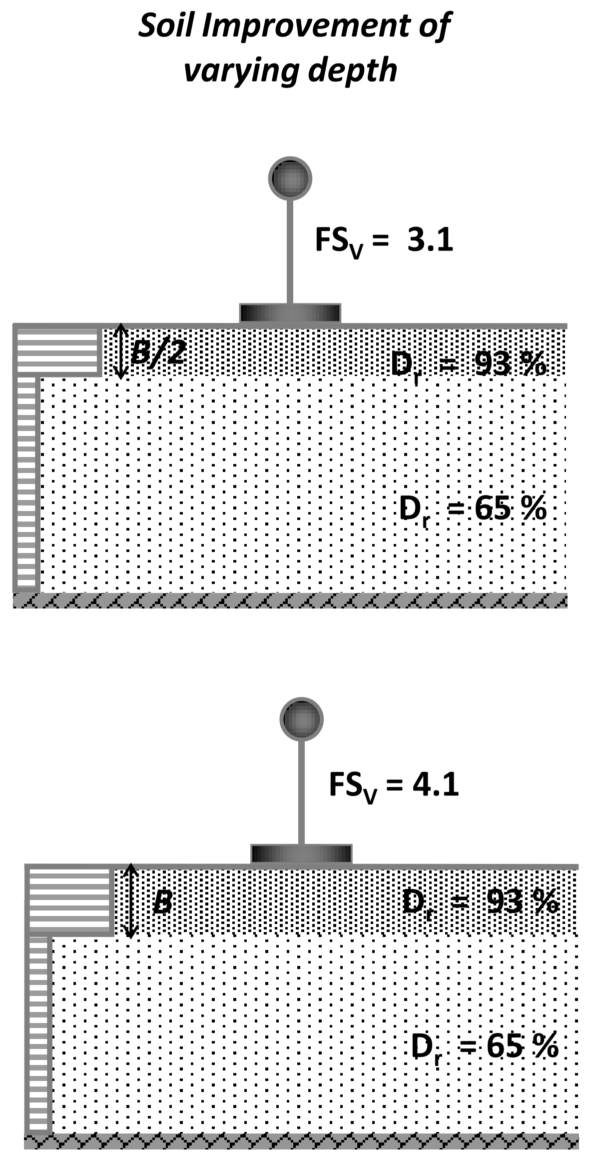

Figure 4.16. Schematic illustration of soil–foundation–superstructure systems studied as a measure of eliminating the uncertainties related to soil properties. The structural mass is $\mathbf{m_{str}}$ **= 100 kg**.

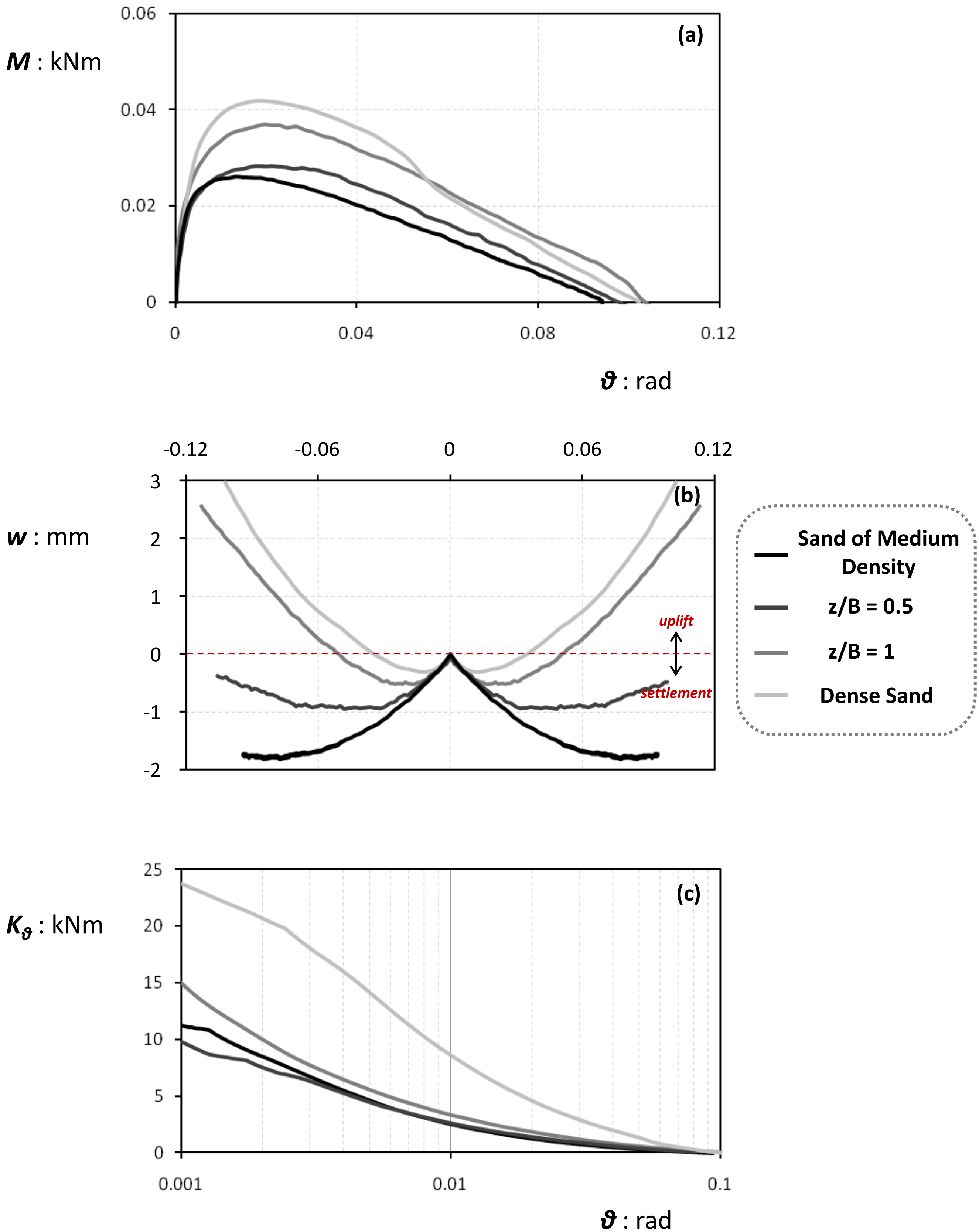

Figure 4.17. Comparison of the performance of the system using the crusts **(a)** Moment–rotation curves, **(b)** settlement–rotation curves, **(c)** rotational stiffness curves derived from monotonic pushover tests for systems lying on homogeneous and two-layered soil deposits. The structural mass is **m_{str} = 100 kg**.

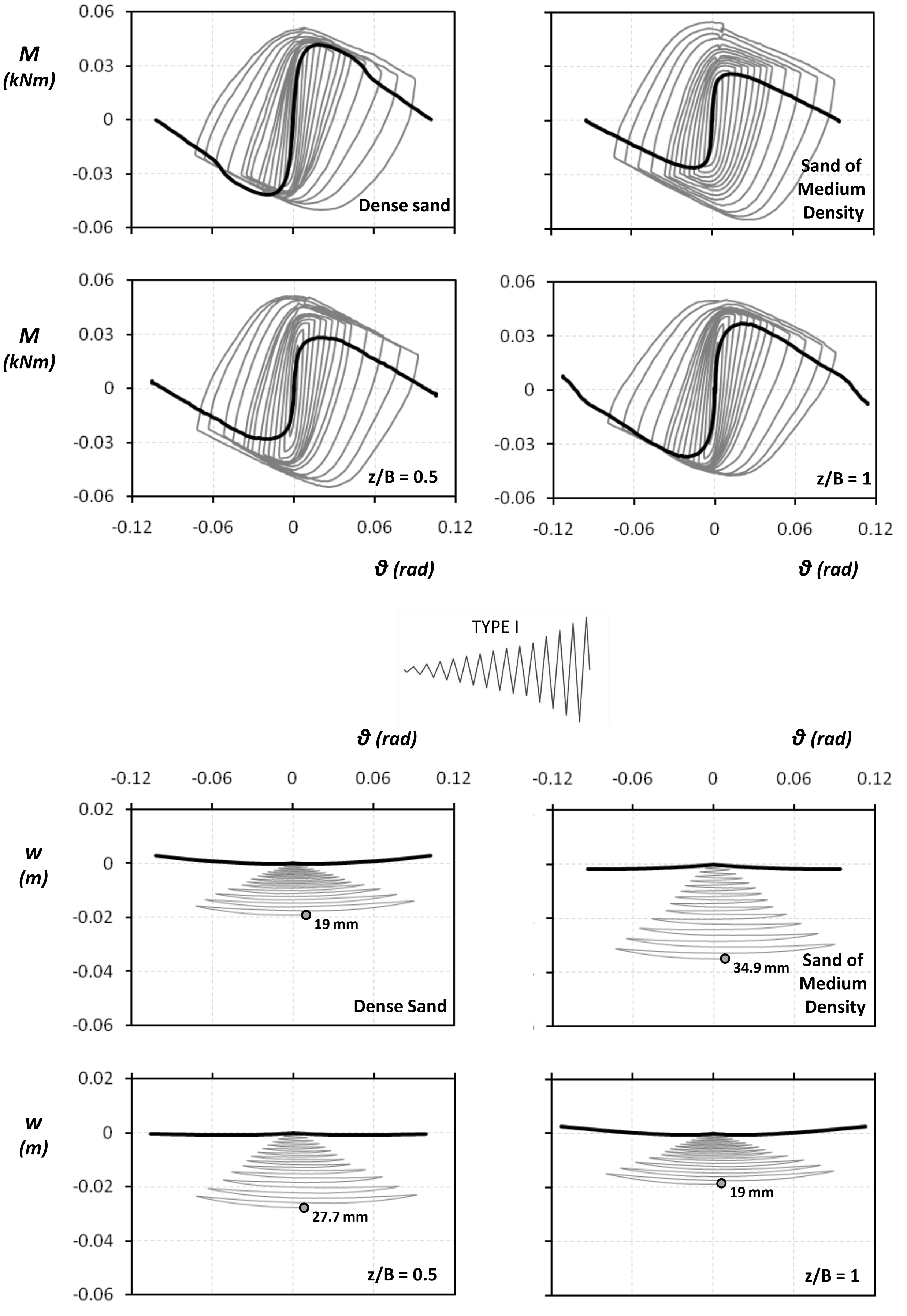

Figure 4.18. Comparison of the performance of the system using the crusts. Moment–rotation and settlement–rotation curves derived from slow cyclic pushover tests (**TYPE I**) for systems lying on homogeneous and two-layered soil deposits. The structural mass is **m_{str} = 100 kg**.

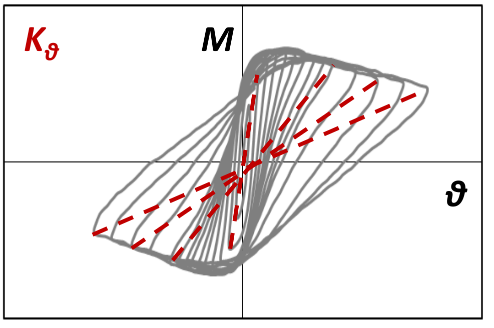

(a)

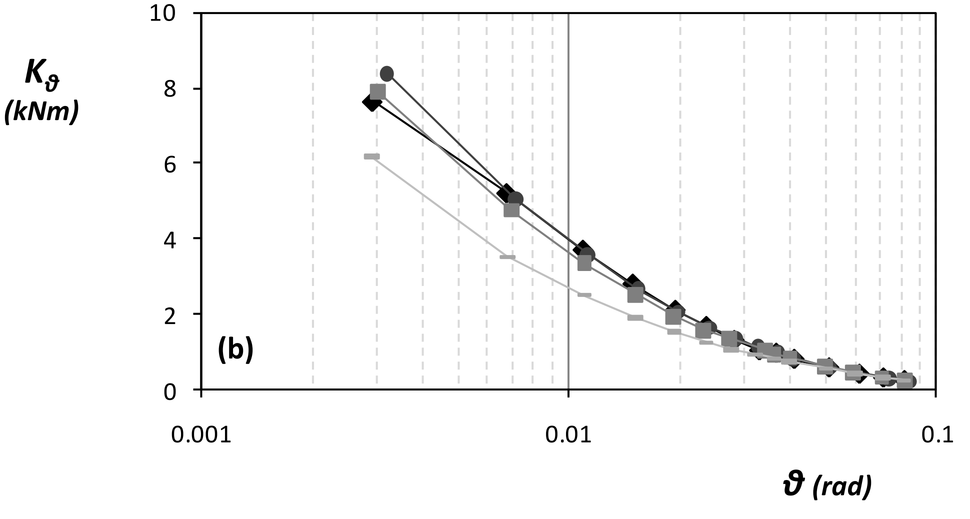

Figure 4.19. (a) Schematic illustration of secant rotational stiffness computed for cyclic loading and **(c)** rotational stiffness curves derived from slow cyclic pushover tests (**TYPE I**) for systems lying on homogeneous and two-layered soil deposits. The structural mass is **m_{str} = 100 kg**.

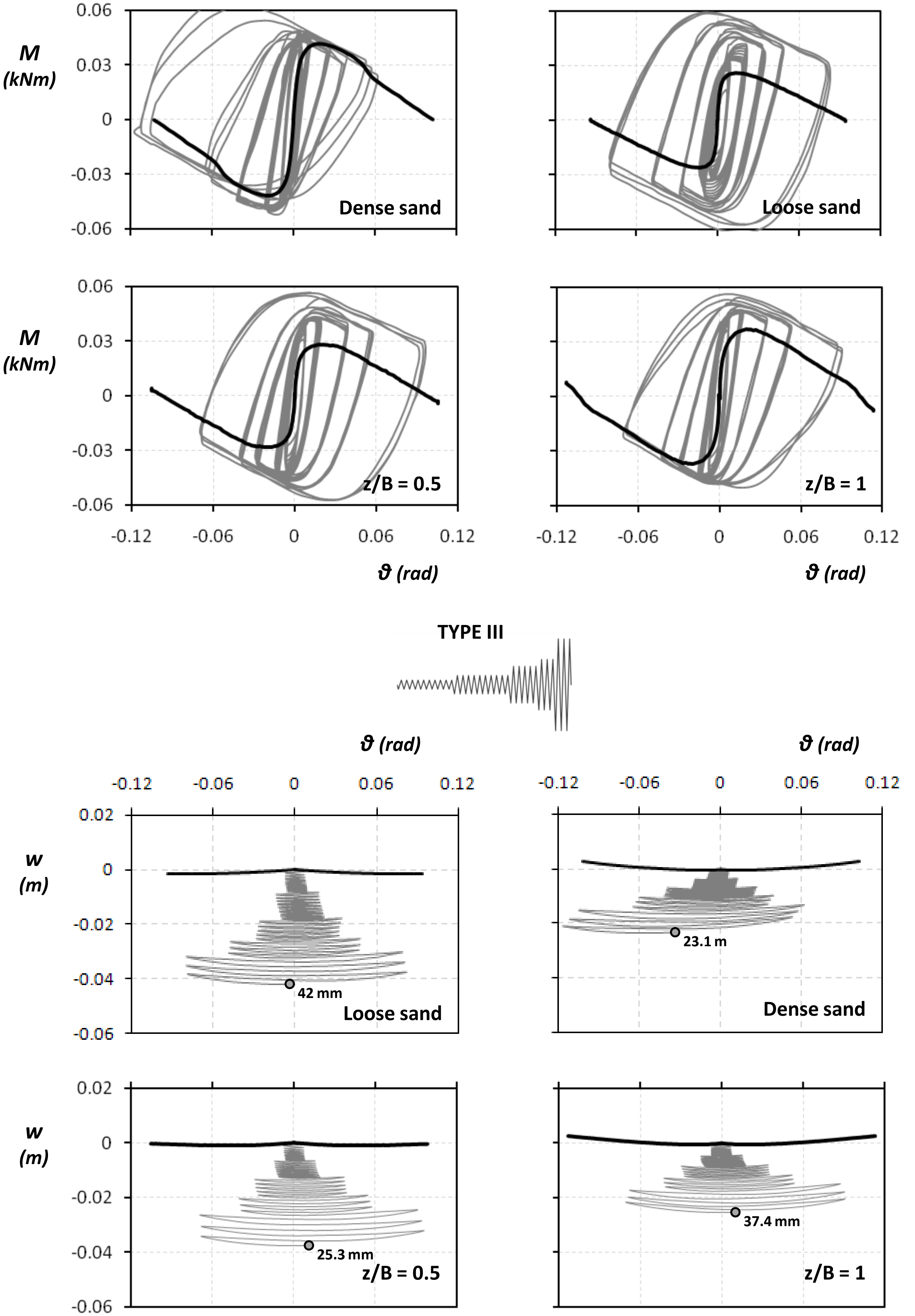

Figure 4.20. Comparison of the performance of the system using the crusts. Moment–rotation and settlement–rotation curves derived from slow cyclic pushover tests (**TYPE III**) for systems lying on homogeneous and two-layered soil deposits. The structural mass is **m_{str} = 100 kg**.

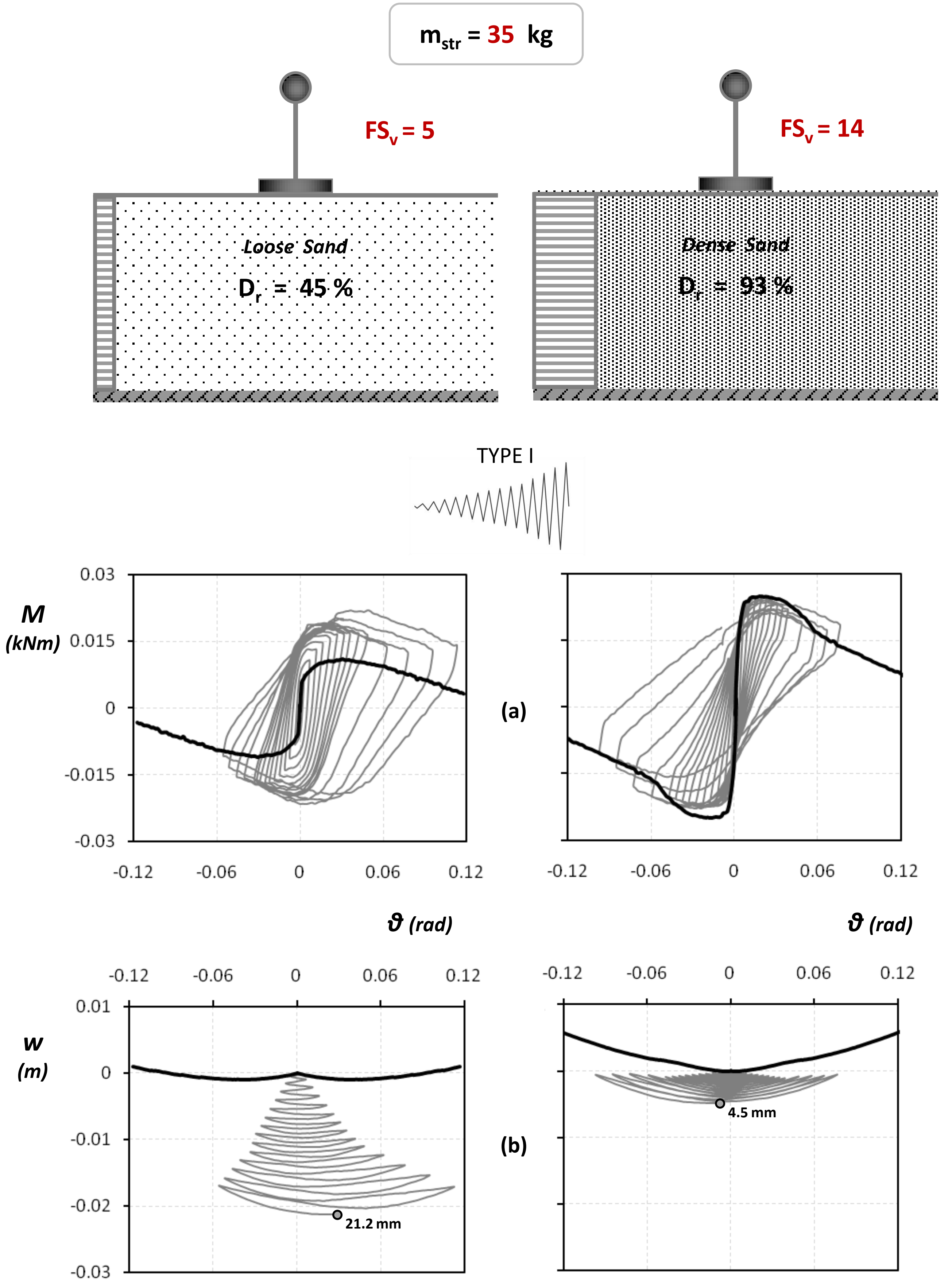

Figure 4.21. (a) Moment–rotation and **(b)** settlement–rotation curves derived from slow cyclic pushover tests (**TYPE I**) for systems with structural mass $\mathbf{m_{str}}$ **= 35 kg** lying on sand of relative density D_r = 93 % (**FS_V = 5**) and D_r = 45 % (**FS_V = 5**).

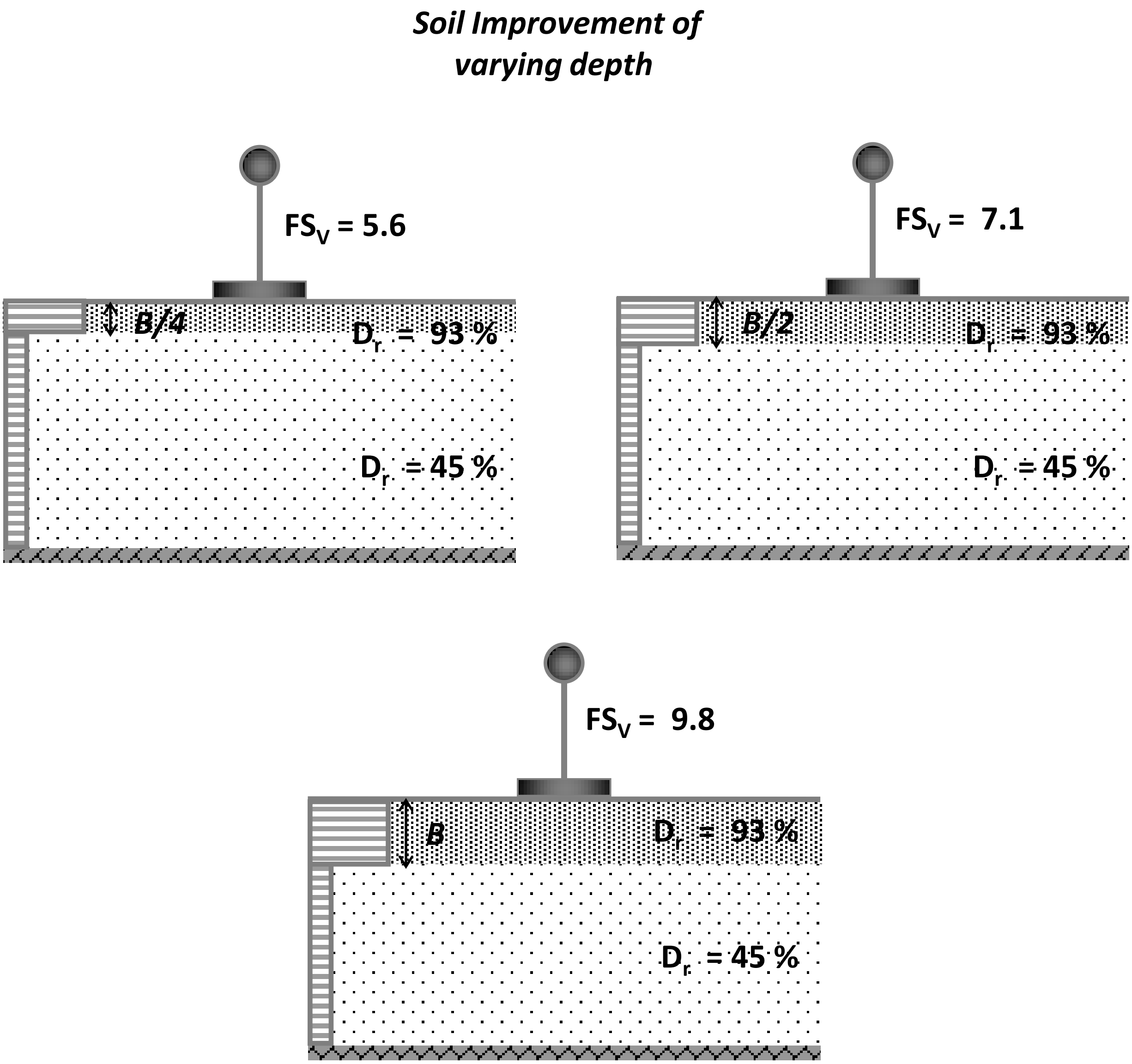

Figure 4.22. Schematic illustration of soil–foundation–superstructure systems studied as measure of performance enhancement. The structural mass is $\mathbf{m_{str} = 35\ kg}$.

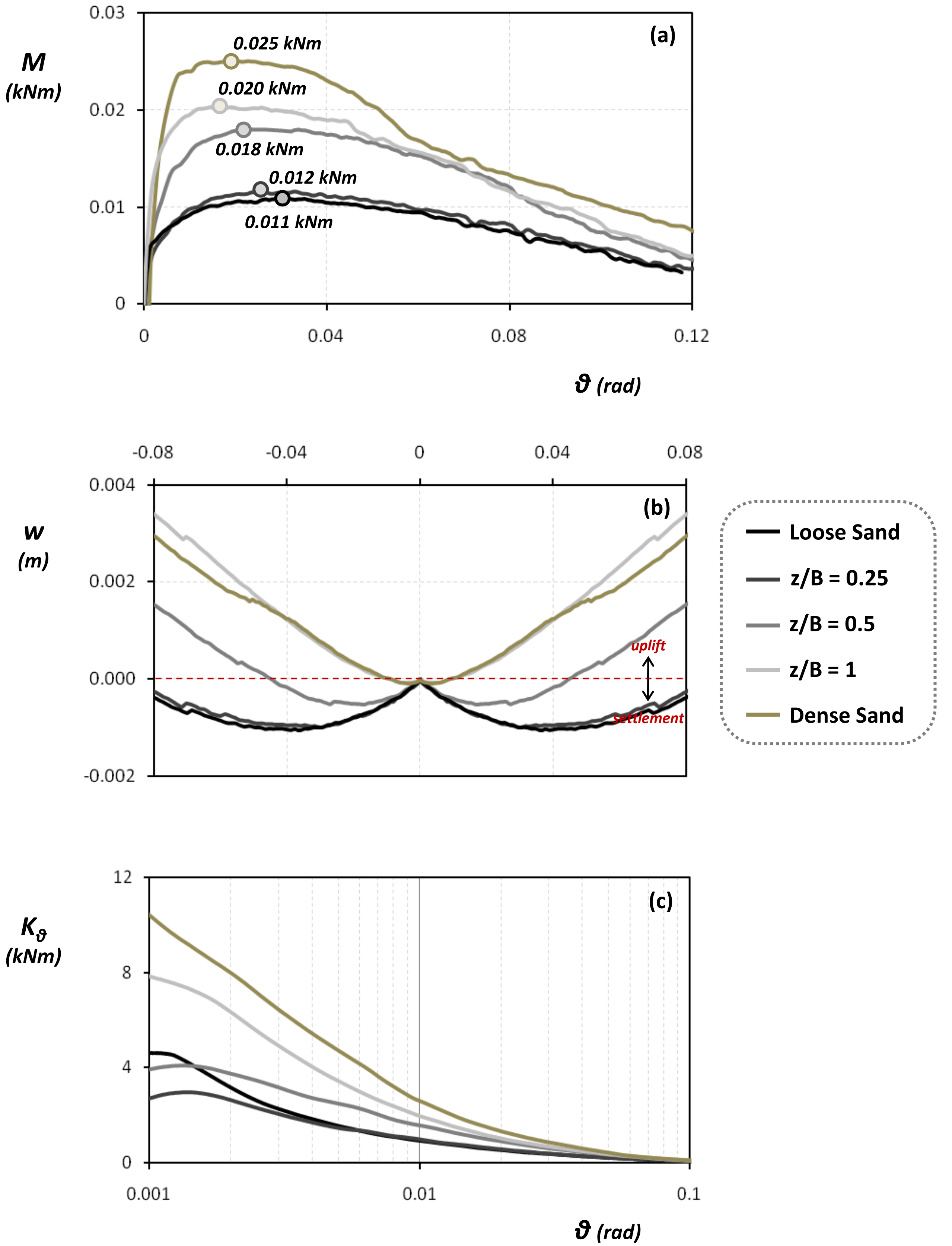

Figure 4.23. Comparison of the performance of the system using the crusts **(a)** Moment–rotation curves, **(b)** settlement–rotation curves, **(c)** rotational stiffness curves derived from monotonic pushover tests for systems lying on homogeneous and two-layered soil deposits. The structural mass is m_{str} = **35 kg**.

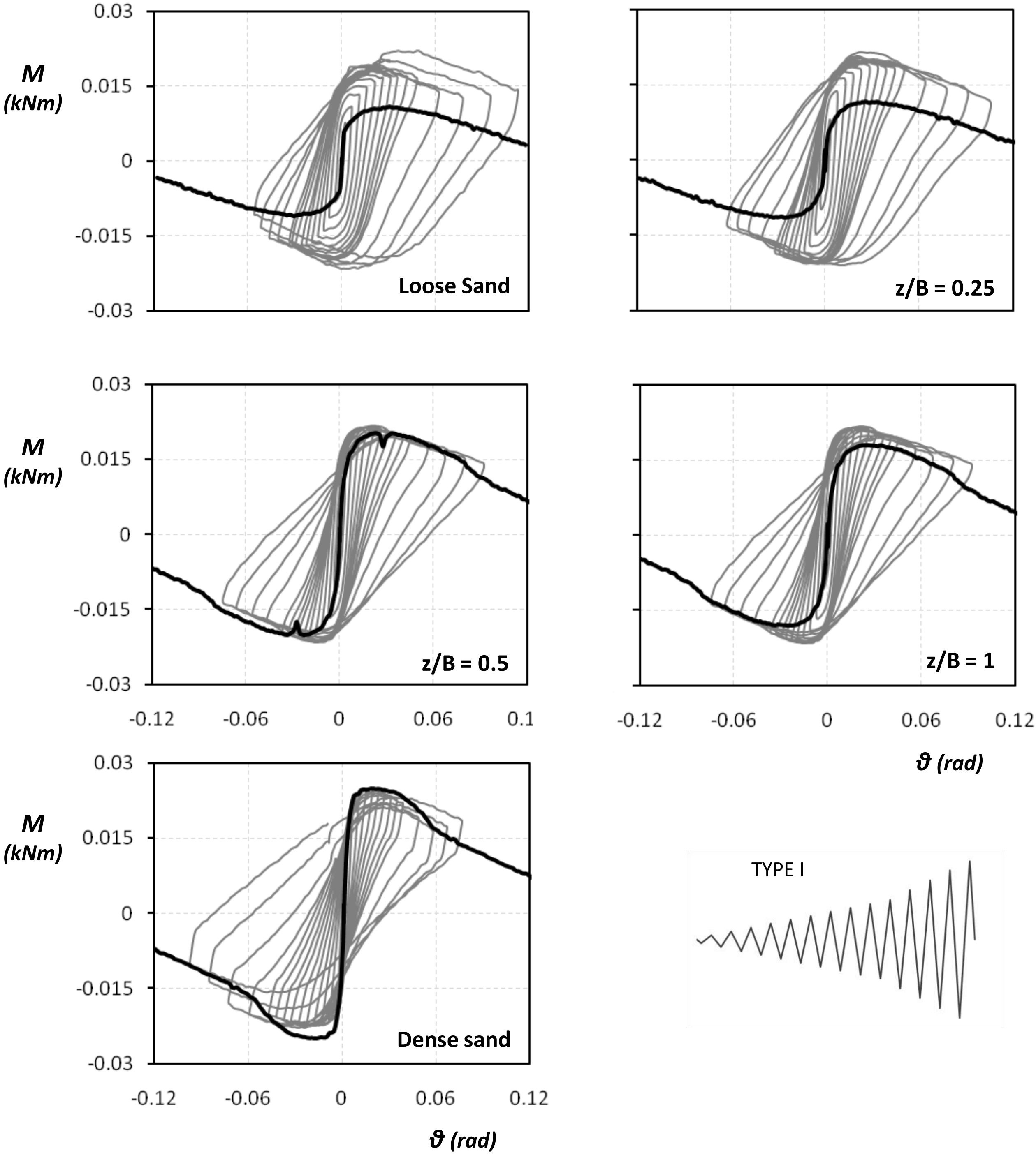

Figure 4.24. Comparison of the performance of the system using the crusts. Moment–rotation curves derived from slow cyclic pushover tests (**TYPE I**) for systems lying on homogeneous and two-layered soil deposits. The structural mass is **m_{str} = 35 kg**.

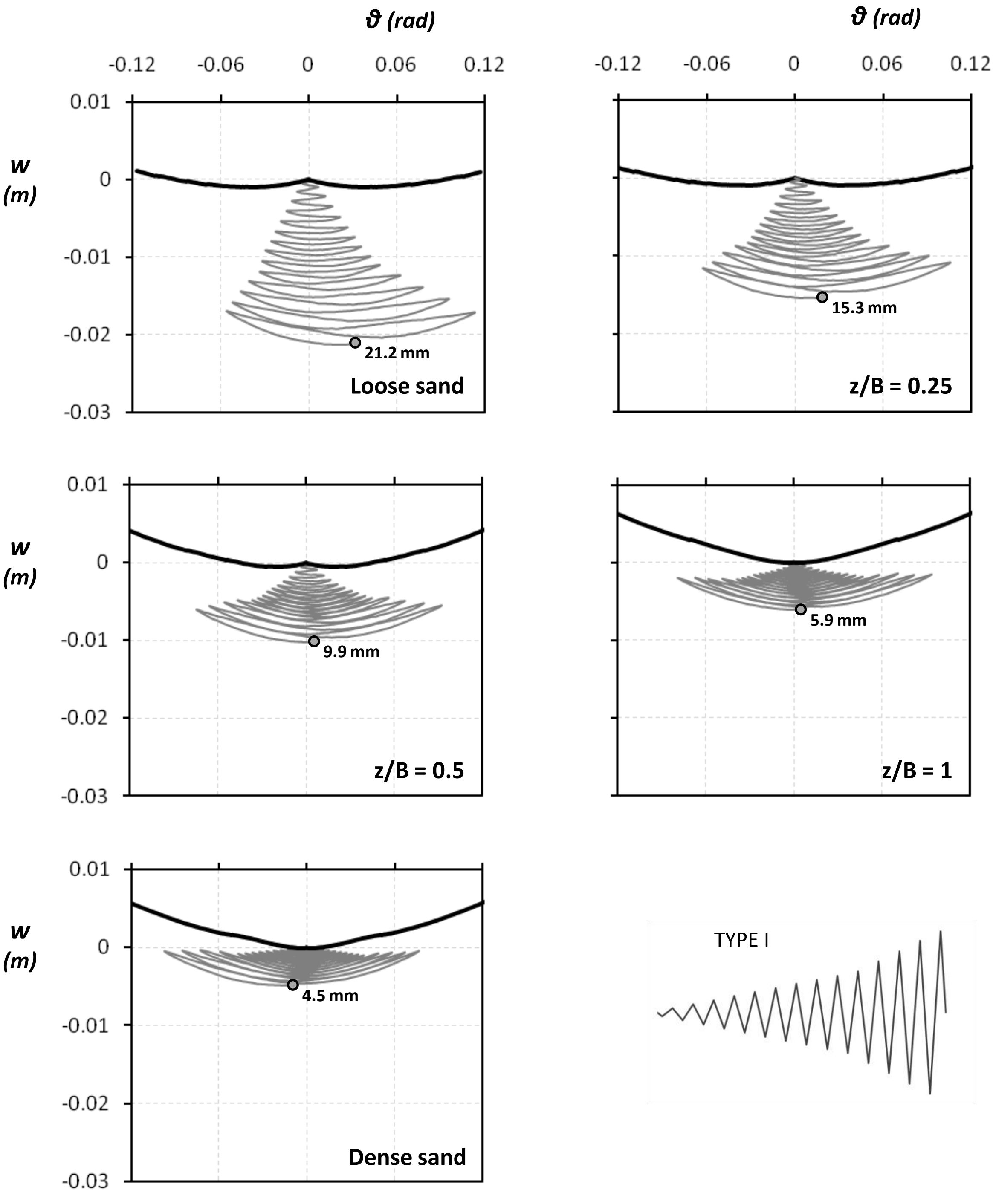

Figure 4.25. Comparison of the performance of the system using the crusts. Settlement–rotation curves derived from slow cyclic pushover tests (**TYPE I**) for systems lying on homogeneous and two-layered soil deposits. The structural mass is **m_{str} = 35 kg**.

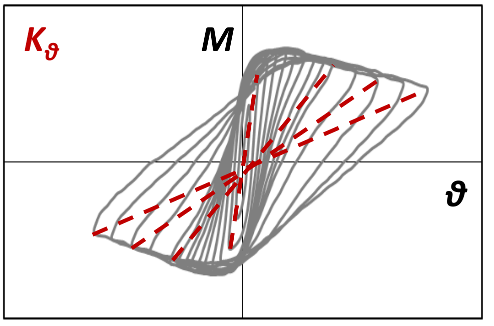

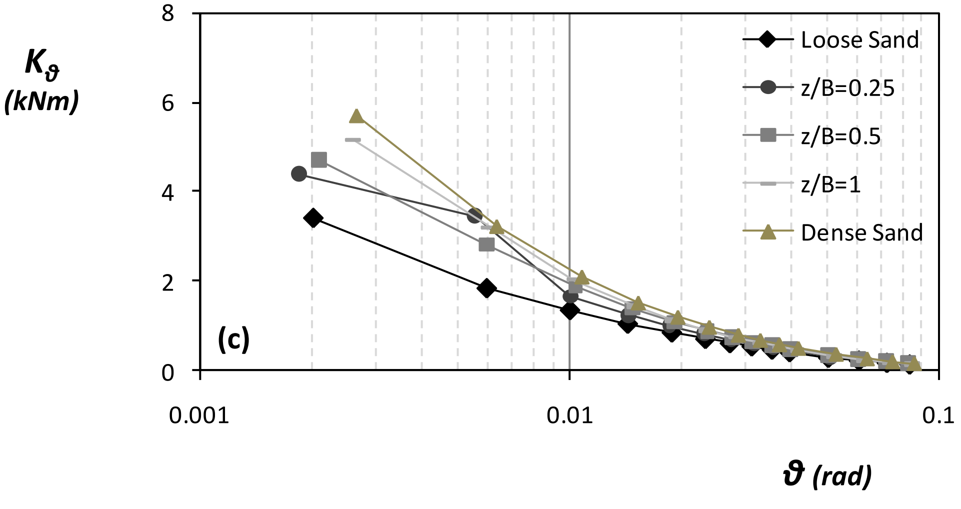

Figure 4.26. (a) Accumulation of settlement per cycle **(b)** schematic illustration of rotational stiffness computed for cyclic loading and **(c)** rotational stiffness curves derived from slow cyclic pushover tests (**TYPE I**) for systems lying on homogeneous and two-layered soil deposits. The structural mass is **m_{str} = 35 kg**.

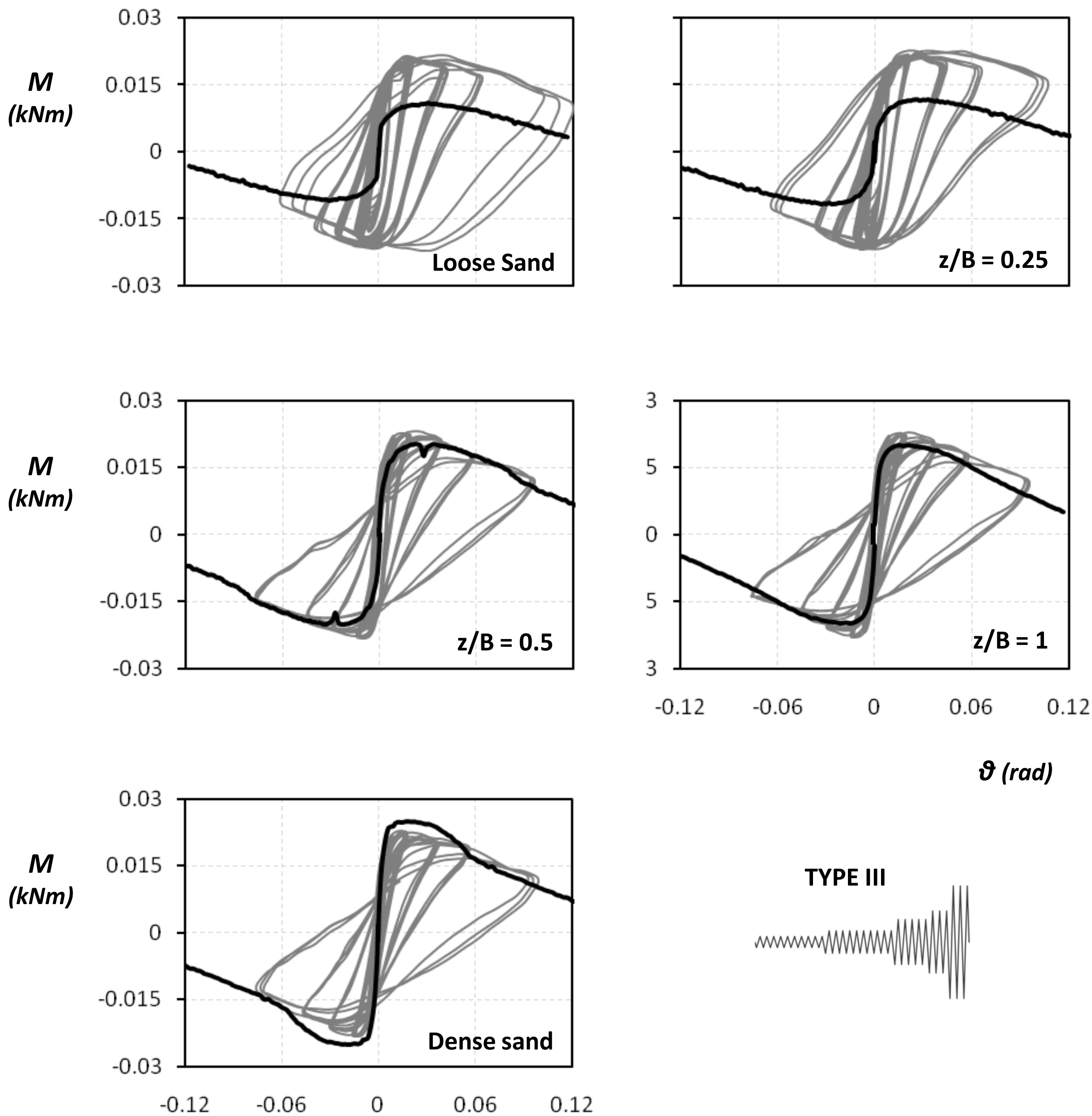

Figure 4.27. Comparison of the performance of the system using the crusts. Moment–rotation curves derived from slow cyclic pushover tests (**TYPE III**) for systems lying on homogeneous and two-layered soil deposits. The structural mass is **m_{str} = 35 kg**.

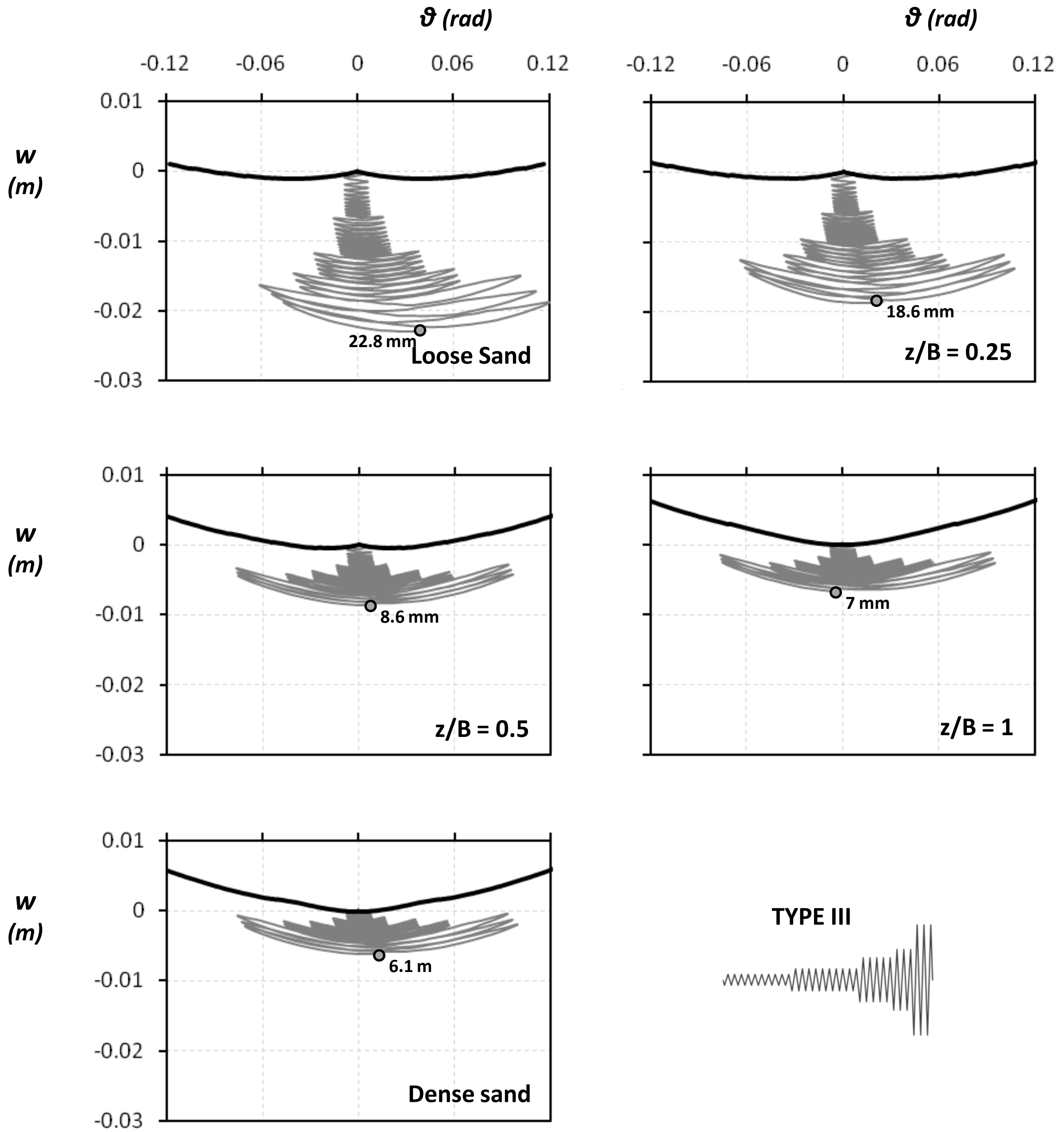

Figure 4.28. Comparison of the performance of the system using the crusts. Settlement–rotation curves derived from slow cyclic pushover tests (**TYPE III**) for systems lying on homogeneous and two-layered soil deposits. The structural mass is **m_{str} = 35 kg**.

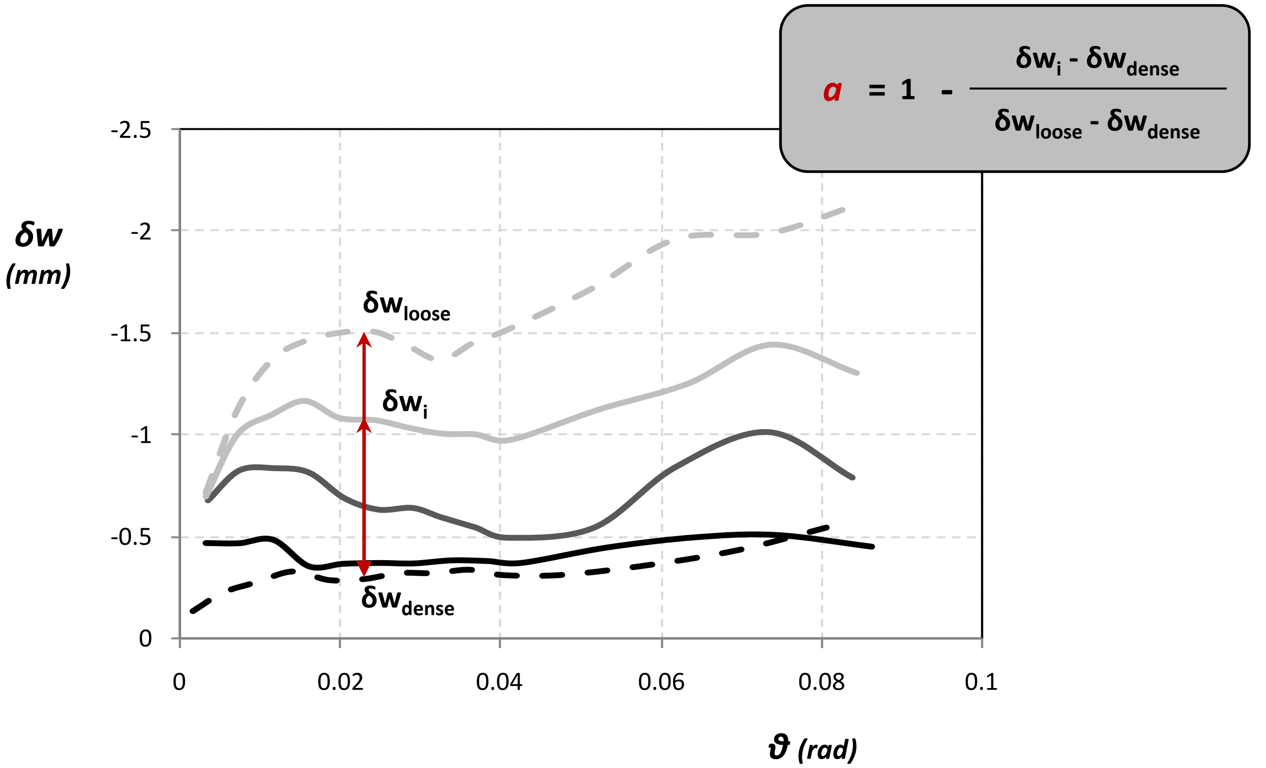

Figure 4.29. Settlement per rotation amplitude derived from slow cyclic pushover tests TYPE I for systems lying on two-layered soil deposits. The structural mass is m_{str} = 35 kg.

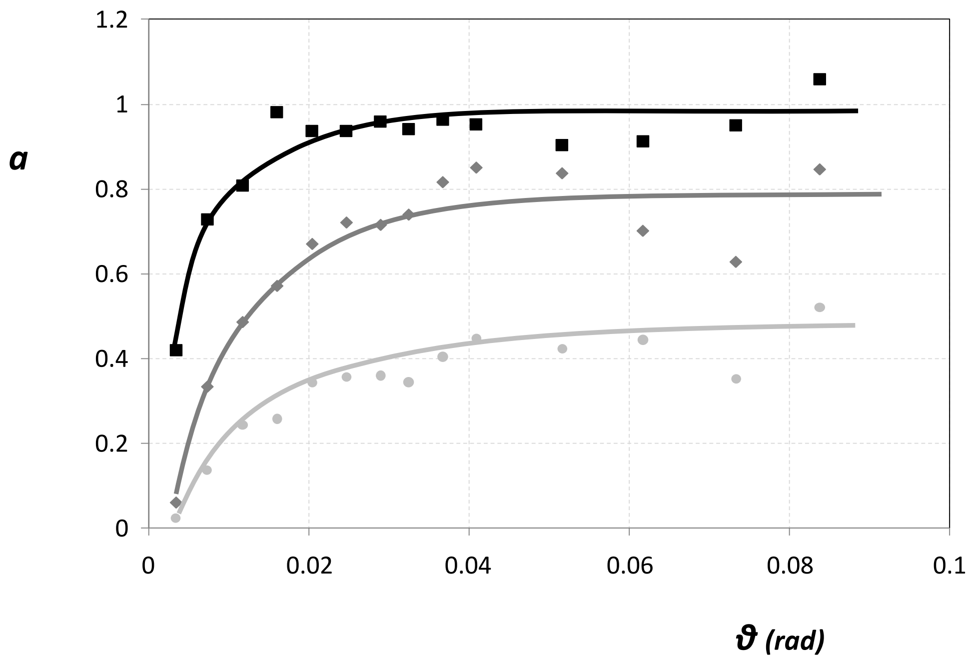

Figure 4.30. Evolution of the effectiveness ratio of each crust presented above with respect to the rotation angle amplitude.

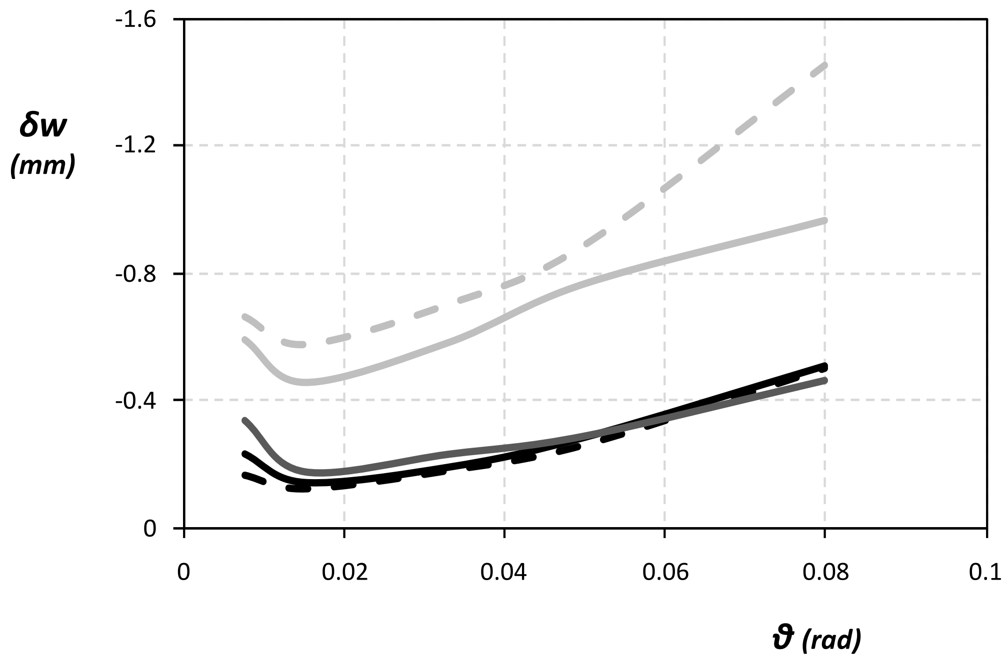

Figure 4.31. Settlement per rotation amplitude derived from slow cyclic pushover tests TYPE III for systems lying on two-layered soil deposits. The structural mass is **m_{str} = 35 kg**. The settlement presented herein refers to the average settlement developed in each load pack of Type III.

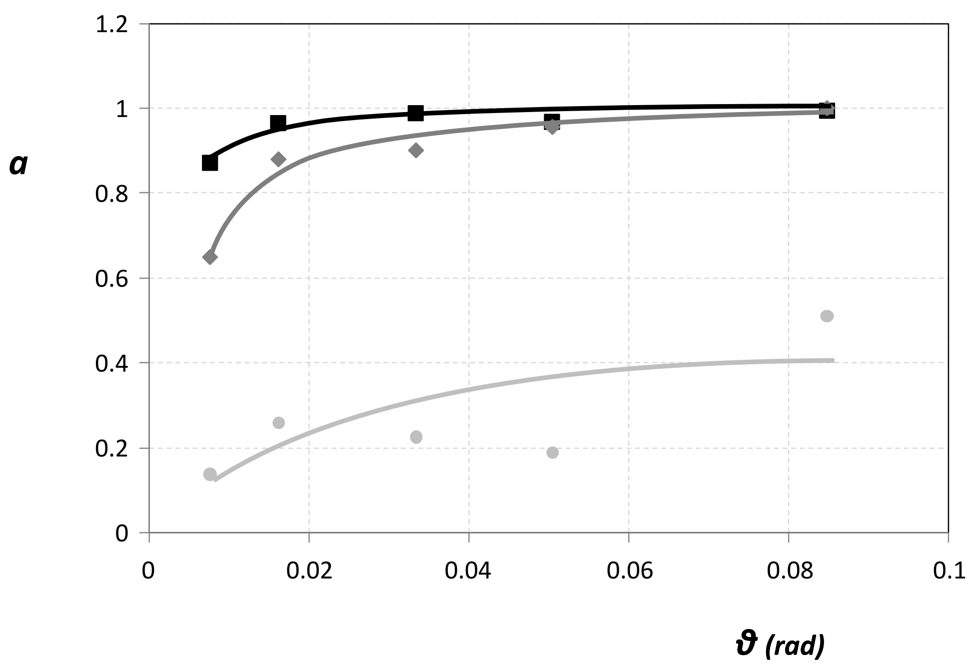

Figure 4.32. Evolution of the effectiveness ratio of each crust presented above with respect to the rotation angle amplitude for loading Type III.